



MSc in Physics

Period variations in the p53 network after protein inhibition

Investigating inhibition responses of p53 *in vitro* and through *in silico*
comparisons across various model formulations

Liv Moretto Sørensen

Supervised by Mogens Høgh Jensen and Mathias Luidor Heltberg
In collaboration with Alba Jiménez Asins

July 2021



Liv Moretto Sørensen

Period variations in the p53 network after protein inhibition

MSc in Physics, July 2021

University of Copenhagen

Faculty of Science

Niels Bohr Institute

Blegdamsvej 17

2100 Copenhagen

Main supervisor: Mogens Høgh Jensen

Co-supervisor: Mathias Luidor Heltberg

In collaboration with:

Harvard Medical School

Department of Systems Biology

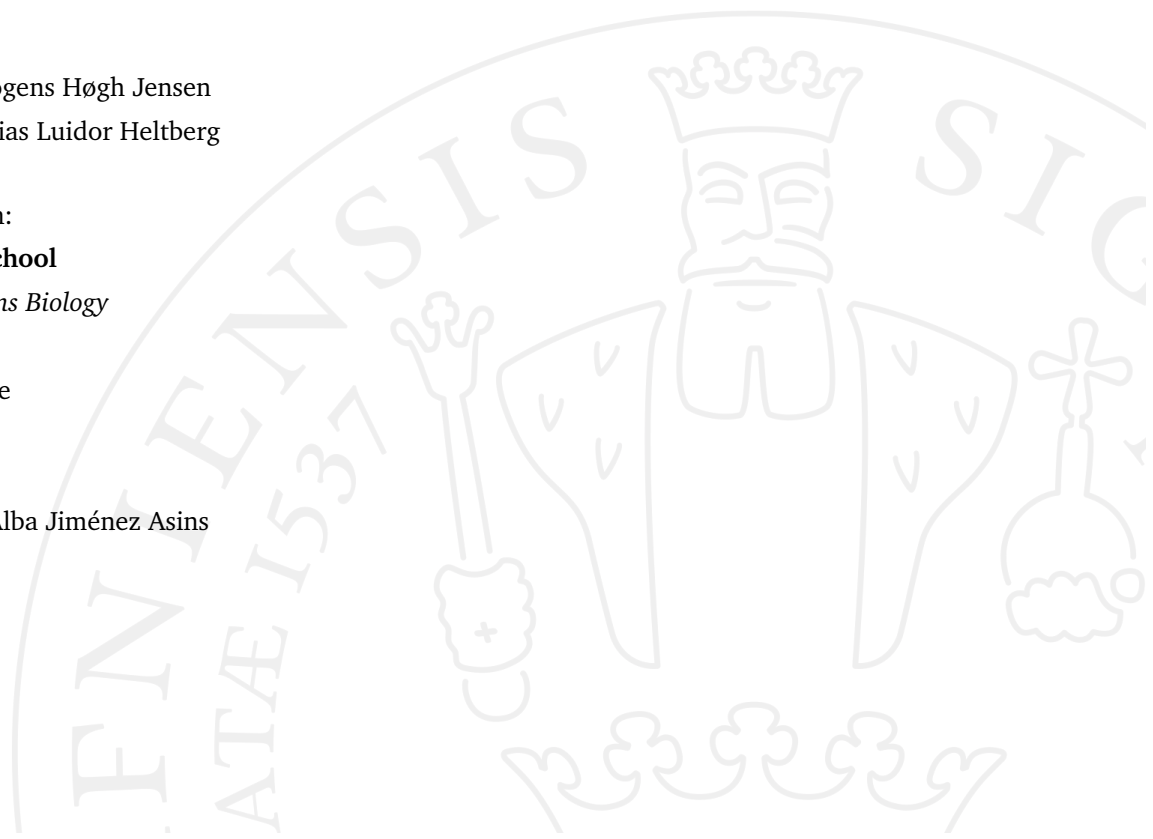
Lahav Lab

10 Longwood Avenue

Armenise Building

Boston, MA 02115

Main collaborator: Alba Jiménez Asins



Abstract

In this work, the regulatory network of the protein p53 is investigated both *in vitro* and *in silico* to understand how the network reacts to inhibition of the regulator protein MdmX. Also known as *the Guardian of the Genome*, p53 functions as a tumour suppressing protein, playing a crucial role regarding the development and progression of cancer. Therefore, understanding how p53 is regulated in the cell is an important step in understanding the mechanisms of cancer development.

Data from experiments conducted by Alba Jiménez Asins in the Lahav Lab at Harvard Medical School has been analysed in this work and four key features of p53 reaction to MdmX inhibition have been identified: a biphasic, oscillatory response can be observed in p53 levels, dividing cells show faster p53 oscillations compared to non-dividing cells, and lastly the proliferation rate decreases and the period of p53 oscillations increases as the inhibition strength increases.

These observations have been investigated analytically and numerically. For this purpose, four previously introduced models have been derived and analysed, and the numerical results have been compared. The investigations in this work propose that the reaction of p53 to MdmX inhibition has global characters across the different model formulations. The *in silico* studies suggest that MdmX levels affect the Mdm2-dependent p53 degradation rate, thereby causing a biphasic oscillatory response with MdmX-dependent period after inhibition of MdmX.

Acknowledgements

During the last year, I have been lucky to work in a fantastic team of people, without whom this work would never have been possible.

I would like to thank my supervisors, Mogens and Mathias, for your trustful and inspiring guidance during the project. The way you have supported and encouraged me to follow my ideas has meant a lot to me. Working with you has included deeply interesting discussions and has provided me with many new perspectives on the complex world we live in. Thank you!

I would also like to thank Alba for the many inspiring talks we have had during the last year. I can't thank you enough for your always cheerful way of keeping me motivated and for all your brilliant explanations that helped me understand the biological aspects of this project. A big thanks to you and the rest of the Lahav Lab!



Figure 0.1: Group meetings in times of a pandemic.

Finally, as this work marks the end of several great years at the Niels Bohr Institute, I would like to thank my friends and colleagues nine million times for making these years so joyful and memorable. Thank you!

Contents

List of abbreviations & technical terms	1
1 Introduction	5
1.1 Outline	6
1.2 Project collaboration	6
2 Introduction to the field of p53 research	9
2.1 p53 - The Guardian of the Genome	9
2.1.1 Tumour suppressor tasks	9
2.1.2 p53 in cancers	10
2.1.3 Regulation of p53 by Mdm2	11
2.1.4 MdmX in the p53/Mdm2 system	12
2.2 Observing p53 dynamics	13
2.2.1 Predicting p53 oscillations	14
2.2.2 Observing oscillatory behaviour	14
2.2.3 Stress dependency of p53 response	15
2.2.4 Re-activation of p53	16
2.3 Working with differential equations	17
2.3.1 Overview of dynamical systems theory	17
2.3.2 Introduction of numerical methods	19
3 MdmX inhibition in cancerous MCF7 cells	23
3.1 Experimental setup & goal	23
3.1.1 Collection of data	23
3.1.2 Choice of cell line and resulting comparability	24
3.1.3 Method for inhibition of MdmX	24
3.1.4 Single cell imaging	24
3.2 Characterising the <i>in vitro</i> p53 response to MdmX inhibition	25
3.2.1 Distinguishing cell fates	25
3.2.2 Categorisation of different cell types	26
3.2.3 Separating single cell dynamics	28
3.2.4 Characterisation of steady oscillations	29
3.2.5 Analysis of oscillatory behaviour	31
3.2.6 Phenotype for MdmX inhibition experiment	32

3.3	Summary of presented results	33
4	Design and analysis of mathematical p53 network models	35
4.1	Modelling p53, Mdm2 and MdmX	35
4.1.1	Scope and level of detail	35
4.1.2	Previous p53/Mdm2 models	36
4.1.3	Incorporating MdmX	36
4.2	Designing a mathematical model	37
4.2.1	Purpose of model	37
4.2.2	Processes in network	38
4.2.3	Adding MdmX	38
4.2.4	Emergence of oscillatory behaviour	39
4.2.5	Necessary assumptions	42
4.3	Derivation and analysis of mathematical p53 models	42
4.3.1	Model A	43
4.3.2	Model B	44
4.3.3	Model C	45
4.3.4	Model D	47
4.3.5	Model overview	48
4.4	Summary of presented results	48
5	Numerical investigations of oscillatory behaviour upon parameter perturbations	51
5.1	Standard system simulations	51
5.1.1	Choice of cooperativity	52
5.1.2	Choice of time delay	52
5.1.3	Temporal dynamics of the simulated standard systems	54
5.1.4	Comparison of mean protein levels	54
5.2	Resulting p53 dynamics across different model formulations	55
5.2.1	Analysis of relative amplitude	58
5.2.2	Period of limit cycle oscillations	58
5.2.3	Phase portrait comparison	58
5.2.4	Visualising spikiness through autocorrelation plots	59
5.3	Simulating the MdmX inhibition phenotype	59
5.3.1	Observation of period variations due to parameter perturbations	59
5.3.2	Change in relative amplitude corresponding to period variations	61
5.3.3	Dynamic responses to MdmX inhibition	62
5.4	Summary of presented results	65
6	Discussion	67
6.1	Experimental results	67
6.2	Numerical simulation results	69

7 Conclusion	73
8 Outlook	75
Handout	77
Bibliography	83
Appendices	89
Appendix A	A
Appendix B	B
Appendix C	C
Appendix D	D
Appendix E	E
Appendix F	F
Appendix G	G
Appendix H	H

List of abbreviations & technical terms

In this list, abbreviations will be explained, and, since most readers of this thesis come from the field of physics, some frequently used technical terms from the field of biology are explained briefly.

For the first appearances of terms from this list, the terms will be marked as [term]*, indicating that an explanation can be found in this list.

Apoptosis	Programmed cell death, which is a highly controlled and regulated process.
ATM	Ataxia-telangiectasia mutated protein. A sensor protein that binds to DSB's, thereby transmitting information about DNA damage to p53.
Cell-cycle arrest	A cellular state in which progression in the cell cycle is temporarily halted.
Depletion	As used here, protein depletion describes a total knock-out of a certain protein.
DNA	Deoxyribonucleic acid, a double helix molecule carrying genetic instructions in organisms.
DSB	Double-strand breaks, a kind of DNA damage occurring after γ -radiation, in which both strands in the double helix are damaged.
Expression	In biology, expression concerns the process in which the information of genes is converted into structures such as mRNA and then into proteins.
Immunoblot	Also called western blotting, the term describes an analytical technique for protein detection within biology.

In silico	Pseudo-latin referring to the silicon in computer chips, the term describes experiments that are performed through computer simulation.
In vitro	Meaning <i>In the glass</i> , describing experiments performed on cells outside their biological context.
In vivo	Latin for <i>Within the living</i> , used to describe experiments done on whole, living organisms.
Inhibition	As used here, protein inhibition describes a partial knock-down of a protein.
MCF7	A human breast-cancer line isolated in 1970, acronym for Michigan Cancer Foundation-7.
MdmX	Also known as Mdm4. Mouse double minute 4, protein with high structural similarity to Mdm2.
Mdm2	Mouse double minute 2 homolog, a protein that in humans is decoded by the Mdm2 gene.
Mdm2 mRNA	Mouse double minute 2 messenger ribonucleic acid, single-stranded RNA corresponding to the genetic sequence of the Mdm2 gene.
Mitosis	A part of the cell cycle, in which two new nuclei are formed from the replicated chromosomes of the mother cell.
mRNA	Messenger ribonucleic acid, a molecule used to carry genetic information.
Proliferation	The cellular process by which cells grow and divide into daughter cells.
p53	In humans, the term p53 covers any protein variant encoded by the homologous tumour suppressor gene TP53.
Senescence	Cellular senescence describes the process of termination of cell division.
siRNA	Small interfering RNA, prevents translation of mRNA.
ssDNA	Single-stranded DNA, this DNA damage occurs for UV-radiation, which is known to cross-link DNA bases.
Transcription	The process describing synthesis of a ribonucleic acid.
Translation	The process where mRNA is translated into its corresponding protein form.
Ubiquitin	If ubiquitin is added to a substrate (process called ubiquitination), the substrate can be affected in several ways. In this work, ubiquitination of p53 is considered, in which case p53 is marked for degradation.

Ubiquitin ligase	A protein that can assist the transfer of ubiquitin to a target protein.
UV-radiation	Electromagnetic radiation of which the short-wave UV-radiation damages DNA.
γ-radiation	Electromagnetic radiation with high photon energy emerging from radioactive decay of atomic nuclei.

Introduction

Oscillatory behaviour is found on all scales in our lives: from planetary orbits to seasonal climates, day-night cycles, heart rates and even in single cells in our bodies. The wide variety of scales does not only apply to physical size, but more importantly also to the period of the oscillator, ranging from fractions of a second to many years. In the case of biology, these kind of rhythms have proven to be greatly important to many processes and can have a wide range of effects. For some processes, the oscillations carry vital information, for other processes the oscillations ensure that the mechanisms work in a well-timed manner.

Examples of vital biological oscillators that human life strongly depends on are the oscillations in genetic networks, which are part of the massively complex mechanism in each and every of our cells. During the last years, the importance of studying these genetic oscillators has become increasingly recognised. In 2017, Jeffrey C. Hall, Michael Rosbash and Michael W. Young received the Nobel Prize in Physiology or Medicine “*for their discoveries of molecular mechanisms controlling the circadian rhythm*” (Karolinska Institutet, 2017).

Besides the genetic oscillators following the circadian rhythm, genetic oscillators following ultradian rhythms (period below 24 hours) have recently been in focus, investigating among other things the immune system, the development of embryos and programmed cell death (Tiana *et al.*, 2002; Monk, 2003; Kruse and Jülicher, 2005; Tiana *et al.*, 2007; Mengel *et al.*, 2010).

The work described in this thesis will focus on the last example mentioned above: the genetic oscillator related to programmed cell death. This genetic oscillator has been under heavy investigation for around 20 years now, with the first oscillations predicted in 2000 by Bar-Or *et al.* and observed in single cells by Lahav *et al.* in 2004. The oscillations are believed to occur due to feedback mechanisms between the tumour suppressor protein p53 and its main negative regulators Mdm2 and MdmX. In this thesis, the p53 dynamics in response to inhibition of MdmX will be of specific interest, and both *in vitro* and *in silico* studies will be carried out to investigate the role of MdmX in the regulatory network of p53.

1.1 Outline

Following the current introduction (Chapter 1), this thesis consists of four main parts. First, an introduction to the research field, followed by presentations of results from three different analyses, all concerning the main question investigated in this work:

How does the regulatory network of p53 respond to inhibition of MdmX and how can these responses be explained and understood from mathematical modelling of the network?

The first part (Chapter 2) will introduce p53 and the network that regulates it, focusing mainly on the negative regulators Mdm2 and MdmX. Previous research in the field of single cell observation of p53 dynamics will also be introduced in this chapter. Furthermore, a short introduction to dynamical systems theory and the numerical methods applied in this work will be included.

The results presented in this work will be divided into three categories: experimental results, analytical results and numerical results. In chapter 3, the experimental data from *in vitro* experiments conducted in the Lahav Lab by Alba Jiménez Asins will be introduced and analysed and a phenotype of the dynamical p53 response to inhibition of MdmX will be designed. In chapter 4, four different models used to simulate and study p53 oscillations will be derived and investigated. The numerical analysis following this analytical study will show the results from the *in silico* investigations of the possible effects of MdmX in the regulatory network models describing the p53/Mdm2 system (Chapter 5).

Lastly, a discussion (Chapter 6) concerning both experimental data from the Lahav Lab and the analytical and numerical investigations of the system will lead to some concluding comments (Chapter 7) and an outlook into future perspectives for this work (Chapter 8).

1.2 Project collaboration

The work presented in this thesis is part of a collaboration between the Lahav Lab at Harvard Medical School (Boston, USA) and the Biocomplexity group at the Niels Bohr Institute (Copenhagen, Denmark).

These two groups have previously collaborated successfully, the results of which have been published in the paper „*Inferring Leading Interactions in the p53/Mdm2/Mdmx*

Circuit through Live-Cell Imaging and Modeling“ by Heltberg, Chen, Jiménez, Jambhekar, Jensen, and Lahav (2019). This research opened up for further investigations of MdmX in the p53/Mdm2 network, of which this thesis is one of the results.

To establish the continuation of this collaboration, a meeting was set up between the two groups in November 2020. For this meeting, I had the responsibility of writing a handout, in which the visions and future perspectives of the suggested research were described. In this task, Alba Jiménez Asins contributed in regard to the experimental ideas and possibilities and Mathias Heltberg assisted in developing ideas concerning the mathematical modelling.

The handout presented three main research ideas:

- MdmX inhibition and reaction to parameter variations across models
- Downstream effects on protein production such as p21
- Entraining p53 oscillations to periodic parameter variations

The subject of this thesis is the first of these three points. Data from MdmX inhibition experiments analysed in this work became available after the meeting in November 2020.

Since then, data for the downstream effect experiments and parts of the entrainment experiments have become available in February and May, opening for further investigations into the remaining two research questions.

The handout has been attached to this thesis at the end, see page 77.

Code availability

The entire code produced in this work has been written and run in Python 3.7. All versions of the code including all commits are available on GitHub and can be accessed through this link

https://github.com/livmoretto/MSc_p53_Mdm2_MdmX_inhibition

Figures 2.5, 2.6, 3.1, 3.2, 3.3, 3.4, 3.5, 3.6, 3.7, 3.8, 5.1, 5.2, 5.3, 5.4, 5.5, 5.6, 5.7, 5.8, 5.9, and 5.10 have been produced in Python 3.7.

The rest, figures 2.1, 2.2, 2.3, 2.4, 4.1, 4.2, 4.2, 4.3, and 4.4 have been created with BioRender.com

Introduction to the field of p53 research

In this chapter, the protein p53^{*1} and its main negative regulators Mdm2* and MdmX* will be introduced in Sec. 2.1. Following this, Sec. 2.2 will describe previous experimental findings focusing on p53 dynamics in single cells. Lastly, Sec. 2.3 will introduce some concepts from dynamical systems theory together with the numerical methods applied in this work.

2.1 p53 - The Guardian of the Genome

The tumour suppressor p53 is one of the most well-studied proteins in human history, mostly due to its great importance in regard to development and progression of cancer. The protein acts as a master stress regulator and can initiate a broad range of cellular outcomes in response to different stresses. Following stresses such as DNA* damage, virus infection or hypoxia the triggered outcomes vary depending on the state of the cell. In some cases, a cell cycle arrest* is initiated while for example DNA repair is going on. In other cases, more ultimate fates are triggered, such as apoptosis* and senescence*, see Fig. 2.1 for a schematic overview.

Although p53 has been studied heavily, the mechanisms underlying this cellular *decision-making process* are yet to be fully understood, making this protein a highly interesting target for research aiming at understanding cellular decision-making and control mechanisms.

2.1.1 Tumour suppressor tasks

The ability to prevent damaged cells from proliferating* and thereby contributing to the maintenance of the genetic stability of the cell has given p53 the nickname *The Guardian of the Genome* (Lane, 1992). It is of great importance in the prevention of

¹Indications such as this are made for the first use of terms explained in the list of abbreviations and technical terms, starting on page 1

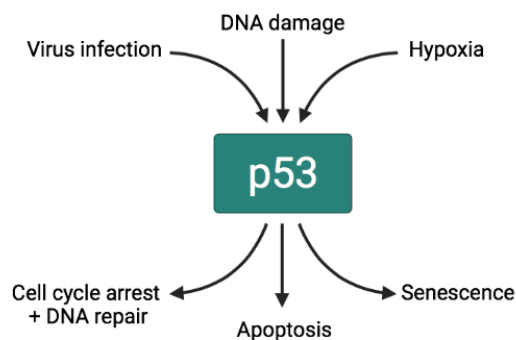


Figure 2.1: Schematic overview of different stresses that can activate p53 and different cellular outcomes that can be triggered.

cancer formation, as damaged cells are more likely to contain mutations that will lead to the development of cancer (Surget *et al.*, 2014).

Various events that also promote cancer cell formation lead to the activation of the p53 protein (Surget *et al.*, 2014). This happens as cellular stresses induce the activation of upstream mediators, which in turn up-regulate p53. Following this, a variety of target genes are activated by p53. The number of target genes that are directly regulated by p53 has been estimated to be over 3600 (Li *et al.*, 2012).

This cascade of activation after cell injury can prevent damaged cells from proliferating. This is very beneficial, as damaged cells more frequently contain mutations that can lead to cancer formation, if the cells are allowed to divide freely. Thereby, p53 plays a crucial role in the *life or death* question for the cell. Understanding how this protein processes input from its upstream activators and forwards this information to its downstream targets is important in understanding how different cell fates arise from different cellular stresses.

2.1.2 p53 in cancers

Several studies have confirmed that p53 mutations have been found in more than 50 % of human cancers (Hollstein *et al.*, 1991; Levine, 1997; Bennett *et al.*, 1999; Vousden and Lu, 2002). As stated by Lane (1992), “*it has become clear that inactivation of its [p53’s, red.] tumour-suppressor activity is an almost universal step in the development of human cancers*”. Loss of p53 activity is usually caused by genetic mutations (Hollstein *et al.*, 1991) and experiments on mice have showed that p53-deficiency leads to tumour development at a very young age (Donehower *et al.*, 1992).

An interesting case shedding light on the importance of a well-functioning p53 network is the Li-Fraumeni syndrome, a rare genetic disorder that predisposes carriers to

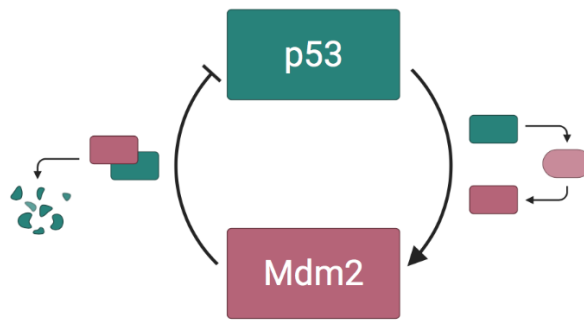


Figure 2.2: Schematic overview of the p53/Mdm2 regulatory system, where p53 stimulates the production of Mdm2, whereas Mdm2 negatively regulates p53 through marking it for degradation. This leads to a negative feedback loop.

cancer development (Li and Fraumeni, 1969). In 1990, Malkin *et al.* showed that patients with this syndrome had inactivating mutations in the p53 gene, explaining the unusually high frequency of cancer cases among these patients.

As p53, a cellular defence mechanism, seems to be deactivated or lost in cancerous cells, understanding the functionality of this protein gives rise to an interesting question in terms of cancer recovery: Could the function of p53 be restored in cancerous cells?

2.1.3 Regulation of p53 by Mdm2

To understand which mechanisms could potentially reactivate the function of p53, the regulatory networks of p53 have to be analysed first. Of these complex networks, the regulatory network between p53 and the protein Mdm2 is of great importance.

In the p53/Mdm2 network, p53 positively regulates the expression* of the Mdm2 gene, of which the protein product, Mdm2, in turn acts as a negative regulator of p53 itself, first described by Momand *et al.* (1992). This is done in two ways: as Mdm2 binds to p53, it decreases its transcriptional* functions, and additionally, Mdm2 functions as an ubiquitin ligase*, marking p53 for degradation (Wu *et al.*, 1993; Kubbutat *et al.*, 1997). This results in a negative feedback loop that contributes to keeping p53 levels low in unstressed conditions as well as terminating the triggered response fast as soon as the p53-activating stress has been resolved (Bar-Or *et al.*, 2000). In addition to degrading p53, Mdm2 also experiences auto-degradation (Fang *et al.*, 2000). The main interactions between p53 and Mdm2 can be seen in Fig. 2.2.

This feedback mechanism is important in order to maintain the correct levels of p53. This is crucial for cells, as too little p53 can allow cancers to form and too much p53

can be lethal for the cells. In fact, experiments on mice have shown that mice deficient of Mdm2 exhibit early embryonal lethality, whereas mice deficient of *both* Mdm2 and p53 develop normally (Jones *et al.*, 1995).

2.1.4 MdmX in the p53/Mdm2 system

Mdmx was discovered a few years after Mdm2 as a p53-associated protein with a “*structural similarity to Mdm2, which is especially notable in the p53-binding domain*” (Shvarts *et al.*, 1996). Due to this similarity to Mdm2, MdmX (also known as Mdm4) is thought to play a role in the regulation of p53 together with Mdm2.

As reported for Mdm2, experiments in mice have shown embryonic lethality for mice with deleted MdmX, while this lethality is rescued after additional deletion of p53 (Parant *et al.*, 2001; Migliorini *et al.*, 2002). Considering that both the deletion of Mdm2 and MdmX lead to embryonic lethality independently, these results indicate non-overlapping functions of Mdm2 and MdmX during early embryonic development and raise the question how MdmX enters the p53/Mdm2 system.

The p53 binding pocket of MdmX is nearly identical to that of Mdm2 (Böttger *et al.*, 1999) and it has been shown that MdmX is able to bind to p53. Jackson and Berberich (2000) have shown that MdmX is “*unable to facilitate nuclear export or induce p53 degradation*”. Furthermore, their investigation yielded that “*expression of MdmX can reverse Mdm2-targeted degradation of p53 while maintaining suppression of p53 transactivation*” (*ibid.*). Although MdmX can not facilitate nuclear export of p53, it has been suggested that MdmX might modulate the Mdm2 driven translocation of p53 from the nucleus to the cytoplasm, resulting in lower p53 transcriptional activity (Wade *et al.*, 2010). As stated by Toledo *et al.* (2006), it seems that “*MdmX regulates p53 activity, while Mdm2 mainly controls p53 stability*”, describing the synergistic nature of the relation between Mdm2 and MdmX.

Contrary to the findings of Jackson and Berberich (2000), Linares *et al.* (2003) have reported that MdmX stimulates Mdm2-mediated ubiquitination* of p53 and that MdmX and Mdm2 facilitate the ubiquitination of each other. They postulate that MdmX might work as a “*stimulator, rather than as an inhibitor*” concerning the degradation activity of Mdm2, and that MdmX is actively involved in the degradation of both Mdm2 and p53 under certain conditions. As this is not in agreement with the results of Jackson and Berberich (2000), it is important to consider any dependencies on cell type and state (Stewart-Ornstein and Lahav, 2017).

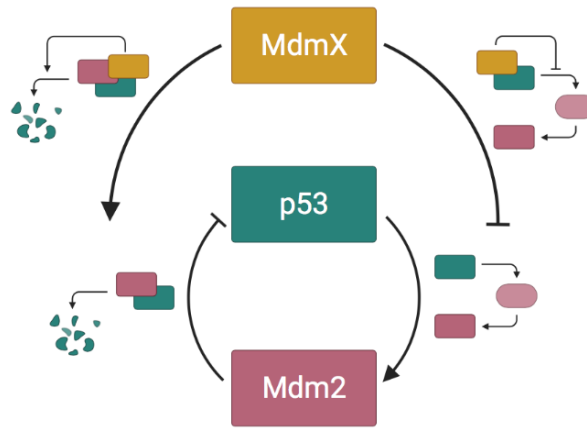


Figure 2.3: Schematic overview of the possible effects of MdmX on the p53/Mdm2 regulatory system. It is proposed that MdmX either enhances degradation of p53 through the complex formation process or that MdmX inhibits the transcriptional activity of p53.

Another important difference between Mdm2 and MdmX is that Mdm2 gene expression is regulated by the amount of p53, whereas expression of the MdmX gene is p53-independent (Shvarts *et al.*, 1996).

The proposed effects of MdmX in the p53/Mdm2 network from Fig. 2.2 are illustrated in Fig. 2.3.

While Mdm2 and MdmX appear to have similar structures, they are both believed to hold important roles in p53 regulation, as none of the two can compensate for the loss of the other (Marine *et al.*, 2006). Additionally, many human cancers express high levels of either Mdm2, MdmX or both (Wasylishen and Lozano, 2016). As the above review of some of the findings concerning MdmX and Mdm2 demonstrates, the network regulating p53 is complex. The exact role of MdmX in the network is the main target of this work.

2.2 Observing p53 dynamics

A way to gain information about the regulatory network of p53 is by analysing p53 levels in cells that undergo different cellular stresses. Several experiments have focused on these p53 reactions to stress, some of which will be presented here.

In 2004, Lahav *et al.* introduced a method for observation of p53 dynamics in single cells. The method uses time-lapse fluorescence microscopy to measure the concentrations of p53 and Mdm2. The approach has achieved great success, since it allows observations of temporal dynamics in single cells, that would often be smeared out by

using immunoblots*, where signals are averaged over cell populations. Most of the results described here have been obtained by using the method introduced by Lahav *et al.* to observe p53 dynamics.

2.2.1 Predicting p53 oscillations

The first mathematical model describing the feedback mechanism between p53 and Mdm2 was presented by Bar-Or *et al.* in 2000. The network consisted of the p53 protein, an intermediary (such as Mdm2 mRNA*) and the Mdm2 protein. In their “*attempt to capture the gross mechanisms of p53-Mdm2 interactions as presently known*” (ibid.), they varied the different parameters in the model, interested in the resulting behaviour of the system.

In their model, the introduction of stress was assumed to affect the transcriptional activities of p53 positively and the degradation of p53 negatively, resulting in a large expression of p53 in response to cellular stress. As this stress response was modelled mathematically, oscillatory behaviour of the level of p53 was observed for stress signals above a certain threshold.

This mathematical prediction was investigated experimentally by exposing cells to ionising radiation, causing double-strand breaks (DSBs*) in the DNA, thereby triggering the cellular stress response system. Oscillations with a period of around 3-4 hours were observed in two different cell types, confirming the theoretically predicted behaviour of p53 after severe DNA damage. These kind of oscillations are illustrated in Fig. 2.4a.

2.2.2 Observing oscillatory behaviour

Observations from single cells revealed a series of pulses in p53 levels over the course of 16 hours post-irradiation (Lahav *et al.*, 2004). Shortly after these results, Geva-Zatorsky *et al.* (2006) reported p53 dynamics observed over the course of several days. In many of the tracked cells, sustained, undamped oscillations could be observed for at least 3 days after γ -irradiation.

In the investigations by Bar-Or *et al.* (2000), Lahav *et al.* (2004), and Geva-Zatorsky *et al.* (2006), observations came from *in vitro** experiments. In addition to these, Hamstra *et al.* (2006) showed that p53 oscillations could be observed *in vivo**. The *in vivo* experiments were done by exposing mice to total body irradiation and observing p53 by bio-luminescent imaging. Hamstra *et al.* reported that “*a distinct oscillatory pattern was observed in radiated mice that was not present in unirradiated control*”.

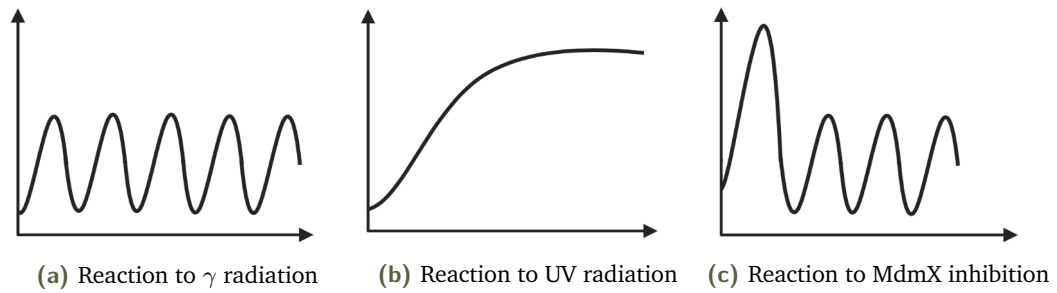


Figure 2.4: The dynamical reaction of p53 levels to different kinds of stresses. The illustrated reactions are caused by (a) γ -irradiation, (b) UV radiation, and (c) MdmX inhibition. For all three plots, p53 concentration is shown on the y -axis and time on the x -axis.

2.2.3 Stress dependency of p53 response

Knowing that γ -irradiation* can trigger oscillatory p53 responses, it is interesting to investigate if the dynamics of p53 response differ between various kinds of cellular stresses.

Using mathematical modelling, Hunziker *et al.* (2010) showed that even a simple negative feedback model was sufficient to trigger different dynamics in the response of the p53/Mdm2 system to different stresses, modelled by varying specific parameters in the model. They computationally investigated the response to cellular stresses such as DNA damage, hypoxia, and introduction of different chemicals.

As DNA damage can happen in several ways, an *in vitro* study by Batchelor *et al.* (2011) aimed at investigating dynamical differences between cells that were irradiated with γ -irradiation and UV-radiation*. Where γ -irradiation causes DSBs, UV-radiation is known to cross-link bases leading to the exposure of single-stranded DNA (ssDNA*). The paper showed that the response of p53 to these two different types of DNA damage was dynamically different. DSBs resulted in oscillations with amplitude, duration, and frequency independent on damage dose (Fig. 2.4a), whereas increased ssDNA damage dose increased both the amplitude and the duration of a single pulse p53 response (Fig. 2.4b). This study is an example of the way that p53 transmits distinct signals by reacting differently to various cellular stresses.

The various p53 dynamics resulting from γ and UV radiation of the cells, leading to distinct cellular outcomes, were further investigated by Purvis *et al.* (2012). In their study, the goal was to alter the dynamics of p53 after γ -irradiation by using the small molecule inhibitor of Mdm2 Nutlin-3 (Vassilev *et al.*, 2004). By adding Nutlin-3 in specific intervals, they succeeded altering the p53 dynamics after γ -irradiation to imitate the dynamics after UV radiation (thus changing the dynamics from the kind illustrated in Fig. 2.4a to the one shown in Fig. 2.4b). Thereby, this study was

meant to investigate if the p53 dynamics carry the main responsibility in terms of cellular outcomes after γ or UV radiation, or if the reaction is additionally controlled by p53-independent events in the cell. The investigation yielded that cells undergoing stress from DSBs caused by γ -irradiation resulted in oscillatory responses and DNA repair, while the cells with altered p53 dynamics underwent senescence. Interestingly, cells exposed to UV radiation show the same dynamics as the altered signal in the γ -radiation experiments, but often the response leads to apoptosis in this case, suggesting that p53 is not the only factor in this cellular decision-making.

2.2.4 Re-activation of p53

A multitude of cancers have been shown to over-express either Mdm2, MdmX or both (Wasylishen and Lozano, 2016). Over-expression of MdmX alone has been reported in around 20 % of human cancers (Toledo and Wahl, 2007). As down-regulation of one or both of these two p53 partners might trigger the reactivation of p53, this is an interesting target for research in terms of new approaches within cancer treatment (Hu *et al.*, 2006; Wang *et al.*, 2011; Haupt *et al.*, 2015; Chen *et al.*, 2016).

After depletion* of MdmX, p53 has been shown to exhibit biphasic behaviour: “*During the first phase, cells show a high-amplitude p53 pulse, and during the second phase, cells experience low-amplitude p53 oscillations*” (Chen *et al.*, 2016). This behaviour is illustrated in Fig. 2.4c. The steady oscillations of the second phase resemble oscillations observed after DSB causing DNA damage in both shape and frequency. This could indicate that the same mechanism is causing both kind of oscillations, but oscillations after MdmX depletion have been shown to not result from activation of the DNA damage signalling pathway. As Kawai *et al.* (2003) showed that MdmX levels are decreased in response to DSBs, it is theorised that a lowered level of MdmX is required for oscillatory behaviour of p53.

Chen *et al.* (2016) furthermore showed that DNA damage during the first phase of the reaction to MdmX depletion promoted apoptosis, while DNA damage during the second phase promoted cell-cycle arrest. Where DNA damage alone caused 66 % cell deaths in normal cells, the number in MdmX-depleted cells went up to 95 % when DNA damage happened during the first phase and down to 16 % when it happened during the second phase. These results indicate the importance of the temporal dynamics of p53 for cellular survival. As several approaches to cancer treatment combine medicines with radiation therapy, these findings motivate a deeper understanding of the dynamical behaviour of p53.

The molecular mechanism causing the biphasic response to depletion of MdmX in otherwise unstressed cells has been further investigated by Heltberg *et al.* (2019). Previous studies have shown that MdmX can interact with the p53/Mdm2 system by either increasing the degradation of p53 (Linares *et al.*, 2003) or by decreasing the transcriptional activity of p53 (Böttger *et al.*, 1999) (see Sec. 2.1.4). Using mathematical modelling, Heltberg *et al.* (2019) investigated how these interactions could explain the biphasic response of p53 to MdmX depletion. To do this, MdmX was incorporated into a minimal mathematical model describing the p53/Mdm2 system through the introduction of impact factors. The response of the system to *in silico**depletion of MdmX was analysed and the effect of MdmX on the degradation of p53 was concluded to be critical for the generation of the biphasic behaviour after MdmX depletion.

2.3 Working with differential equations

The models simulating the regulatory network of p53 presented in this work are systems of differential equations. To analyse these models, both analytical and numerical methods will be applied, and a brief sketch of the technical aspects of these approaches will be explained in the following sections.

2.3.1 Overview of dynamical systems theory

The core idea behind dynamical systems theory is to design a framework that allows analysis of a system's evolution in time. Especially characterisation of the long-term behaviour such as steady or oscillatory dynamics are of interest in these types of analyses.

In general terms, ordinary differential equations can be described by a set of equations

$$\begin{aligned}\dot{x}_1 &= f_1(x_1, \dots, x_n) \\ &\vdots \\ \dot{x}_n &= f_n(x_1, \dots, x_n)\end{aligned}$$

In this formulation, \dot{x} denotes the differentiation of x with respect to time t . In this work, the variables x_1, \dots, x_n represent the different parts of the regulatory network of p53, such as p53 and Mdm2.

For most systems, it is not possible to solve for these variables analytically, but a lot of information can be gained from considering the qualitative behaviour of the system. These kind of analytical considerations can lead to visualising the system in a *phase portrait*. From this, it can be observed if there are fixed points x^* ($f(x^*) = 0$) or limit cycles of length $T > 0$ ($x(t + T) = x(t)$) present for the system, illustrating equilibrium and periodic solutions, respectively.

The stability of a fixed point can be classified through linear stability analysis. One can consider some two-dimensional system

$$\begin{aligned}\dot{x} &= f(x, y) \\ \dot{y} &= g(x, y)\end{aligned}$$

The fixed points can be described as $f(x^*, y^*) = 0$ and $g(x^*, y^*) = 0$. Introducing small disturbances around these points as $u = x - x^*$ and $v = y - y^*$ now allows for Taylor expansion around these fixed points (Strogatz, 2016)

$$\begin{aligned}\dot{u} &= u \frac{\partial f}{\partial x} + v \frac{\partial f}{\partial y} + O(u^2, v^2, uv) \\ \dot{v} &= u \frac{\partial g}{\partial x} + v \frac{\partial g}{\partial y} + O(u^2, v^2, uv)\end{aligned}$$

Hence, the perturbations around the fixed point results in disturbances according to

$$\begin{aligned}\begin{pmatrix} \dot{u} \\ \dot{v} \end{pmatrix} &= \begin{pmatrix} \frac{\partial f}{\partial x} & \frac{\partial f}{\partial y} \\ \frac{\partial g}{\partial x} & \frac{\partial g}{\partial y} \end{pmatrix} \begin{pmatrix} u \\ v \end{pmatrix} + O(u^2, v^2, uv) \\ &= A \begin{pmatrix} u \\ v \end{pmatrix} + O(u^2, v^2, uv)\end{aligned}$$

In this linearized system, the matrix A is called the *Jacobian matrix* at the fixed point (x^*, y^*) . When characterising the stability of a fixed point, it is sufficient to analyse the trace and determinant of the Jacobian.

For most systems, the phase portrait can change as parameters are varied in the system. Some parameter variations only create small changes in the phase portrait, whereas others result in drastic responses. For the latter kind, the system is said to have gone through a bifurcation. In this process, fixed points and limit cycles can appear or disappear in the system, or the stability of these can change.

A helpful tool for analysis of periodic signals is the Poincaré map. For a n -dimensional system of equations, a Poincaré map is a $(n - 1)$ -dimensional surface through which the flow is travelling. For periodic signals, the Poincaré mapping yields a fixed point, where x^* returns to its value after some period T . This mapping indicates a closed

orbit for the system, whereby detection of closed orbits can be simplified to detection of fixed points of the mapping.

2.3.2 Introduction of numerical methods

The fourth order Runge-Kutta method, known also as RK4, is a widely used iterative method for solving differential equations. Incrementing the time t , by a step of Δt , the value of a given function $\dot{y} = f(t, y)$ is given at the next time step $t + \Delta t$ by

$$y_{t+\Delta t} = y_t + \frac{1}{6}\Delta t(k_1 + k_2 + k_3 + k_4)$$

In this formula, the slopes at different points (k_1 , k_2 , k_3 and k_4) are defined as

$$\begin{aligned} k_1 &= f(t, y_t) \\ k_2 &= f\left(t + \frac{\Delta t}{2}, y_t + \Delta t \frac{k_1}{2}\right) \\ k_3 &= f\left(t + \frac{\Delta t}{2}, y_t + \Delta t \frac{k_2}{2}\right) \\ k_4 &= f(t + \Delta t, y_t + \Delta t k_3) \end{aligned}$$

In the solution, $y_{t+\Delta t}$ is the Runge-Kutta approximation of the value $y(t + \Delta t)$ and is calculated from the preceding value y_t and a weighted average of four different slopes around the point.

It is of interest to be able to classify the dynamics resulting from numerically solving the differential equations that represent the models. For this purpose, a step-wise solver using Poincare lines to analyse the dynamical behaviour of the systems has been designed as part of this work.

A Poincare line is a one-dimensional Poincare map, which is useful to analyse oscillating dynamic systems. Using this Poincare map it is possible to analyse closed orbits as fixed points of the mapping, as the shape of the trajectory is mapped to the intersection points on the Poincare map. If these intersections are found at the same point after a period T , the analysed trajectory must be a closed orbit (Strogatz, 2016).

Two examples of this are shown in Fig. 2.5, figure (a) showing a damped oscillation reaching a fixed point (intersections shown in red) and figure (b) showing a limit cycle as it is reached from the outside (red intersections) and the inside (blue intersections) of the limit cycle.

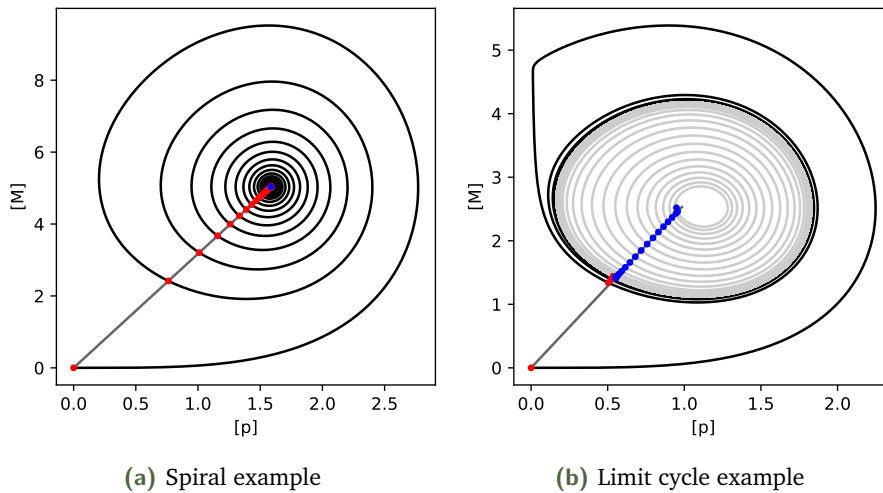


Figure 2.5: Illustration of Poincaré intersection mappings with the concentration of p53 on the x-axis and the concentration of Mdm2 on the y-axis. Figure (a) shows a damped oscillation, where the intersections of the trajectory and the Poincaré line are shown in red. Figure (b) shows a limit cycle as it is reached from the outside (intersections are shown in red) and from the inside (intersections shown in blue).

The characteristics of the dynamical behaviour can be found from analysing the intersections with the Poincaré line. If these intersections are found to happen at different points along the line, the system is spiralling towards a steady state. If the intersections on the other hand happen at the same points on the Poincaré line, the system is in steady state, yielding either a fixed point or a limit cycle.

Calculating the ratio between the intersection values p_{cross} and the mean of the values between intersections p_{final} allows classification of the system, as the logarithm of this value will approach zero for fixed points and a non-zero value for limit cycles, as can be seen from Fig. 2.6.

To avoid stopping the simulation before a steady state is reached or continuing simulation long after it is reached, a step-wise solver is designed. For this, the system is solved for time steps of T_{int} and the dynamics are analysed after each time step. If a steady state is reached, the simulation is stopped, but if no steady state is reached yet, the simulation is continued for another interval of length T_{int} .

This is also visible in Fig. 2.6, where the time interval has been set to $T_{\text{int}} = 50$. Small discontinuities can be seen as new intervals of simulation are started, as the values of p_{final} are narrowed down for each repetition.

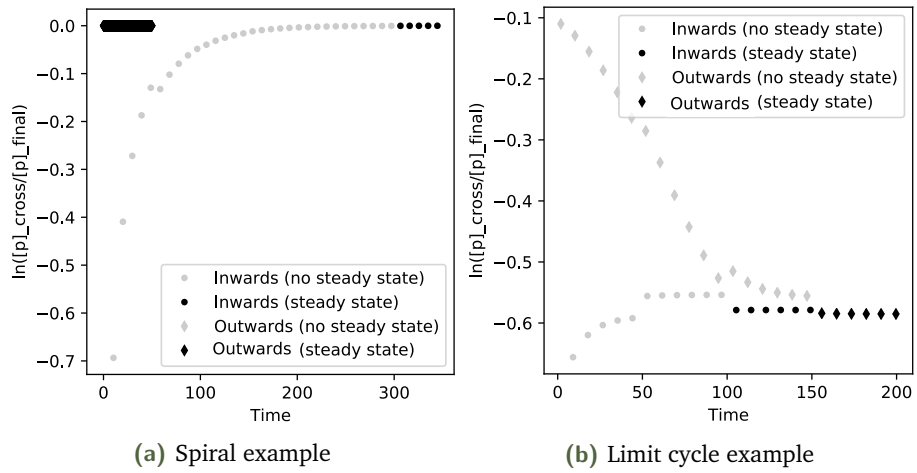


Figure 2.6: Steady state analysis for same systems as presented in Fig. 2.5. As long as the system is not in steady state, the logarithm of the ratio is marked in grey. When a steady state is detected, this changes to black. For the spiral towards a fixed point in figure (a), the final value approaches zero. For the limit cycle case in figure (b), the final value is non-zero.

MdmX inhibition in cancerous MCF7 cells

In this chapter, the first part, Sec. 3.1, will focus on the experimental setup. The second part, Sec. 3.2, contains the analysis of the experimental data, presentation of the main results, and lastly the introduction of a phenotype describing the experimental findings in short. At the end of this chapter, Sec. 3.3 will briefly summarise the results obtained through the chapter.

3.1 Experimental setup & goal

Depletion of MdmX leads to biphasic behaviour in terms of p53 dynamics, where the first phase exhibits a large pulse and the second phase exhibits steady oscillations in the p53 level (Chen *et al.*, 2016). *In silico* investigation of the p53/Mdm2 system has successfully simulated the observed dynamics after MdmX depletion (Heltberg *et al.*, 2019).

A natural next step after these investigations of MdmX depletion is the investigation of partial MdmX inhibition*, where MdmX is not fully removed from the system, but the amount is decreased. The goal of the experiment described and analysed in this chapter is to investigate such a partial inhibition of MdmX at different strengths.

3.1.1 Collection of data

The data analysed in this chapter has been kindly provided by Alba Jiménez Asins from the Lahav Lab, who has designed and conducted the experiments. As this work focuses on the results of these experiments and the computational investigation hereof, there will only be a brief description of the experimental setup here.

3.1.2 Choice of cell line and resulting comparability

The dynamics of p53 have been shown to vary across different species (Stewart-Ornstein *et al.*, 2017), different tissues in mice (Stewart-Ornstein *et al.*, 2021), and different human cell lines (Stewart-Ornstein and Lahav, 2017). Therefore, the choice of cells for the experiment is an important factor regarding comparability to other studies.

For the experiment analysed here, human breast cancer MCF7* cells are investigated, which have also been used by Bar-Or *et al.* (2000), Lahav *et al.* (2004), Geva-Zatorsky *et al.* (2006), Loewer *et al.* (2010), Batchelor *et al.* (2011), Purvis *et al.* (2012), Haupt *et al.* (2015), Chen *et al.* (2016), Stewart-Ornstein *et al.* (2017), and Heltberg *et al.* (2019), enabling a comparison of the results of this experiment to most of the results described in the previous chapter. The clonal MCF7 cells used in this experiment express a fluorescently tagged p53, which enables observation of the protein levels.

3.1.3 Method for inhibition of MdmX

In the previous MdmX depletion investigations, small interfering RNA (siRNA*) has been used for MdmX depletion. In the experiments described here, small interfering molecules have been used instead to inhibit MdmX with different strengths.

3.1.4 Single cell imaging

The cells for this experiment are grown for two days in glass-bottom plates before the imaging is started. For the measurements, a Nikon Eclipse TE-2000 inverted microscope with a Hamamatsu Orca ER camera is used. The entire experiment is conducted in an environmental chamber that controls the temperature, atmosphere, and humidity during the experiment. As six different conditions are investigated in this experiment, six different glass-bottom plates are used during the experiment. The experiment has been conducted twice, and the full data set analysed in this chapter consists of the combined data from both experimental runs.

Measurements are taken each 15 minutes over the course of 48 hours in total by measuring the light intensity from each of the six groups, indicating the amounts of fluorescently tagged p53. After this, the video is analysed by tracking the light intensity from single cells in each group.

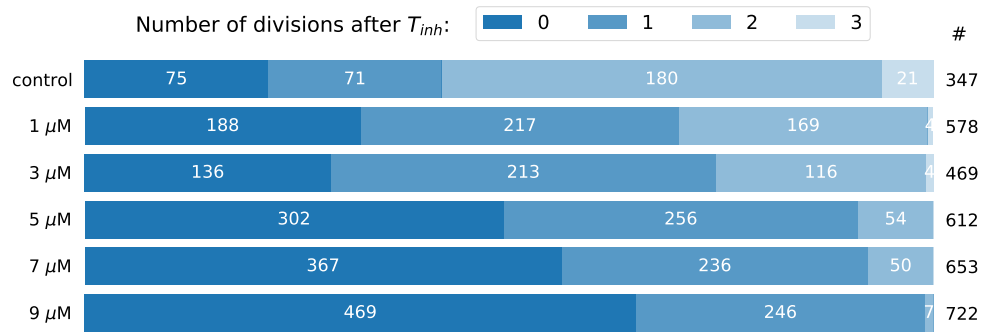


Figure 3.1: Number of cell divisions after time of MdmX inhibition (T_{inh}) for the six different groups of cells. The number of divisions is illustrated by colour and the total number of cells in each group is shown to the right in black.

3.2 Characterising the *in vitro* p53 response to MdmX inhibition

A total of 3381 cells from six groups have been tracked in the experiment. The six groups are: groups with concentrations of MdmX inhibitor of 1 μM , 3 μM , 5 μM , 7 μM , and 9 μM and a control group with no inhibition. For the rest of this work, these will be referred to as *inhibition strength 1, 3, 5, 7, and 9*.

3.2.1 Distinguishing cell fates

The dynamics of p53 have been closely related to cellular fate decisions (Purvis *et al.*, 2012). This makes the proliferation rates of the cells a good target for investigating the effects of MdmX inhibition, as these are an expression of the cellular fate decisions. The cell-cycle length of MCF7 cells is around 25 hours (Chen *et al.*, 2016), hence a standard of two divisions is expected for the non-stressed cells during the experiment of 48 hours duration.

The number of divisions during the time of the experiment are illustrated in Fig. 3.1. As expected, most of the control cells (52 %) divide two times during the experiment, whereas 26.5 % of the cells divide 1 or 3 times and 21.5 % do not divide during the course of the experiment. These numbers change quite drastically when MdmX is inhibited. For the weaker inhibitions of MdmX, most of the cells only divide once. This can be seen for the inhibition strengths 1 and 3, for which 38 % and 45 % of the observed cells divide once only, respectively. For stronger inhibition, the majority of the cells do not divide during the course of the experiment, with non-dividing cells making up 49 % for inhibition strength 5, 56 % for inhibition strength 7, and 65 % of all cells for inhibition strength 9.

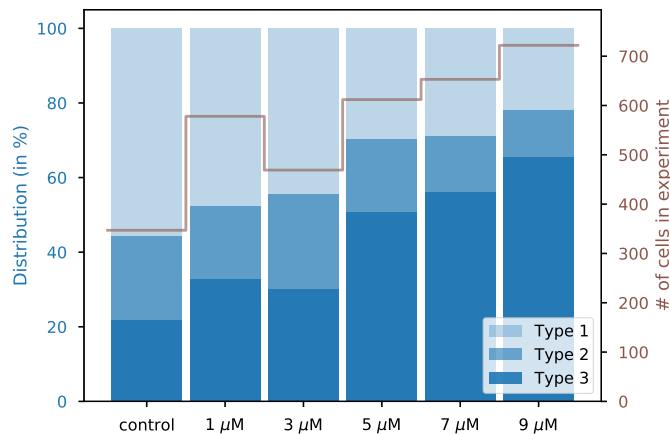


Figure 3.2: Distribution of type 1, type 2 and type 3 cells for the control group and different inhibition strengths. As can be seen from this figure, the fraction of cells belonging to type 1 goes down as the inhibition strength goes up. The total number of cells for each inhibition strength is indicated on the y-axis on the right-hand side of the plot.

Where 52 % of all cells divided twice in the group of control cells, this number gradually decreases to 29 %, 25 %, 9 %, 8 %, and finally 1 %, as inhibition strength goes up. This trend is a clear indicator that the inhibition of MdmX affects mechanisms that assist cellular decision-making.

3.2.2 Categorisation of different cell types

Considering that cell proliferation changes as MdmX is inhibited, the dynamical behaviour of cells with different proliferation rates is an interesting target for further investigation. To enable systematic analysis of the differences between dividing and non-dividing cells, the cells are categorised into three different types:

- Type 1** Cells divide at least once and the first division happens within the first 15 hours after MdmX inhibition
- Type 2** Cells of type 2 divide at least once, but for these cells the first division happens more than 15 hours after inhibition of MdmX
- Type 3** Type 3 cells do not divide during the course of the experiment

Using these classification rules, the distribution of type 1, 2, and 3 cells can be seen for the six different groups in Fig. 3.2. The distribution shows that the number of type 1 and 2 cells goes down as inhibition strength goes up, leaving the majority of cells for inhibition strengths 5, 7, and 9 being of the non-dividing type 3, as can also be seen from Fig. 3.1.

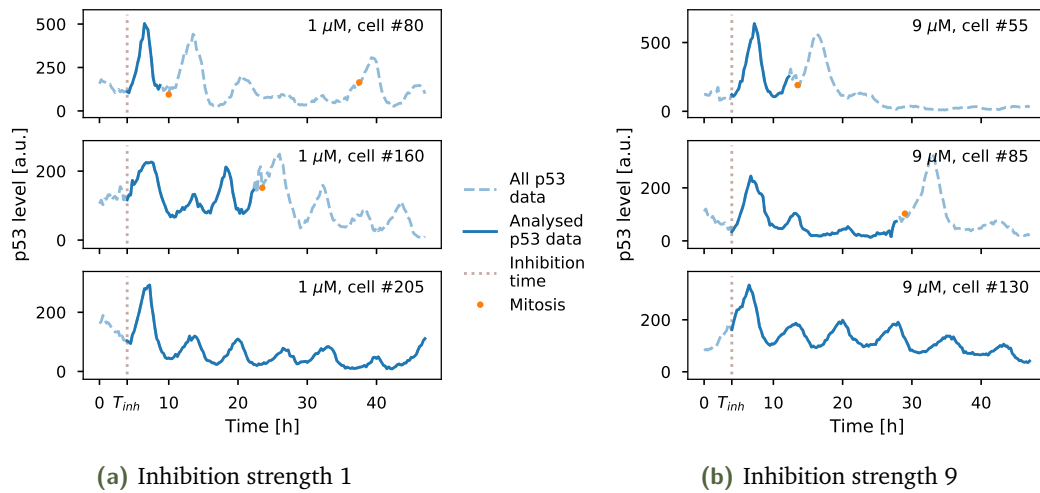


Figure 3.3: Examples of temporal dynamics in p53 levels for type 1 (upper panels), type 2 (middle panels) and type 3 (lower panels) cells. Plot (a) shows examples for inhibition strength 1 and plot (b) for inhibition strength 9. All the sampled data is indicated as dashed blue line and the part of the data used for analysis is shown in solid blue line. The experimental data shown in this plot is unpublished data from the Lahav Lab at Harvard Medical School.

Examples of single cell traces for the different types of cells can be seen in Fig. 3.3 for inhibition strengths 1 and 9 (see App. A for other inhibition strengths). As has previously been described for MdmX depletion by Chen *et al.* (2016) and Heltberg *et al.* (2019), a biphasic p53 response can be observed after MdmX inhibition for all strengths of inhibition.

A large peak can be observed for all cells immediately after inhibition of MdmX and taking a closer look at the type 1 and 2 cells, another large peak can be observed in relation to cell division right after mitosis*, as expected from investigations by Loewer *et al.* (2010). For cells of type 2 and 3 the second phase of the biphasic response to MdmX inhibition can be observed as steady p53 oscillations at lower levels compared to the first phase (Chen *et al.*, 2016; Heltberg *et al.*, 2019).

The main point of interest of this work is the biphasic response of p53 dynamics to inhibition of MdmX. Since cell division interferes with this dynamical response by stimulating a post-mitotic pulse in p53 levels, the dynamics after cell division will not be considered in the following analyses and only the data marked with solid blue lines in Fig. 3.3 will be analysed.

Since the analysed data for type 1 cells will always be shorter than 15 hours of observation, the data from these cells is considered insufficient in terms of analysing the biphasic behaviour. Consequently, only type 2 and 3 cells will be considered in the next analyses.

3.2.3 Separating single cell dynamics

Some of the cells in the experiment show dynamics that are vastly different to the expected biphasic behaviour after inhibition of MdmX. Examples can be seen in the upper panels of Fig. 3.4 (see App. B for other inhibition strengths). These cells will act as a source of noise in the further analyses of the biphasic p53 response and it is therefore desirable to sort out these traces.

For this task, an algorithm has been designed as part of this work to classify traces into the categories *oscillating* and *non-oscillating*. First, high frequency noise is smoothed out by using the running average as a simple low-pass filter. Then, peaks are detected in the data, making it possible to cut away the first big pulse for each trace, thereby only analysing phase 2 of the response. The phase 2 data is zero-padded to length 2^{11} followed by Fourier transformation to obtain the spectrum in frequency space, where the zero-padding ensures the same spectral resolution for all cells. Lastly, all type 2 and 3 cells are assumed to exhibit oscillatory behaviour with a period equal to the location of the highest peak in the power spectrum.

Cells to which any of the points below apply are classified as *non-oscillatory*:

- Several main periods** If the second-highest peak in the power spectrum is above 90 % of the highest peak in intensity, a single main period is not detectable and the cell is classified as non-oscillatory.
- Too short phase 2** If there are less than 8 hours of phase 2 data, the cell is classified as non-oscillatory, as this is too little to analyse oscillatory behaviour with the expected period of around 5.5 hours.
- Main period too high** If the main period detected is above 10 hours, the cell is classified as non-oscillatory, as low-frequency oscillations are expected to stem from systematic noise such as the slow decay of fluorescence in the system.
- Main period too low** If the main period detected is below 2 hours, the cell is classified as non-oscillatory, as high-frequency oscillations stem from noise in the system or in the signal, making these traces unfit for analysis.

Looking at the distribution of oscillating and non-oscillating cells as classified by this algorithm in Fig. 3.5, it does not seem as if the inhibition strength has an impact on the fraction of oscillating cells compared to non-oscillating cells. Therefore, the non-oscillating behaviour can be attributed to systematic noise in the experiment, and

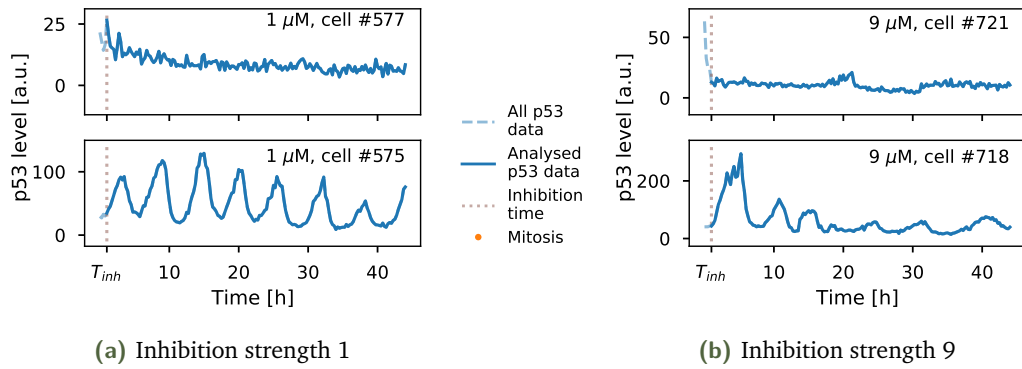


Figure 3.4: Examples of non-oscillating (upper panels) and oscillating cells (lower panels) for inhibition strengths 1 in figure (a) and 9 in figure (b). The experimental data shown in this plot is unpublished data from the Lahav Lab at Harvard Medical School.

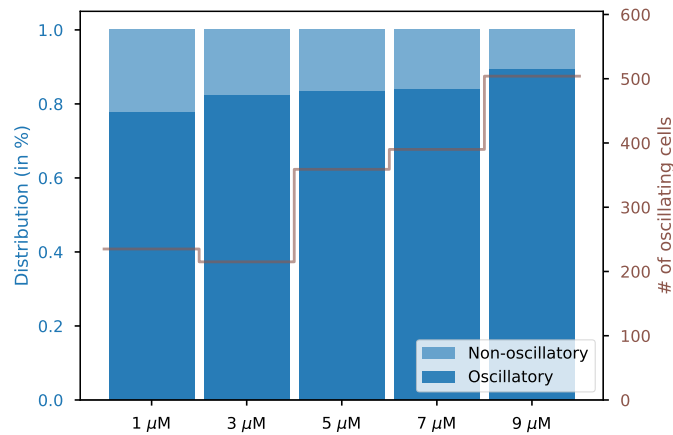


Figure 3.5: Distribution of oscillating and non-oscillating cells across the different inhibition strengths. Seemingly, the inhibition strength does not have an influence on the distribution of oscillating and non-oscillating cells. Note that fewer cells are analysed for low inhibition strengths compared to high inhibition strengths, since only type 2 and type 3 cells are analysed (according to Fig. 3.2).

the non-oscillating cells will not be considered in further analyses. Since only cells of type 2 and 3 are considered, the amount of cells analysed for low inhibition strength is lower than for high inhibition strength, which is indicated on the right-hand side axis.

3.2.4 Characterisation of steady oscillations

In the case of MdmX inhibition, the system transitions from one state *before* to another state *after* the inhibition of MdmX. Steady oscillations can be observed in the second phase of the reaction to MdmX inhibition, indicating that the system has entered the Hopf bifurcation, transitioning from a fixed point to a limit cycle. As such, the first phase can be thought of as a transient phase that the system undergoes to reach the

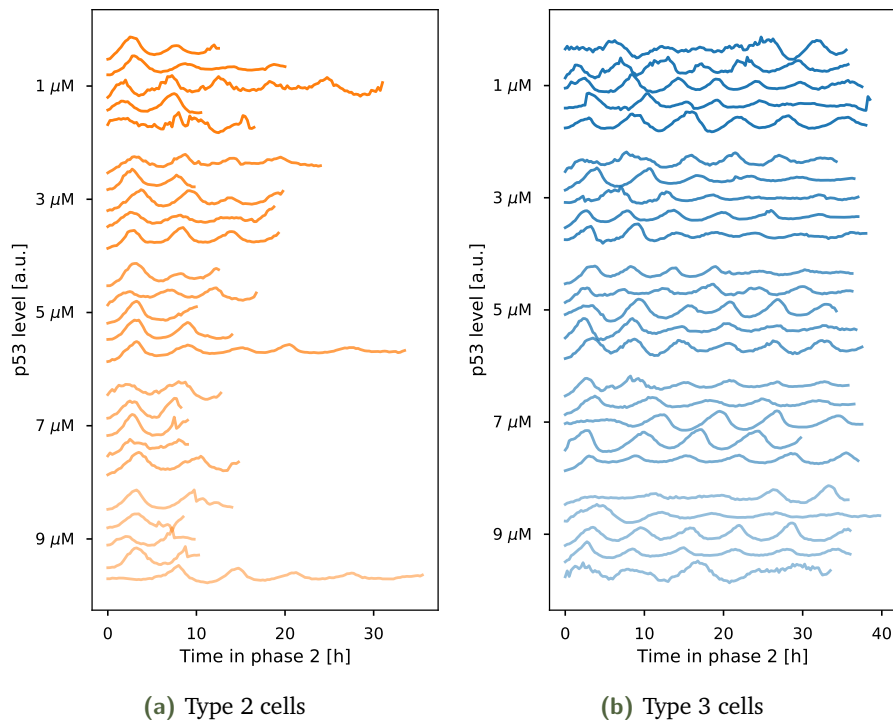


Figure 3.6: Phase 2 oscillatory dynamics for randomly selected cells for each inhibition strength. Figure (a) shows type 2 cells and figure (b) shows type 3 cells. The length of each trace differs, as the beginning is defined as the valley after the big phase 1 peak and the end is defined depending on the type of cell considered. The experimental data shown in this plot is unpublished data from the Lahav Lab at Harvard Medical School.

limit cycle. For the numerical investigations following later in this work the limit cycle oscillations observed in phase 2 will be of main interest.

In Fig. 3.6, the phase 2 oscillations are shown for some randomly selected cells for each inhibition strength. Here, time is set to zero at the end of the big phase 1 pulse, thereby aligning the phase 2 traces from all the cells. Analysing the illustrated traces, it is clear that there are slight differences in the oscillatory phases of the different traces across the cells within each group.

To analyse the level of coherence between the oscillations, a practical approach is to analyse the autocorrelation of the traces. For this analysis, each trace is compared to itself as a function of time. For oscillatory signals, the temporal dynamics repeat in intervals of the period. Thereby, by shifting an oscillatory signal by its period, the signal resembles itself, leading to the maximal autocorrelation of 1.

For a group of cells, the mean of all the autocorrelations for single cell traces serves as an indicator of the coherence between the cells. These mean autocorrelations are shown for type 2 and 3 cells in Fig. 3.7 for inhibition strength 1 and 9 (see App. C for

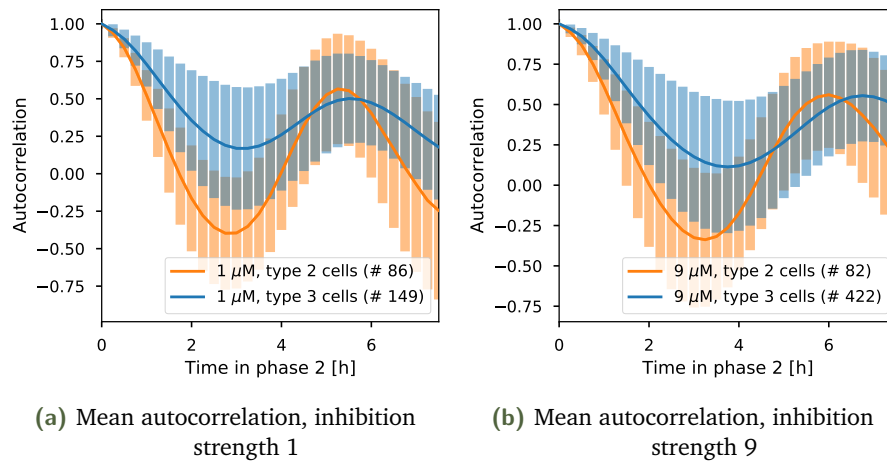


Figure 3.7: Mean autocorrelation plots for (a) inhibition strength 1 and (b) inhibition strength 9. Each plot shows both the mean autocorrelation for type 2 and type 3 cells, including the standard deviation of the mean shaded in colour. The number of autocorrelations that have been averaged in figure (a) are 86 (type 2) and 149 (type 3), the numbers are 82 and 422 for figure (b).

other inhibition strengths). Inspecting these plots, two things become apparent. Firstly, it seems that the type 2 cells are more strongly correlated to each other. Secondly, it seems that the autocorrelation of type 3 cells peaks later than the one of type 2 cells, indicating that the two types of cell oscillate with different periods.

Also worth noting in Fig. 3.7 is that the mean autocorrelations oscillate in a slightly less damped way for the inhibition strength 9 case compared to the inhibition strength 1 case. This could indicate, that the system has transitioned further into the bifurcation for strong inhibition compared to weak inhibition of MdmX.

3.2.5 Analysis of oscillatory behaviour

The autocorrelation plots indicate that there is a period difference between type 2 and type 3 cell steady oscillations in phase 2. This can be further investigated by analysing the distribution of main periods, which can be seen in Fig. 3.8.

For the weak MdmX inhibition strength 1, type 2 cells oscillate with a period of 5.50 ± 0.08 h and type 3 cells with a longer period of 6.09 ± 0.09 h. This trend continues for the stronger MdmX inhibitions, where type 2 cells consistently exhibit faster p53 oscillations compared to type 3 cells. This observation points to some very interesting mechanisms within cellular decision-making, where oscillatory signals with different periods might trigger different outcomes in terms of cellular fate.

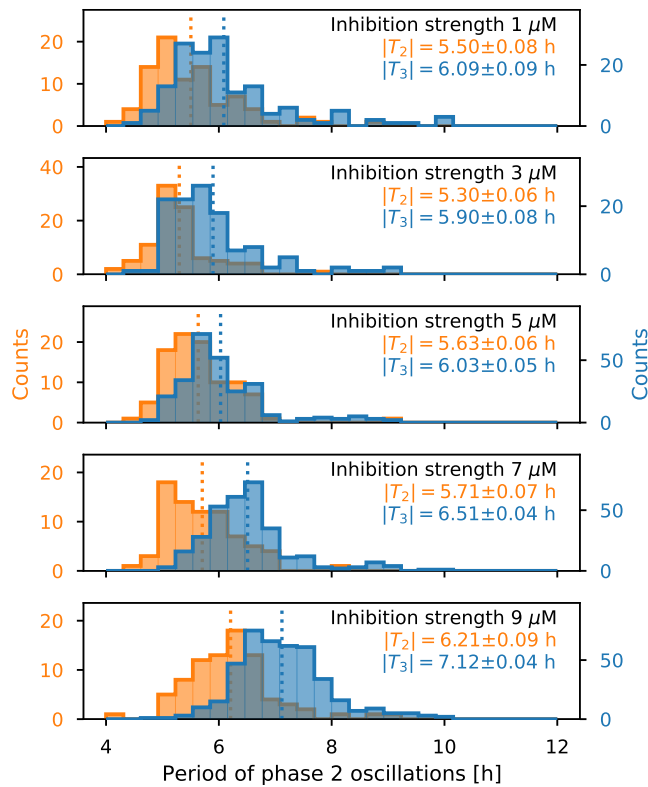


Figure 3.8: Distribution of phase 2 oscillation periods for the dividing type 2 (orange) and the non-dividing type 3 (blue) cells. The mean period of type 2 cells consistently lies below the mean period of type 3 cells, indicating that the period could play a role in determining the fate of a cell. Furthermore, the period of phase 2 oscillations increases as the inhibition strength is increased. The mean periods are indicated in the figure by text, $|T_2|$ being for type 2 and $|T_3|$ for type 3 cells.

Another interesting trend that can be observed in Fig. 3.8 is that both type 2 and type 3 mean periods increase as the inhibition strength increases. For the low inhibition strengths 1, 3, and 5, the periods do not vary strongly (5.50 ± 0.08 h, 5.30 ± 0.06 h, and 5.63 ± 0.06 h for type 2 and 6.09 ± 0.09 h, 5.90 ± 0.08 h, and 6.03 ± 0.05 h for type 3 cells). For the higher inhibition strengths of 7 and 9, the mean periods of type 2 cells rise to 5.71 ± 0.07 h and 6.21 ± 0.09 h, whereas the mean periods for type 3 cells rise to 6.51 ± 0.04 h and 7.12 ± 0.04 h. Thereby, the mean period increases by 13 % for type 2 cells between inhibition strength 1 and 9 and by more than 16 % for type 3 cells.

3.2.6 Phenotype for MdmX inhibition experiment

Having analysed the data from the MdmX inhibition experiment, a phenotype consisting of the most prominent features of the p53 response to MdmX inhibition can be designed.

Four characteristics of the p53 response have been chosen in the design of the phenotype, as elaborated below:

- Biphasic response** The response of p53 to inhibition of Mdmx is biphasic. Phase 1 consists of a single big pulse, followed by phase 2 in which steady oscillations are exhibited.
- Proliferation** The strength of MdmX inhibition has an effect on the number of cell divisions observed after inhibition. For cells that experience weak MdmX inhibition, most cells divide once or twice during the course of the experiment, whereas the majority of cells having experienced strong MdmX inhibition do not divide during the experiment.
- Type 2 & type 3** Analysing phase 2 of the biphasic p53 response to MdmX inhibition, it is observed that the mean period of oscillation is consistently lower for the dividing type 2 cells compared to the non-dividing type 3 cells across all inhibition strengths. In addition, the type 2 cells seem to be more strongly correlated to each other compared to type 3 cells.
- Period increase** When the strength of MdmX inhibition is increased, the period of phase 2 oscillations is increased as well. This holds true from inhibition strength 1 to inhibition strength 9 for both the cells of type 2 and the cells of type 3, where the period increases by 13 % and 16 %, respectively.

3.3 Summary of presented results

In this chapter, we have analysed the still unpublished data from MdmX inhibition experiments conducted at the Lahav Lab at Harvard Medical School. We have successfully designed a set of rules that enables classification of several cell types through which the 3381 p53 traces can be separated into groups. This separation of different dynamics has allowed us to correlate differences in the observed p53 dynamics to the cellular fate outcomes. Through the analysis of the biphasic p53 reaction we have designed a four-point phenotype that summarises our observations.

Design and analysis of mathematical p53 network models

In this chapter, Sec. 4.1 will introduce the modelling of the p53/Mdm2 network in general terms, considering some earlier introduced models and the effect of MdmX. Sec. 4.2 will investigate the process of designing a mathematical model, with emphasis on the p53/Mdm2 network. These model design principles will be applied in Sec. 4.3, where four models will be derived and their characteristics analysed. Finally, Sec. 4.4 will summarise the results obtained in this chapter.

4.1 Modelling p53, Mdm2 and MdmX

The application of mathematical models to investigate biological networks systematically has seen an increase as numerical simulations have become more accessible. This has allowed system biologists to understand results from laboratory experiments in greater detail, as well as enabling new biological investigations inspired by predictions made by numerical simulations. However, as the use of numerical network modelling increases, the amount of different models also increases, and the results from *in silico* investigations can become less transparent and hard to compare across different implementations.

4.1.1 Scope and level of detail

One might ask, why scientists don't agree on one model that is *the right one* and stick to this across different analyses. As all models are approximate descriptions of simplified systems, the bitter truth inevitably is that *all models are wrong*. The right- or wrongfulness of a model is solely dependent on the purpose of the model itself.

The purpose of modelling is often not to describe all aspects of large biological systems, but rather to unravel yet unseen structures and characteristics. This also increases the need to develop new models often, as new investigations focus on different properties

of a network, often expanding from or changing the perspective of previously known models.

In most cases, models show very different levels of detail. Some models focus on describing many processes in a biological network in detail, whereas other models aim at using mathematically simple models that contain less parameters. This again leads to models that cannot always be compared directly, as various simplifying assumptions can lie behind the different model designs.

4.1.2 Previous p53/Mdm2 models

Several papers have investigated the interactions between p53 and Mdm2 through numerical modelling of the network, examples being Bar-Or *et al.* (2000) where p53 oscillations were predicted mathematically and Tiana *et al.* (2002) that argued how time delay mechanisms are essential for the appearance of oscillations. In the paper by Geva-Zatorsky *et al.* (2006), six different model families were introduced and investigated, one of which has later been used for numerical analysis of the p53/Mdm2 system by Mengel *et al.* (2010) and Stewart-Ornstein *et al.* (2017). Batchelor *et al.* (2008) used mathematical modelling to investigate if oscillations arise intrinsically in the p53/Mdm2 loop or stem from upstream mediators of p53. Numerical investigations by Hunziker *et al.* (2010) concentrated on the ability of p53 to react in specific ways to different stresses and Heltberg *et al.* (2019) have used a similar approach to understand how oscillations occur after depletion of MdmX in the cells.

The papers mentioned above have inspired the following work, where the main questions asked are: What choices lie behind different model designs and how do the models relate to each other?

4.1.3 Incorporating MdmX

The biphasic reaction of p53 to MdmX depletion has previously been investigated *in silico* by Heltberg *et al.* (2019) by introducing a minimal mathematical model. As described in Sec. 2.1.4, MdmX is theorised to have several possible effects on the p53/Mdm2 system. Heltberg *et al.* (2019) concluded that the stimulating effect on Mdm2-dependent p53 degradation through complex formation is the most critical to achieve the biphasic behaviour observed in experiments.

The main goal of the numerical investigations performed in this work is to analyse if this conclusion has a *global* character across different previously introduced models describing the interactions in the p53/Mdm2 system.

4.2 Designing a mathematical model

When considering how to design a mathematical model of a biological system, there are several important aspects that should be considered. As cellular protein regulation is a very complex problem, simplifying assumptions and limitations are inevitable when designing a mathematical model, but the choice of these can affect the output of simulations.

Therefore, keeping the following questions in mind is of great importance: What is the purpose of the model? Which assumptions are made of the system and are these reasonable in a biological sense? And, which processes should the model describe? These questions will be considered in the following sections.

4.2.1 Purpose of model

As previously mentioned, there is no one-model-fits-all solution within numerical modelling. The quality of a model is defined by its ability to model the interactions of interest, making it important to consciously consider the purpose of modelling.

The purpose of the models introduced in this work is to investigate how MdmX affects the interactions between p53 and Mdm2. Considering the phenotype described in Sec. 3.2.6, there are four known effects of MdmX inhibition: biphasic reaction, changed proliferation rates, different dynamics between type 2 and type 3 cells, and an increase in the period as the inhibition gets stronger.

The models that will be considered in this work only take into account the interactions between p53 and Mdm2. Consequently, they cannot model cellular states or proliferation rates of cells. Therefore, the biphasic reaction and the period increase will be in focus for the numerical analyses in this work.

For the models designed in this work, there are two main purposes for numerical investigations (illustrated in Fig. 4.1):

- Purpose (1)** Model the biphasic oscillatory reaction to MdmX inhibition, where phase 2 oscillations are steady and have a period of around 5.5 h.
- Purpose (2)** Model an increase in period of phase 2 oscillations as the inhibition strength is increased.

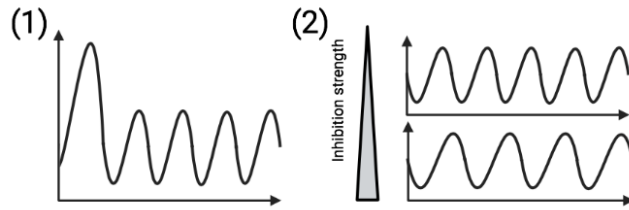


Figure 4.1: Graphical illustration of the purposes of the presented models in this work. Purpose (1) is to be able to model the biphasic reaction of p53 to MdmX inhibition and purpose (2) is to model the increase in oscillation period as inhibition strength is increased, as reported in chapter 3.

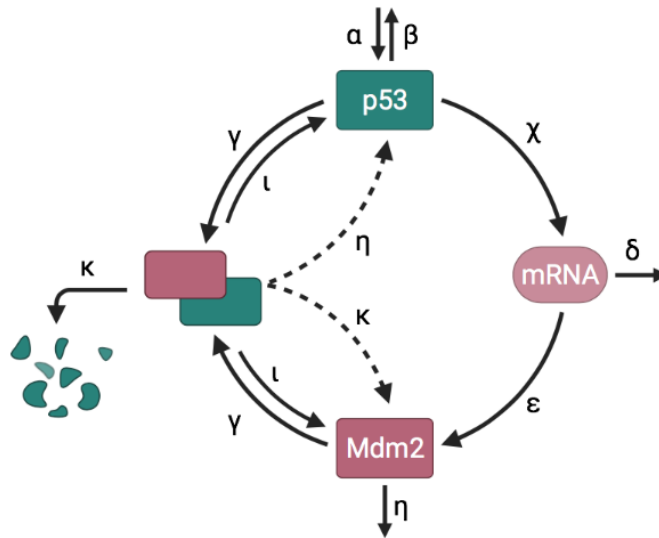


Figure 4.2: A more detailed version of the p53/Mdm2 regulatory network of Fig. 2.2 with rates added to each process.

4.2.2 Processes in network

Considering the interactions previously illustrated in Fig. 2.2 in more detail, each of the processes can be considered to happen at a certain rate. This yields the more detailed illustration of the network shown in Fig. 4.2.

Using these rates, differential equations can be set up for each part of the network, describing how the levels vary over time. The set of differential equations can then be solved numerically to obtain the temporal dynamics described by the model.

4.2.3 Adding MdmX

The effect of MdmX on the p53/Mdm2 network is of special interest for this work, thus MdmX has to be incorporated in the model design. Previous analysis has yielded that the complex formation process is the most critical impact point of MdmX on the

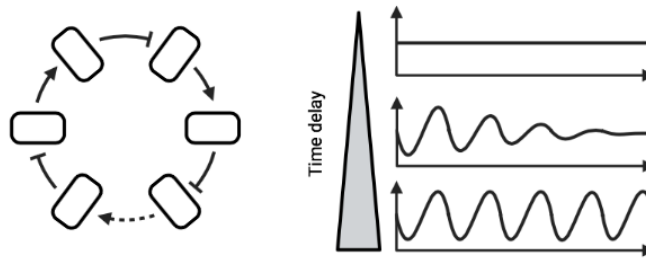


Figure 4.3: An example of a negative feedback loop, where inhibitory links are marked with bars and stimulating links with arrowheads. The plots to the right show the typical temporal dynamics: steady state dynamics, damped oscillations and steady oscillations. The necessary time delay to obtain these dynamics is indicated to the left of the plots.

p53/Mdm2 system (Heltberg *et al.*, 2019). Therefore, the following parameters are of interest when analysing the potential effect of MdmX on the complex formation process between Mdm2 and p53:

- Complex formation rate γ
- Complex break apart rate ι
- Mdm2-dependent p53 degradation rate κ

The effect of varying these parameters will be of interest to understand how the different models react to inhibition of MdmX.

4.2.4 Emergence of oscillatory behaviour

A model describing the p53/Mdm2 network should be able to generate oscillatory dynamics. The simplest system exhibiting oscillatory behaviour is a negative feedback-loop with a time delay (Tiana *et al.*, 2002). The p53/Mdm2 network can be considered as such a feedback-loop and the oscillatory dynamics arise through the finite amount of time that is spent on transcription and translation*, which can be described as a time-delay in the self-inhibitory system (Tiana *et al.*, 2007).

Mathematically speaking, a negative feedback loop is a feedback loop with an odd number of inhibitory links, see Fig. 4.3. If a perturbation in the system is signalled around a negative feedback loop fast, the perturbation is quickly cancelled and a steady state is reached in the form of a fixed point, a homeostasis in biological terms. If the speed of the signalling on the other hand is lower, values can repeatedly overshoot the fixed point values and thereby either exhibit damped or steady oscillations, see right side of Fig. 4.3.

Considering a very general negative feedback loop describing the interactions between p53 (denoted p) and Mdm2 (denoted m) yields the equations

$$\begin{aligned}\dot{p} &= a - bf(p)g(m) \\ \dot{m} &= ch(p) - dm\end{aligned}$$

For these equations, the Jacobian matrix yields a trace τ and determinant Δ of

$$\begin{aligned}\tau &= -b \frac{\partial f(p)}{\partial p} g(m) - d \\ \Delta &= bd \frac{\partial f(p)}{\partial p} g(m) + bcf(p) \frac{\partial g(m)}{\partial m} \frac{\partial h(p)}{\partial p}\end{aligned}$$

Assuming that the parameters take positive values ($a, b, c, d > 0$), that $p, m > 0$ at all times, and that the functions and their derivatives can be assumed to be positive, this yields that τ is negative and Δ is positive for any configuration of the system. For this reason, the system presented here can not exhibit oscillatory dynamics, as complex eigenvalues only occur for systems satisfying $\tau^2 - 4\Delta < 0$. Consequently, the introduction of a time delay is necessary to model oscillatory dynamics.

An effective time delay can be obtained in several ways (Mengel *et al.*, 2010), some of which are illustrated in Fig. 4.4 and described below:

Many steps in the loop

If the feedback loop consists of many steps, propagation of information will naturally be slowed down and every link adds to the total time-delay of the system

Time-consuming process

For these systems, an explicit time-delay τ is introduced, which results in direct dependence on earlier states of the system

Degradation through binding

If a regulator is degraded through binding to another regulator in a complex, the degradation is delayed and the complex formation process will be saturated

Introducing an explicit time delay or several equations to the system unfortunately makes analytical analysis much more complicated. Considering the above system *without* time delay allows for analytical analysis of the system. As the Jacobian describes the behaviour close to a fixed point, the damped oscillations around this fixed point can be analysed analytically in terms of the frequency. From the trace and determinant, this frequency can be found analytically as (Strogatz, 2016)

$$\omega = \frac{1}{2} \sqrt{4\Delta - \tau^2}$$

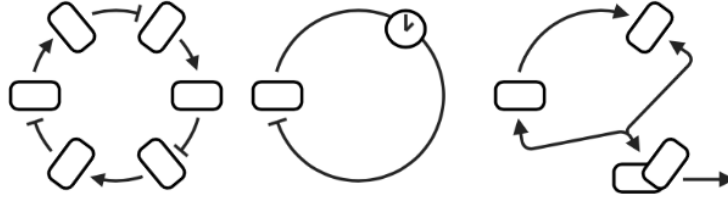


Figure 4.4: Graphical illustration of the feedback mechanisms discussed in this work. From left to right: *Many steps in the loop*, *Time-consuming process* and *Degradation through binding*. Stimulating links are marked with arrowheads and inhibiting links marked with bars.

Now analysing how the frequency changes as the parameters in the system are varied yields

$$\begin{aligned} \frac{\partial \omega}{\partial a} &= 0 \\ \frac{\partial \omega}{\partial b} &= \frac{\frac{\partial f(p)}{\partial p} g(m) \left(d - b \frac{\partial f(p)}{\partial p} g(m) \right) + 2c f(p) \frac{\partial g(m)}{\partial m} \frac{\partial h(p)}{\partial p}}{2\sqrt{4bc f(p) \frac{\partial g(m)}{\partial m} \frac{\partial h(p)}{\partial p} - \left(d - b \frac{\partial f(p)}{\partial p} g(m) \right)^2}} \\ \frac{\partial \omega}{\partial c} &= \frac{b f(p) \frac{\partial g(m)}{\partial m} \frac{\partial h(p)}{\partial p}}{\sqrt{4bc f(p) \frac{\partial g(m)}{\partial m} \frac{\partial h(p)}{\partial p} - \left(d - b \frac{\partial f(p)}{\partial p} g(m) \right)^2}} \\ \frac{\partial \omega}{\partial d} &= \frac{b \frac{\partial f(p)}{\partial p} g(m) - d}{2\sqrt{4bc f(p) \frac{\partial g(m)}{\partial m} \frac{\partial h(p)}{\partial p} - \left(d - b \frac{\partial f(p)}{\partial p} g(m) \right)^2}} \end{aligned}$$

These derivatives reveal that changes in the parameter c will always result in changes of the same size regarding the frequency of the damped oscillations, independently of the parameter values and functions $f(p)$, $g(m)$, and $h(p)$. For the other parameters of the system, this is not the case, and the frequency can decrease or increase depending on the chosen parameters and functions.

From the above equations it can be concluded that it is difficult to analytically predict how parameter changes will affect the resulting dynamics, even for a simple system without time delay such as the one considered here.

Adding a time delay to the considered system reveals a bifurcation, as limit cycles will appear for sufficiently large values of the time delay (recall Fig. 4.3). Assuming that the rates of change act similarly for these limit cycle systems this reveals that the effect of the MdmX inhibition on the period is not directly obtainable through analytical studies for this case either. Therefore, numerical analysis will be used in this work to analyse the period variations caused by MdmX inhibition.

4.2.5 Necessary assumptions

For the models analysed in this work, the assumptions will be stated explicitly for each model. There are, however, some general assumptions that concern all the models considered. One of the general assumptions is that the regulatory network of p53 can be isolated, thereby numerically modelling the p53 levels that are observed experimentally simply by considering the interactions between p53, Mdm2 and MdmX. Additionally, for all models it will be assumed that the MdmX level is neither regulated by p53 or Mdm2 and that it can be considered constant both before and after MdmX inhibition. Another assumption valid for all models is that the described processes happen at constant rates over time, thereby assuming that no external factors are affecting the different reaction rates. As the experimental setup includes an environmental chamber, such effects from the environment surrounding the cells are expected to be at a minimum.

4.3 Derivation and analysis of mathematical p53 models

The four models analysed in this work are the following:

- Model A** From Hunziker *et al.* (2010), originally used to investigate the stress-specific responses in the p53/Mdm2 feedback loop
- Model B** From Tiana *et al.* (2002), introduced to investigate the importance of time delay mechanisms for the existence of oscillations
- Model C** From Mengel *et al.* (2010), presented as a deterministic model of oscillations with particular focus on the process of saturated degradation
- Model D** From Heltberg *et al.* (2019), used to model reaction to MdmX depletion with focus on the specific role of MdmX in the network

In the four following sections, the models will be derived to shed light on the relations between the different models. First, model A will be introduced. Then, both model B and model C will be derived from model A. Lastly, model D will be derived mainly from model C.

As there is no agreement among previous models as to whether p53 binds to the Mdm2 promoter site in the DNA as a single protein or as a pair of two proteins, it has for the derivations in this part been decided to introduce the function $g(p)$ that can be set to $g(p) = p$ or $g(p) = p^2$ depending on the assumed binding cooperativity.

4.3.1 Model A

Model A will be designed as a detailed model in which all processes described in Sec. 4.2.2 are modelled directly. This results in four equations that can be set up in straightforward manner from considering each of the described processes. In the model, p_f denotes the concentration of free p53, m_m denotes the concentration of Mdm2 mRNA, m_f the concentration of free Mdm2, and c the concentration of p53-Mdm2 complex. This results in a 4-dimensional model with a total of 9 parameters,

$$\begin{aligned}
 \dot{p}_f &= \alpha - \beta p_f - \gamma p_f m_f + \iota c + \eta c \\
 \dot{m}_m &= \chi g(p_f) - \delta m_m \\
 \dot{m}_f &= \epsilon m_m - \gamma p_f m_f + \iota c + \kappa c - \eta m_f \\
 \dot{c} &= \gamma p_f m_f - \iota c - \kappa c - \eta c
 \end{aligned} \tag{4.1}$$

Two delay mechanisms can be recognised from these equations. One is introduced by modelling the step between p53 and Mdm2 separately by describing the Mdm2 mRNA transcription and translation directly through the equation concerning Mdm2 mRNA dynamics (delay mechanism *Many steps in the loop* is used here). This mechanism is controlled by parameters χ , δ and ϵ . The other delay mechanism is the degradation through p53-Mdm2 complex formation (*Degradation through binding*), which is also modelled explicitly. The complex formation and resulting Mdm2-dependent p53 degradation are described by parameters γ , ι , κ and η .

An identical model to model A has previously been introduced by Hunziker *et al.* (2010) in the following form (rate parameter names as in the original presentation)

$$\begin{aligned}
 \dot{p}_f &= \sigma - \alpha p_f - k_f p_f m_f + k_b c + \gamma c \\
 \dot{m}_m &= k_t p_f^2 - \beta m_m \\
 \dot{m}_f &= k_{tl} m_m - k_f p_f m_f + k_b c + \delta c - \gamma m_f \\
 \dot{c} &= k_f p_f m_f - k_b c - \delta c - \gamma c
 \end{aligned}$$

The chosen cooperativity of p53 binding to the Mdm2 promoter site was thereby 2, resulting in $g(p_f) = p_f^2$.

The assumptions that have been made besides the general assumptions to reach the model in Eq. 4.1 are

- Degradation of Mdm2 happens at the same rate for free and bound Mdm2
- The p53-Mdm2 complex is assembled from one of each of the proteins

4.3.2 Model B

For the derivation of model B, the total amounts of proteins will be considered. This can be done by introducing $p = p_f + c$ and $m = m_f + c$. Reformulating Eq. 4.1 yields

$$\begin{aligned}\dot{p} &= \alpha - \beta p - (\kappa - \beta)c \\ \dot{m}_m &= \chi g(p - c) - \delta m_m \\ \dot{m} &= \epsilon m_m - \eta m \\ \dot{c} &= \gamma(p - c)(m - c) - \iota c - \kappa c - \eta c\end{aligned}$$

As a next step, both the binding between p53 and Mdm2, but also the binding between p53 and the Mdm2 promoter site will be considered. Treating the Mdm2 mRNA as bound p53 and Mdm2 promoter site (denoted d), the following binding process can be considered

$$\begin{aligned}\dot{p}_f &= -\chi g(p - c)(d - m_m) + \delta m_m \\ \dot{m}_m &= \chi g(p - c)(d - m_m) - \delta m_m\end{aligned}$$

For this model, it will be assumed that both types of complexes are in equilibrium, which entails $\dot{c} = 0$ and $\dot{m}_m = 0$. This assumption is justified by considering the dissociation times of the complexes, which are much shorter than for the other processes considered here (Tiana *et al.*, 2002). This yields steady complex concentrations of

$$\begin{aligned}c &= \frac{1}{2} \left[(p + m + \lambda) - \sqrt{(p + m + \lambda)^2 - 4pm} \right] \\ m_m &= \frac{g(p - c)}{\mu + g(p - c)}\end{aligned}$$

Here, it has been assumed that there is only one Mdm2 promoter and two new parameters have been introduced to simplify the expressions, $\lambda = \frac{\iota + \kappa + \eta}{\gamma}$ and $\mu = \frac{\delta}{\chi}$.

For the full system of equations, these re-formulations now yield model B

$$\begin{aligned}\dot{p} &= \alpha - \beta p - (\kappa - \beta)c \\ \dot{m} &= \epsilon \frac{g(p(t - \tau) - c(t - \tau))}{\mu + g(p(t - \tau) - c(t - \tau))} - \eta m \\ c &= \frac{1}{2} \left[(p + m + \lambda) - \sqrt{(p + m + \lambda)^2 - 4pm} \right]\end{aligned}\tag{4.2}$$

Where the explicit time-delay τ has been introduced in the Mdm2 production, as the skipped Mdm2 mRNA step takes a finite amount of time which still has to be accounted for.

This model introduces time delay to the negative feedback system by having explicit complex formation, where the amount of complex is described by the variable c (*Degradation through binding*). Concerning p53-activated transcription and translation of Mdm2, this process is not modelled in an explicit way as in Eq. 4.1, but instead, the time spent on this process is accounted for by introducing a time-delay τ to the equations (*Time-consuming process*).

A model similar to model B has been introduced by Tiana *et al.* (2002) and is as follows

$$\begin{aligned}\dot{p} &= S - ac - bp \\ \dot{m} &= c_p \frac{p(t-\tau) - c(t-\tau)}{k_g + p(t-\tau) - c(t-\tau)} - dm \\ c &= \frac{1}{2} \left[(p + m + k) - \sqrt{(p + m + k)^2 - 4pm} \right]\end{aligned}$$

The cooperativity is set to one, leading to $g(p_f) = g(p - c) = p - c$, in this case with an added time delay τ .

The assumptions that have been made to derive model B are

- Degradation of Mdm2 happens at the same rate for free and bound Mdm2
- The p53-Mdm2 complex is assembled from one of each of the proteins
- The p53-Mdm2 complex is in equilibrium ($\dot{c} = 0$)
- The p53-DNA complex is in equilibrium ($\dot{m}_m = 0$)
- Mdm2 is produced with time delay τ from p53

4.3.3 Model C

For the next derivation, the total amounts of p53 are again considered, and the p53-Mdm2 complex is assumed in equilibrium just as before

$$\dot{c} = 0 = \gamma(p - c)(m - c) - \iota c - \kappa c - \eta c$$

Assuming that the total amount of p53 is much bigger than the amount of p53-Mdm2 complex ($p \gg c$) yields

$$c = m \frac{p}{p + \lambda}$$

This temporarily leaves model C to take the form

$$\begin{aligned}\dot{p} &= \alpha - \beta p - (\kappa - \beta)m \frac{p}{p + \lambda} \\ \dot{m}_m &= \chi g(p - c) - \delta m_m \\ \dot{m} &= \epsilon m_m - \eta m\end{aligned}$$

A similar model introduced by Geva-Zatorsky *et al.* (2006) (model IV in the paper) and later directly implemented by Stewart-Ornstein *et al.* (2017) looks as follows

$$\begin{aligned}\dot{p} &= \beta_x - \alpha_x p - \alpha_k m \frac{p}{k + p} \\ \dot{m}_m &= \beta_y p - \alpha_0 m_m \\ \dot{m} &= \alpha_0 m_m - \alpha_y m\end{aligned}$$

Furthermore, a similar model has been introduced by Mengel *et al.* (2010)

$$\begin{aligned}\dot{p} &= k_s - \delta m \frac{p}{k + p} \\ \dot{m}_m &= k_{c2} p^2 - \beta m_m \\ \dot{m} &= k_t m_m - \alpha m\end{aligned}$$

As can be seen from these two models, the first one uses $g(p - c) = p$ and the second uses $g(p - c) = p^2$, thus both of these models do not consider the amounts of p53-Mdm2 complex in the function $g(p - c)$. This difference can be explained by considering the approximation stating that the total amount of p53 is much bigger than the amount of p53-Mdm2 complex, thus $g(p_f)$ can be approximated as $g(p)$.

Additionally, for the model by Geva-Zatorsky *et al.* (2006) it is stated that the Mdm2-independent degradation rate of p53 (α_x) should be very close to zero. The model introduced by Mengel *et al.* (2010) does not contain this degradation term. Therefore, it will for model C in this work be assumed that the Mdm2-independent degradation of p53 is zero, yielding $\beta = 0$ for model C.

Implementing this, the final version of model C looks as follows

$$\begin{aligned}\dot{p} &= \alpha - \kappa m \frac{p}{p + \lambda} \\ \dot{m}_m &= \chi g(p) - \delta m_m \\ \dot{m} &= \epsilon m_m - \eta m\end{aligned} \tag{4.3}$$

For this set of differential equations, a delay mechanism has been introduced through the term describing the saturated degradation process that p53 undergoes after complex formation with Mdm2 (*Degradation through binding*). Furthermore, a delay

is introduced by computing the translation and transcription of Mdm2 explicitly, adding a further step to the feedback-loop (*Many steps in the loop*).

The assumptions that have been made to derive model C are

- Degradation of Mdm2 happens at the same rate for free and bound Mdm2
- The p53-Mdm2 complex is assembled from one of each of the proteins
- The p53-Mdm2 complex is in equilibrium ($\dot{c} = 0$)
- The total amount of p53 is much larger than amount of p53-Mdm2 complex ($p \gg c$)
- There is no Mdm2-independent degradation of p53 ($\beta = 0$)

4.3.4 Model D

To derive the last model which will be analysed in this work, model D, the derivations are started at the recently derived version of model C in Eq. 4.3. Assuming, as for model B, that the Mdm2 mRNA is in equilibrium yields

$$m_m = \frac{\chi}{\delta} g(p)$$

This can now be added to the differential equations by inserting a time delay for the production of Mdm2 and introducing $\nu = \frac{\epsilon\chi}{\delta}$, which leaves the final formulation of model D described by

$$\begin{aligned} \dot{p} &= \alpha - \kappa m \frac{p}{p + \lambda} \\ \dot{m} &= \nu g(p(t - \tau)) - \eta m \end{aligned} \quad (4.4)$$

In this model, the necessary time delay mechanisms are introduced through an explicit time delay τ describing the finite amounts of time spent on transcription and translation (*Time-consuming process*) and by describing the saturated degradation process, which is done implicitly in the last term of the first equation (*Degradation through binding*).

A similar model has previously been introduced by Heltberg *et al.* (2016)

$$\begin{aligned} \dot{p} &= \alpha - \beta m \frac{p}{\gamma + p} \\ \dot{m} &= \psi p(t - \tau) - \delta m \end{aligned}$$

For this formulation of the model, the function binding function has been set to $g(p) = p$, indicating that a cooperativity of 1 has been assumed for this model.

The assumptions that have been made to derive model D are

- Degradation of Mdm2 happens at the same rate for free and bound Mdm2
- The p53-Mdm2 complex is assembled from one of each of the proteins
- The p53-Mdm2 complex is in equilibrium ($\dot{c} = 0$)
- Amount of Mdm2 mRNA is in equilibrium ($\dot{m}_m = 0$)
- Mdm2 is produced with time delay τ from p53
- The total amount of p53 is much larger than amount of p53-Mdm2 complex ($p \gg c$)
- There is no Mdm2-independent degradation of p53 ($\beta = 0$)

4.3.5 Model overview

The four models derived in the previous sections are shown together in Tab. 4.1.

Model	Equations
A	$\dot{p}_f = \alpha - \beta p_f - \gamma p_f m_f + \iota c + \eta c$ $\dot{m}_m = \chi g(p_f) - \delta m_m$ $\dot{m}_f = \epsilon m_m - \gamma p_f m_f + \iota c + \kappa c - \eta m_f$ $\dot{c} = \gamma p_f m_f - \iota c - \kappa c - \eta c$
B	$\dot{p} = \alpha - \beta p - (\kappa - \beta)c$ $\dot{m} = \epsilon \frac{g(p(t-\tau) - c(t-\tau))}{\mu + g(p(t-\tau) - c(t-\tau))} - \eta m$ $c = \frac{1}{2} \left[(p + m + \lambda) - \sqrt{(p + m + \lambda)^2 - 4pm} \right]$
C	$\dot{p} = \alpha - \kappa m \frac{p}{p+\lambda}$ $\dot{m}_m = \chi g(p) - \delta m_m$ $\dot{m} = \epsilon m_m - \eta m$
D	$\dot{p} = \alpha - \kappa m \frac{p}{p+\lambda}$ $\dot{m} = \nu g(p(t - \tau)) - \eta m$

Table 4.1: Table overview of the four introduced models.

4.4 Summary of presented results

In this chapter, we have presented the main ideas behind designing mathematical models and have implemented these principles to derive four different models. We have also discussed how oscillations can occur from simple feedback mechanisms and how these oscillations can be investigated through analytical studies. The models that we introduce in this chapter span from very detailed models to mathematically more simple models. In this span, the detailed models are characterised by containing many parameters. The simple models on the other hand are characterised by the fact

that the number of assumptions that have to be made in order to obtain the simple mathematical formulations is higher. We have successfully derived four different model formulations that describe the same processes in the regulatory network of p53. In addition to the model derivations, we have presented similar models from the literature previously used for modelling the p53 regulatory network, providing an overview of some of the central models within the field of p53 modelling.

Numerical investigations of oscillatory behaviour upon parameter perturbations

The results presented in this chapter stem from a range of numerical investigations of the models introduced in the previous chapter. Sec. 5.1 contains a presentation of the standard parameters and the obtained dynamics resulting from simulation with these. In the next part, Sec. 5.2, emphasis will lie on the p53 dynamics and their characteristics across the different models. Following this, Sec. 5.3 introduces results from simulations where MdmX has been incorporated. Lastly, Sec. 5.4 contains a short summary of the results presented in this chapter.

5.1 Standard system simulations

The four different models from Tab. 4.1 are formulated using the same parameters to describe the same processes in the p53/Mdm2 network. This allows a direct comparison of the resulting dynamics between the different models.

A set of parameters is chosen to be the *standard configuration* of the system. As many of the parameters are not known, the set of parameters is chosen to yield a period of the expected 5.5 hours for model A when using a cooperativity of 2. The standard system configuration can be seen in Tab. 5.1.

Parameter	α	β	χ	δ	ϵ	η	γ	ι	κ
Value	10	0	0.01	0.25	10	1	100	1	10
Parameter	$\lambda = \frac{\eta + \iota + \kappa}{\gamma}$		$\mu = \frac{\delta}{\chi}$	$\nu = \frac{\epsilon \chi}{\delta}$	τ_1	τ_2			
Value	0.12		25	0.4	1.6	1.1			

Table 5.1: Standard parameter values

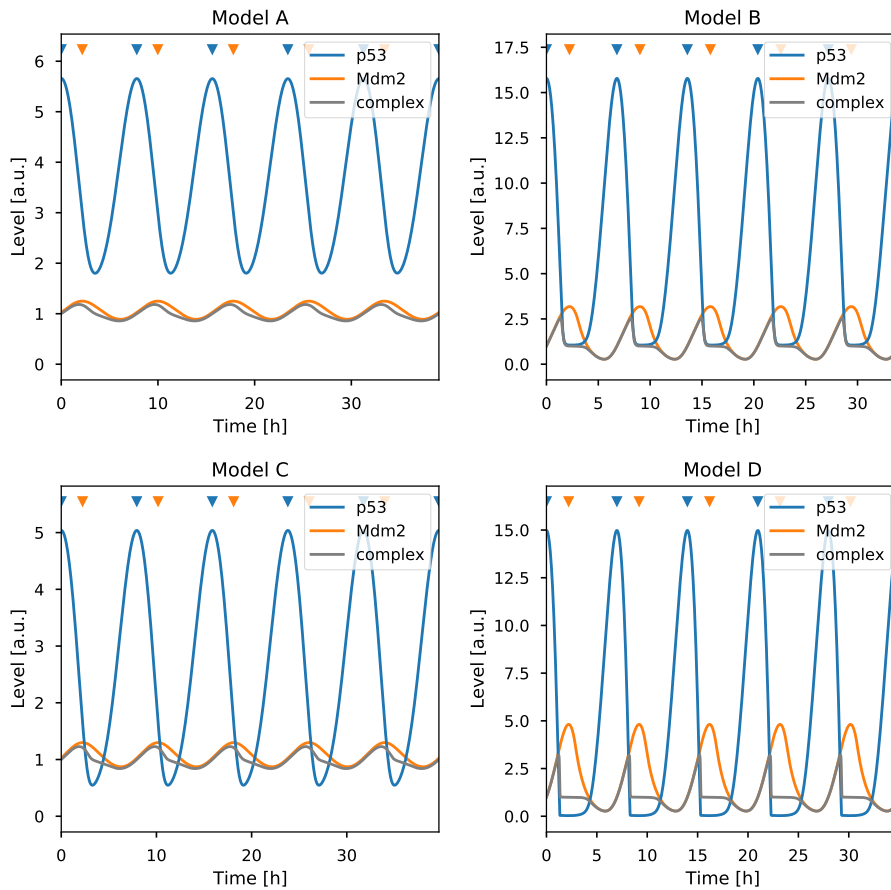


Figure 5.1: Steady state oscillations of p53, Mdm2 and p53-Mdm2 complex as a function of time for the four different models when using $g(p) = p$. The peaks of p53 level and Mdm2 level are indicated by blue and orange triangles, respectively.

5.1.1 Choice of cooperativity

Despite the similarities of the various models, agreement on the cooperativity between p53 and the Mdm2 promoter site is still lacking. Some of the models considered in this work have previously been introduced using the function $g(p) = p$ (Tiana *et al.*, 2002; Geva-Zatorsky *et al.*, 2006; Stewart-Ornstein *et al.*, 2017; Heltberg *et al.*, 2019) while others have used $g(p) = p^2$ (Hunziker *et al.*, 2010; Mengel *et al.*, 2010).

The results introduced here will consider both of these cooperativities to shed light on possible differences across models as the cooperativity is changed from 1 to 2.

5.1.2 Choice of time delay

The explicit time delay τ is the only parameter that can not be directly related to the other parameters in the system. As the time delay describes the delay that arises due to the finite amount of time used to transcribe and translate the Mdm2 mRNA, a

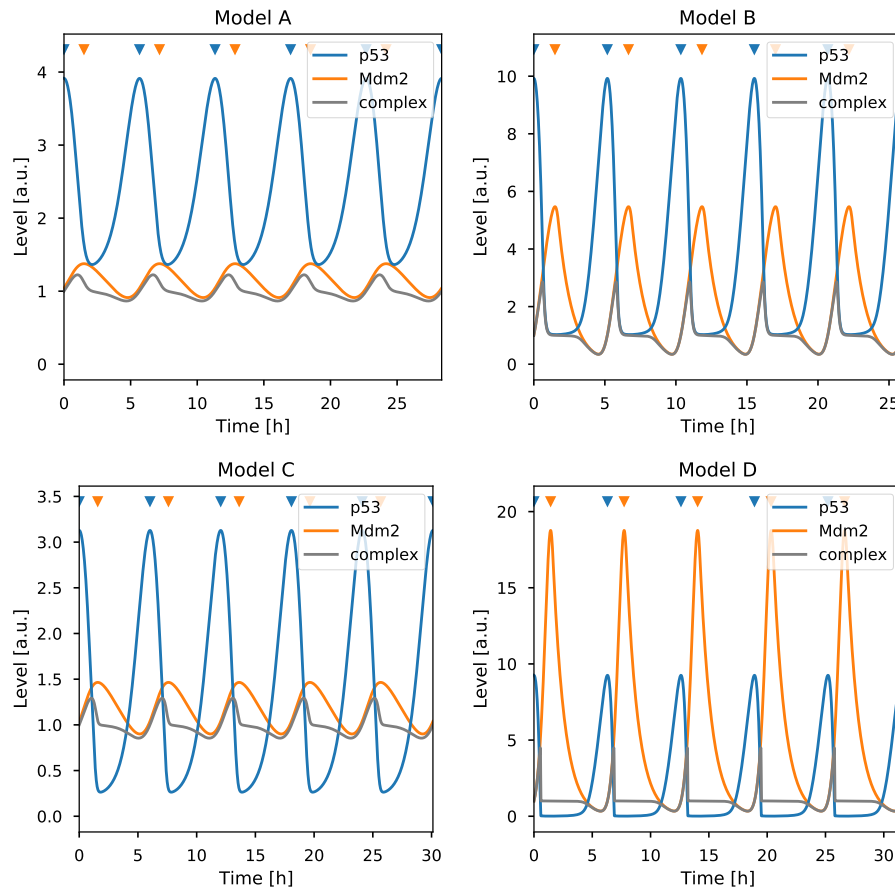


Figure 5.2: Steady state oscillations of p53, Mdm2 and p53-Mdm2 complex as a function of time for the four different models when using $g(p) = p^2$. The peaks of p53 level and Mdm2 level are indicated by blue and orange triangles, respectively.

good measure is to look at the difference in time between p53 and Mdm2 peaks when simulating.

This has been done in Fig. 5.1 for cooperativity 1 and in Fig. 5.2 for cooperativity 2, where the p53 peaks are marked by blue triangles and the Mdm2 peaks by orange triangles. The explicit time delays that result in equal distances between the peaks for all models are τ_1 equalling 1.6 h and τ_2 equalling 1.1 h, where the subscript indicates the cooperativity. For the rest of this analysis the cooperativity 1 results will be mentioned first, followed by the cooperativity 2 results in parenthesis.

With these choices of τ_1 and τ_2 , the delay for model A becomes 2.17 h (1.50 h). For model B, where the time delay is used for simulation, the delay between peaks is 2.22 h (1.49 h). Model C shows a delay of 2.24 h (1.57 h) and finally model D a delay of 2.20 h (1.43 h). As the delay between p53 and Mdm2 is comparable across the different models when introducing the explicit time delay of 1.6 h (1.1 h), this has been chosen as the standard parameter value.

5.1.3 Temporal dynamics of the simulated standard systems

As seen in both Fig. 5.1 and Fig. 5.2, all four models show oscillatory dynamics when simulated with the standard parameters for both high and low cooperativity.

In Fig. 5.1 the qualitative resemblance between models A and C and models B and D is striking, indicating that the introduction of an explicit time delay does affect the resulting dynamics. For all four models, the level of Mdm2 and p53-Mdm2 complex is quite low compared to the level of p53, which points to the fact that none of the changes made when deriving the models has affected the balance between the simulated models for the cooperativity 1 case.

A closer look at Fig. 5.2 reveals that the differences are more apparent for the case with cooperativity 2. Considering that a nonlinearity has been introduced for these cases, it seems natural that the resulting dynamics vary to a higher degree compared to before. For the cooperativity 2 case, model A and C still have a high resemblance, just as in Fig. 5.1. Models B and D on the other hand look quite different in their dynamics, as the levels of Mdm2 overshoot the levels of p53 in model D now. Furthermore, the oscillations for both models B and D are more spiky as the cooperativity is increased to 2.

5.1.4 Comparison of mean protein levels

As the experimental data does not include information about the levels of Mdm2 or the p53-Mdm2 complex it is not an aim of this work to analyse the respective levels and how they compare to each other. Although the distribution of proteins is not known from the experimental data, there are still reasons to analyse them.

For one, it was assumed in the derivations of models C and D that the amount of total p53 is much higher than the amount of p53-Mdm2 complex. In general, the motivation for introducing four different models is to compare these models, why any similarities or differences between the models help get a better understanding of the relations between models.

Investigation of Fig. 5.1 and Fig. 5.2 yields some differences in the levels of p53, Mdm2, and the p53-Mdm2 complex. The mean levels have been investigated by averaging over the five full oscillations shown for each model in these figures, which leaves the results shown in Fig. 5.3.

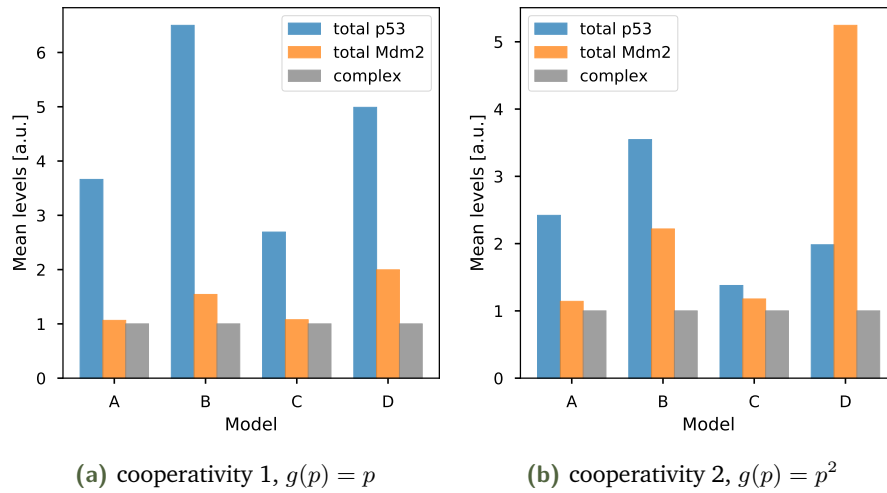


Figure 5.3: Mean levels of p53, Mdm2 and the p53/Mdm2 complex for the five full oscillations shown in (a) Fig. 5.1 and (b) Fig. 5.2. Note, that the amount of complex is also included in both the total amount of p53 and Mdm2, as $p = p_f + c$ and $m = m_f + c$.

From these figures it is clear that the cooperativity of the binding between p53 and Mdm2 plays an important role for the proportions of the levels of p53, Mdm2, and the complex. For a cooperativity of 1, the models behave similarly, whereas larger differences are observed in the distributions for a cooperativity of 2. This again points to the fact that the introduction of the nonlinearity for the high cooperativity case results in greater differences across the models.

5.2 Resulting p53 dynamics across different model formulations

The purposes of modelling the dynamics of p53 are to understand how a biphasic reaction to MdmX inhibition can occur and to investigate how the period of phase 2 p53 oscillations can increase as inhibition becomes stronger. As both of these purposes are concerned with p53 levels, the dynamics of these are of special interest in these simulations.

The results from simulating all four models with the standard parameters can be seen in Fig. 5.4 for $g(p) = p$ and in Fig. 5.5 for $g(p) = p^2$, this time only portraying the dynamics of p53. Three plots are shown for each model to illustrate several aspects of the temporal dynamics resulting from the simulations.

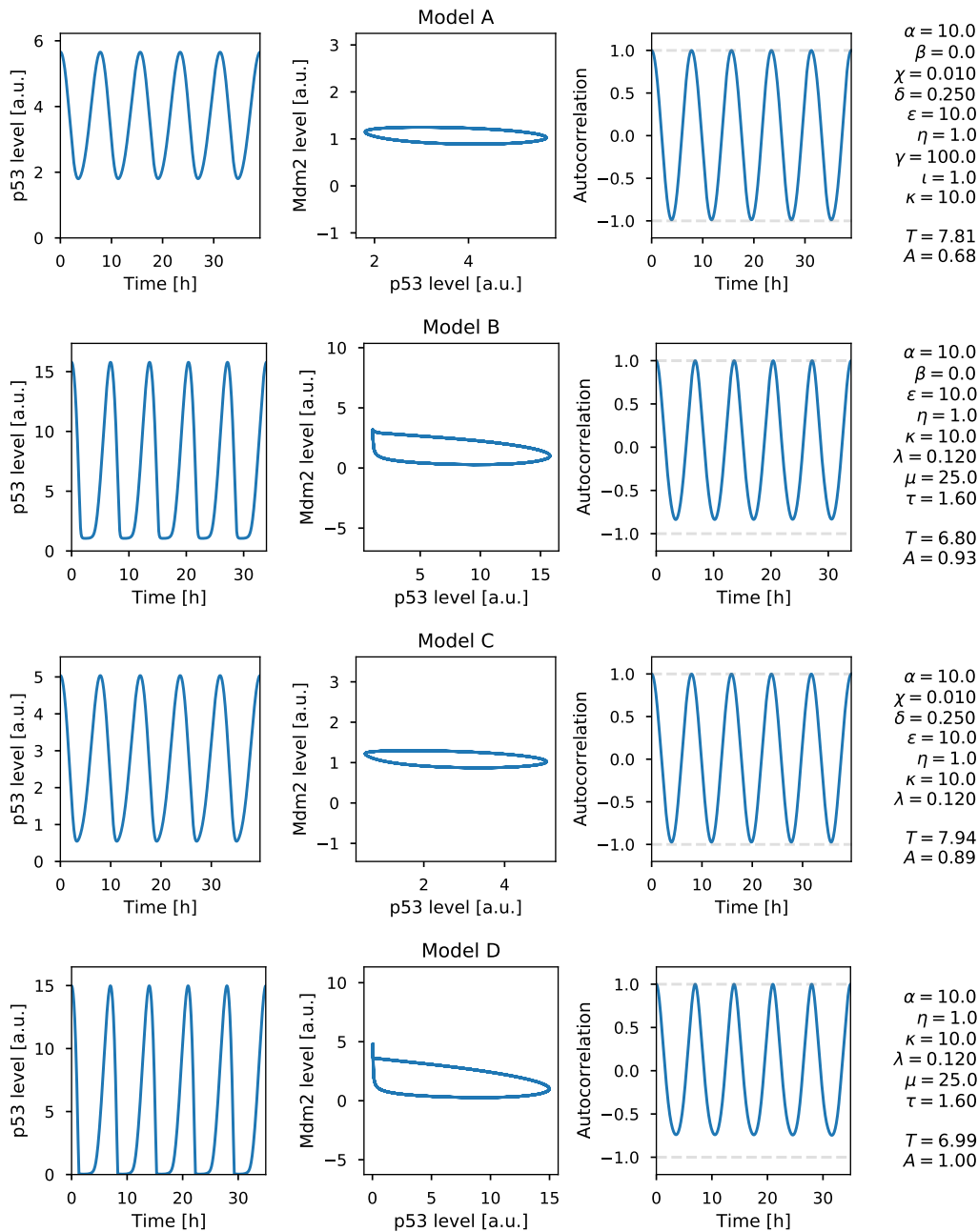


Figure 5.4: Dynamics for standard configuration of the four different p53/Mdm2 system models with $g(p) = p$. The left column shows the phase 2 p53 level as a function of time. The middle column shows the phase portrait in p53/Mdm2 phase space. The right column shows the autocorrelation of the p53 signal, where -1 and +1 have been indicated in grey. The parameters used are shown at the right (as in Tab. 5.1) together with the period of the oscillations and the relative amplitude for each of the models.

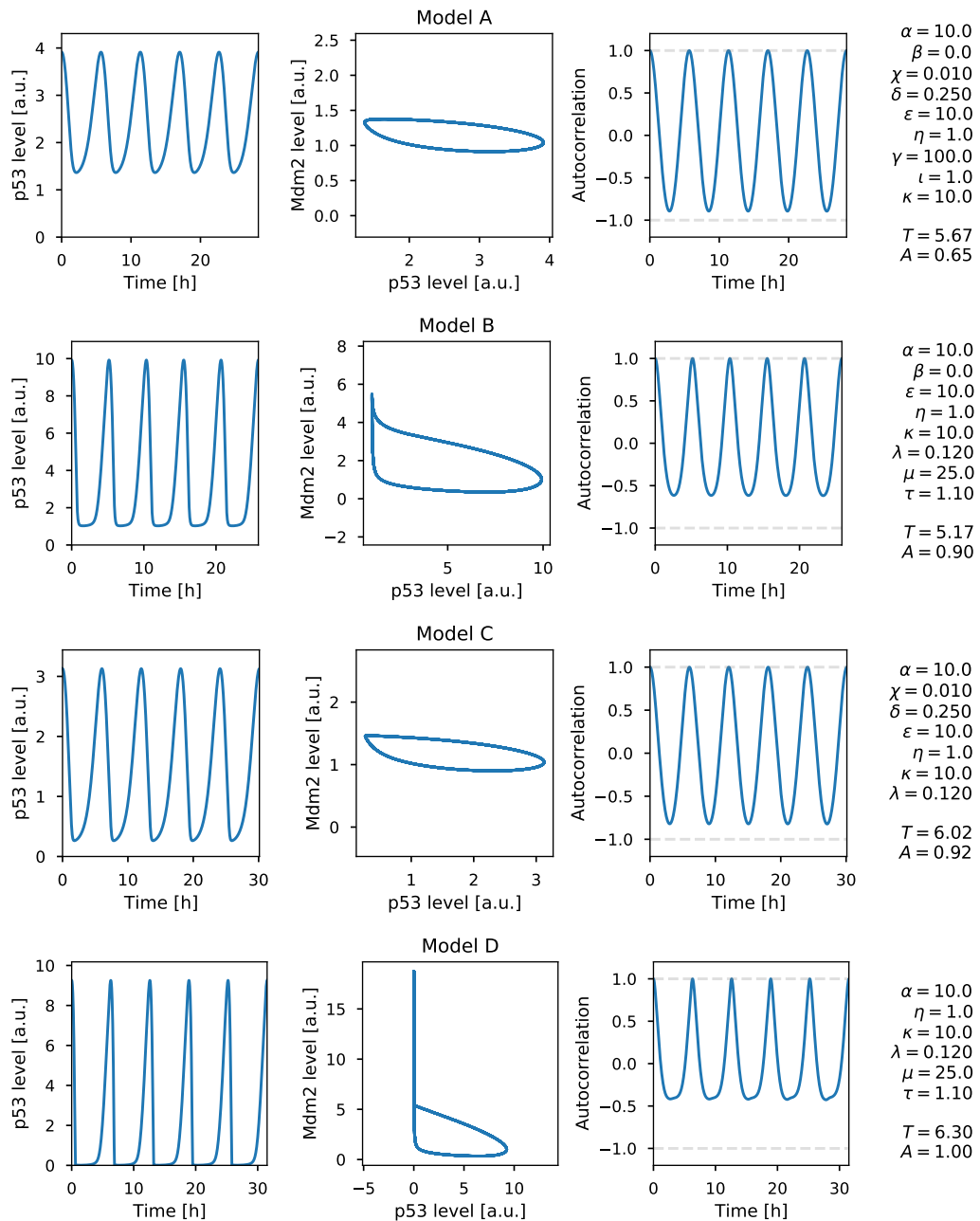


Figure 5.5: Dynamics for standard configuration of the four different p53/Mdm2 system models with $g(p) = p^2$. The left column shows the phase 2 p53 level as a function of time. The middle column shows the phase portrait in p53/Mdm2 phase space. The right column shows the autocorrelation of the p53 signal, where -1 and +1 have been indicated in grey. The parameters used are shown at the right (as in Tab. 5.1) together with the period of the oscillations and the relative amplitude for each of the models.

5.2.1 Analysis of relative amplitude

Taking a closer look at the left columns of Fig. 5.4 and Fig. 5.5, one can note how the p53 levels at the valleys of the oscillations change across the models. To characterise this behaviour, the term *relative amplitude* is introduced, which is calculated as

$$A = 1 - p_{\min}/p_{\max}$$

Calculating this relative amplitude yields 0.68 (0.65) for model A, 0.93 (0.90) for model B, 0.89 (0.92) for model C, and 1.00 (1.00) for model D.

5.2.2 Period of limit cycle oscillations

The period of oscillation for the different models can be seen from the text to the right in Fig. 5.4 and Fig. 5.5. For model A, the period is 7.81 h (5.67 h). Here it should be noted, that the model A period for cooperativity 2 has worked as reference when defining the standard parameters. Therefore, this period is close to the experimentally expected 5.5 h, whereas the period for the cooperativity 1 case is higher. This is not essential for the results presented here, as the comparison between different model formulations is the main goal.

The first re-formulation of the system, model B, simulates p53 oscillations with a period of 6.80 h (5.17 h). The oscillations for model C show a period of 7.94 h (6.02 h) and lastly, the model D oscillations in p53 level have a period of 6.99 h (6.30 h).

Differences in the period between models A and C can only stem from the reformulations of the equations, as all the described processes are the same. The period found for model C is 0.13 h (0.35 h) higher compared to that of model A. The same is the case for models B and D, where the period of model D is 0.19 h (1.13 h) higher compared to model B. Again, the models agree to a higher degree for the low cooperativity case.

5.2.3 Phase portrait comparison

The middle columns of Fig. 5.4 and Fig. 5.5 show the relation between p53 and Mdm2 levels in a phase portrait. For model A and model C, the phase portraits are close to harmonic and exhibit very similar shapes for both cooperativities. Looking at the levels of p53 and Mdm2 in Fig. 5.1 and Fig. 5.2 reflects this fact, as both the oscillations of p53 and Mdm2 are close to being harmonic.

Model B and model D on the other hand show very different phase portraits. For these models, the phase portraits get affected by the fact that the models are designed such that the protein levels are not allowed to take negative values. As a consequence, spiky oscillations can appear, as one protein *hits the wall* at zero while the level of the other protein keeps rising. This behaviour is especially visible for model D.

5.2.4 Visualising spikiness through autocorrelation plots

The autocorrelation is shown for all four models in the right-most columns of Fig. 5.4 and Fig. 5.5. As all four models reach a limit cycle oscillation when simulated with the standard parameters, the maximum value of the autocorrelation must be 1 for all models, as they resemble each other after a full period. The information that can be collected from the autocorrelation plot thereby lies in the shape and in the minimum value of the autocorrelation.

Analysing the autocorrelation plots, it is apparent that the amplitude of the autocorrelation is in general larger for cooperativity 1 cases compared to cooperativity 2 cases, indicating more harmonic oscillations for $g(p) = p$. For both cooperativities it can furthermore be observed that model B and D show more spiky oscillations, hence resulting in less harmonic autocorrelations.

5.3 Simulating the MdmX inhibition phenotype

To investigate how the models react to parameter changes such as the ones that can be caused by MdmX inhibition, the parameters of interest (κ , γ , and ι) are varied in the different systems and the resulting dynamics are then analysed. This also allows for comparison between the reactions to parameter perturbations across different models and across the two cooperativities.

5.3.1 Observation of period variations due to parameter perturbations

Multiple scans across different values of parameters can create a picture of the system's reaction to parameter changes. This has been done for all models in Fig. 5.6 for cooperativity 1 and in Fig. 5.7 for cooperativity 2. In these figures, the Mdm2-independent p53 degradation rate κ and the complex formation rate γ are varied. Each parameter is varied between 30 different values ranging from 10 times the standard value to 0.1 times the standard value. Notice the logarithmic scales on

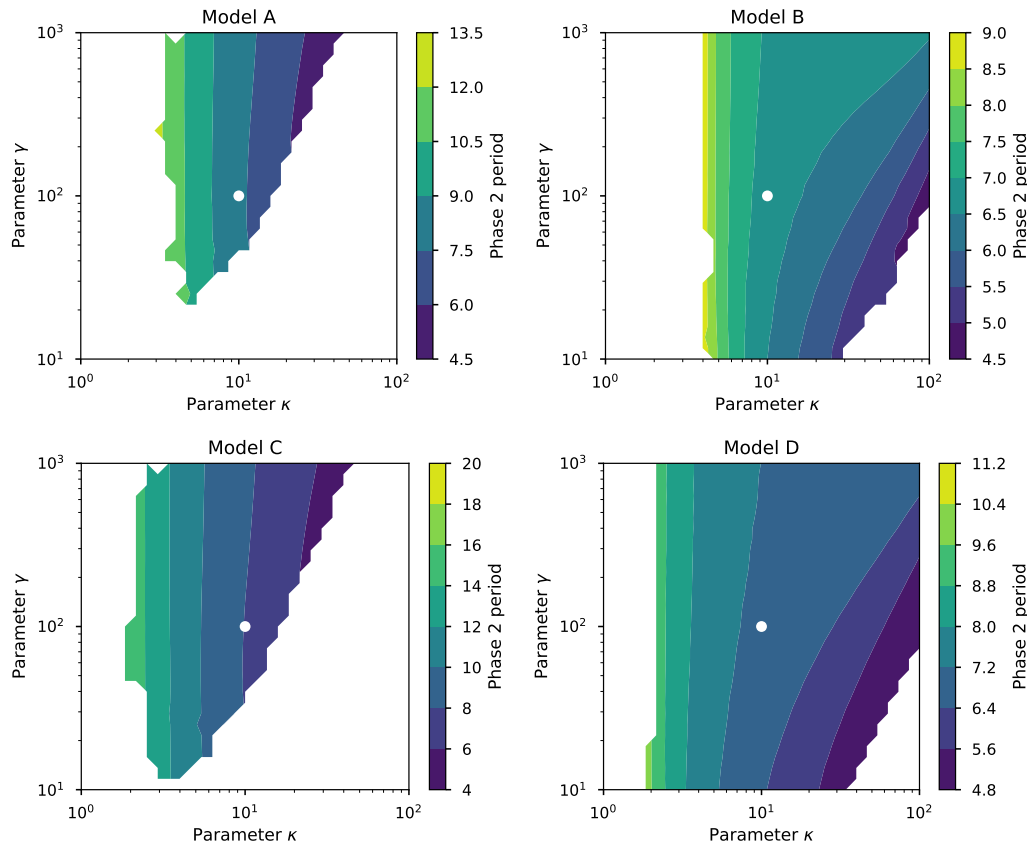


Figure 5.6: Bifurcation analysis for parameters κ and γ using $g(p) = p$. Parameter combinations that result in limit cycle oscillations are indicated in colour, also showing the period of the limit cycle oscillation as indicated for each plot by the colour-bar. The white dot represents the standard system configuration for each model, where parameters from Tab. 5.1 are used. Each parameter has been varied between 30 different values, thus this plot represents results from 900 parameter combinations.

both axes. For each parameter combination for which the system exhibits oscillatory dynamics, the period of oscillation is found and indicated by colour in the figures.

Decreasing the Mdm2-independent p53 degradation rate κ can lead to an increase in the period. This is valid across all four models for both cooperativity 1 and 2. For the cooperativity 2 case, an increase of the complex formation rate γ also results in a period increase.

Considering model A as an example, the standard period is 7.81 h (5.67 h). Scanning across the different values of κ and γ yields that the maximum period reached is around 13.5 h (7.2 h) and the minimum around 4.5 h (3.6 h). For cooperativity 1, this corresponds to an increase of around 70 % and decrease of 40 % from the standard system period, whereas these numbers are approximately 30 % and 35 % for cooperativity 2 when scanning across the exact same parameter combinations. The development is the same for the remaining models, indicating that smaller parameter

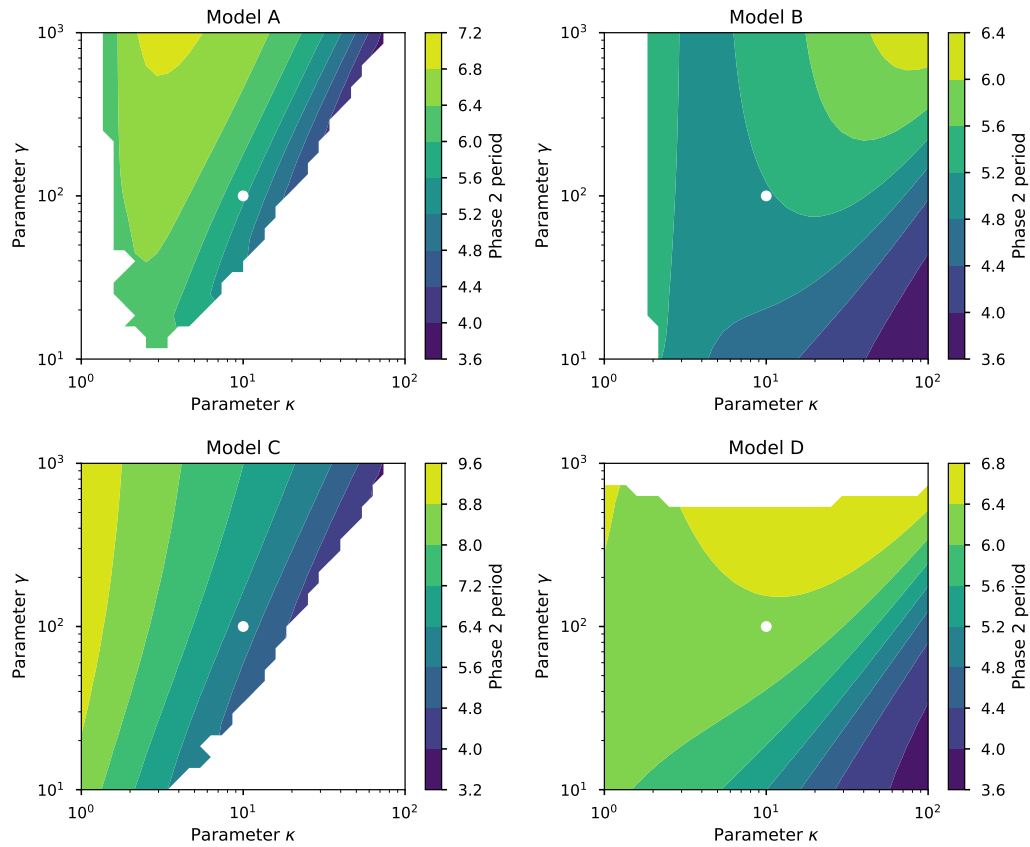


Figure 5.7: Bifurcation analysis for parameters κ and γ and $g(p) = p^2$. Parameter combinations that result in limit cycle oscillations are indicated in colour, also showing the period of the limit cycle oscillation as indicated for each plot by the colour-bar. The white dot represents the standard system configuration for each model, where parameters from Tab. 5.1 are used. Each parameter has been varied between 30 different values, thus this plot represents results from 900 parameter combinations.

changes are necessary to achieve the same change of period for cooperativity 1 compared to cooperativity 2. This can also be observed by comparing the scale of the oscillatory regimes found for the models in Fig. 5.6 and Fig. 5.7.

Figures showing results for scans across different values of κ and ι as well as γ and ι can be seen in App. D and App. E. Inspecting these figures, it is apparent that the complex break apart rate ι does not have a strong effect on the period of oscillation.

5.3.2 Change in relative amplitude corresponding to period variations

Besides knowing the period of oscillation, the relative amplitude is also of interest, as Fig. 5.4 and Fig. 5.5 have shown that this measure is not conserved across models when modelling the standard configuration of the system.

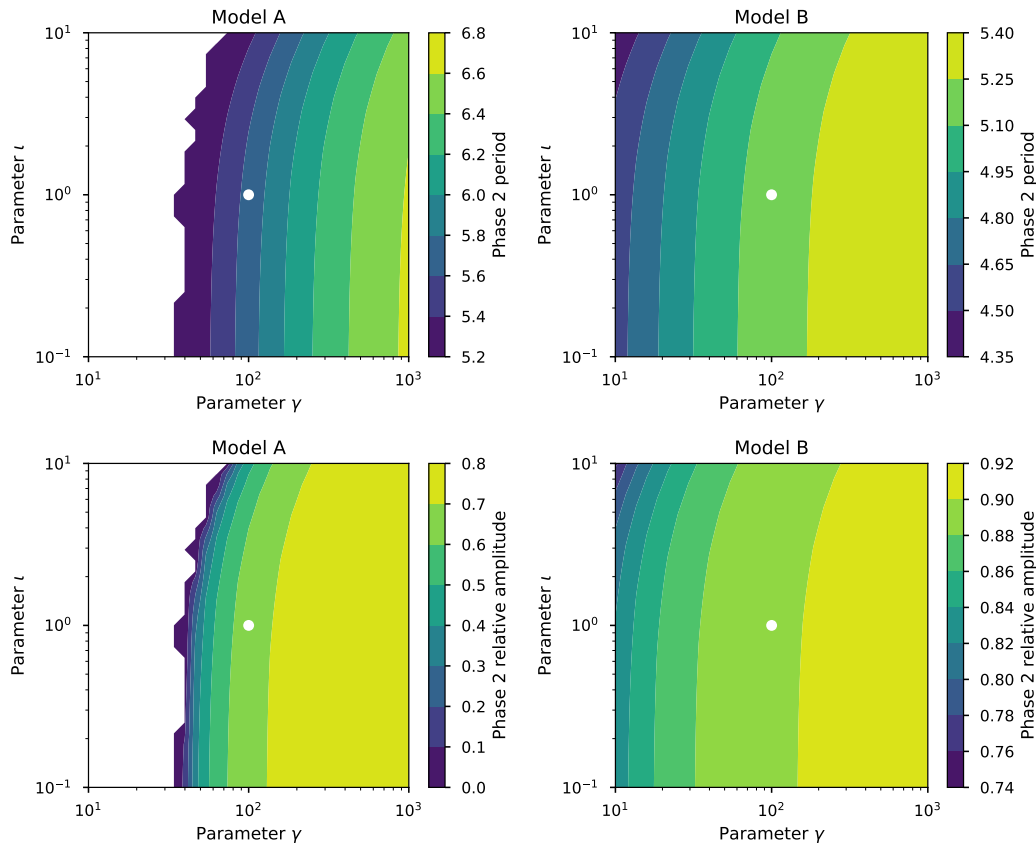


Figure 5.8: Bifurcation analysis for parameters γ and ι for model A (left column) and model B (right column) with cooperativity 2. The upper row shows the period diagrams and the lower row shows the according relative amplitude. The white dot represents the standard system configuration for each model, where parameters from Tab. 5.1 are used.

In Fig. 5.8 the period and relative amplitude are shown for model A (left column) and model B (right column) for the scan across parameters γ and ι with cooperativity 2. From these two sets of figures it is apparent that the relative amplitude rises the further the system enters the oscillatory regime. As the explicit time delay model B seems to be deeper into this regime, this can help explain the difference in the relative amplitude between the different models.

The results showing the relative amplitude for other models, parameter combinations, and different cooperativities can be seen in App. F, App. G, and App. H.

5.3.3 Dynamic responses to MdmX inhibition

Having shown that the complex formation parameters can induce period increases in all four models leaves the other purpose of modelling up to analysis: the biphasic response of p53 to MdmX inhibition. To analyse this, the effect of MdmX is introduced

to parameter κ , as this parameter has been shown to influence the period of oscillation for both cooperativities:

$$\kappa \rightarrow \kappa h(m_x)$$

Here, m_x is the level of MdmX in the system and h is a function of m_x .

Before MdmX inhibition, MdmX levels are set to be high, as MdmX is known to be over-expressed in the MCF7 cells analysed in Chapter 3. Furthermore, p53 levels are assumed to be constant, as oscillations have not been reported for non-stressed cells. This state can be achieved by choosing a high value of m_x , which results in a value of κ outside of the bifurcation regime, thereby leading to constant levels of p53.

After MdmX inhibition, the MdmX level should be lower compared to before, and p53 should exhibit oscillatory dynamics. Thereby, the system has to go through the Hopf bifurcation to reach the oscillatory dynamics after inhibition. Also, the stronger the inhibition of MdmX is, the higher should the period of oscillation be.

This behaviour can be achieved by switching between the points indicated by dots in Fig. 5.9, with a weak inhibition resulting in a smaller change in the parameter and a strong inhibition in a bigger change.

This leads to the dynamics shown in Fig. 5.10. The upper panel shows the cooperativity 1 results and the lower panel the cooperativity 2 results. From left to right the weak, medium and strong inhibition of MdmX are shown. As can be seen from these, changing parameter κ from a high value to a lower value induces the experimentally expected biphasic reaction of p53 levels to MdmX inhibition. Furthermore, the period of the phase 2 oscillation can be seen to rise as the inhibition strength is increased.

For the case with cooperativity 1, the weak inhibition is simulated by changing κ from 2.5 times to 1.2 times the standard value. This leads to biphasic oscillations with phase 2 period of 7.32 h. For the medium strength inhibition, the value is decreased from 2.5 to 1.0 times the standard value, yielding a phase 2 period of 7.81 h and for the strong inhibition the change is from 2.5 to 0.8 times the standard value, resulting in a period of 8.33 h. Thereby, both the period increase and the biphasic reaction can be obtained by varying κ .

For the cooperativity 2 case, the value of κ is varied from 5 times to 1, 0.5, and 0.25 times the standard value for weak, medium, and strong inhibition, respectively. For this scan, the periods are 5.67 h, 6.35 h, and 6.61 h, thereby also recreating the period increase as well as the biphasic reaction.

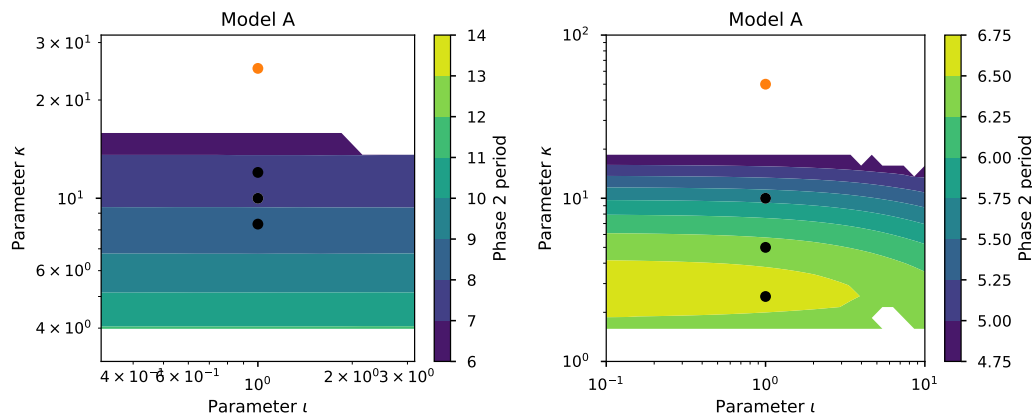


Figure 5.9: Before MdmX inhibition, the MdmX level is high and the p53 levels constant (orange dot). After inhibition of different strengths (weak, medium and strong), the system enters the oscillatory regime with different periods (black dots). The points representing states after inhibition have been scaled to approximately yielding the period increases detected in the experimental data. Left shows the case for cooperativity 1 and right the case for cooperativity 2.

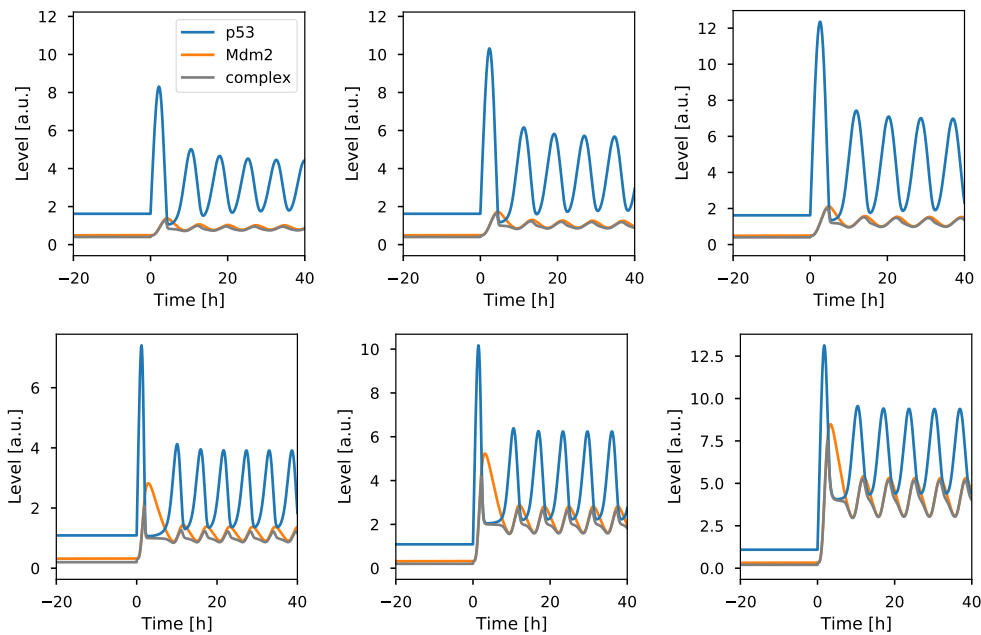


Figure 5.10: Temporal dynamics before ($t < 0$) and after ($t > 0$) inhibition of MdmX. The left-most plots show the weak inhibition, then medium inhibition and to the right the high inhibition cases (all marked by black dots in Fig. 5.9). Upper row shows the results for cooperativity 1 and lower row for cooperativity 2. The phase 2 periods for weak, medium and strong MdmX inhibition are 7.32 h, 7.81 h, and 8.33 h for cooperativity 1 and 5.67 h, 6.35 h, and 6.61 h for cooperativity 2, respectively.

5.4 Summary of presented results

In this chapter, we have successfully shown that the p53 dynamics achieved from simulating the four different models derived in the previous chapter are comparable across the different model formulations when simulated for the same set of parameters. To do so, the so-called standard configuration of the systems was introduced, and the dynamics obtained when simulating with these parameters were analysed and compared in detail. We found that there is a difference in dynamics between the models that use an explicit time delay and the models that do not, where the latter display more harmonic oscillations compared to the first. The analysis also showed that the relation between mean protein levels is affected by the choice of cooperativity, whereas the dynamics do not change drastically. Scanning across a broad range of parameter combinations, we found that changes in κ (and γ for cooperativity 2) can yield period variations in the phase 2 oscillations. Investigating the effect of changing κ in more detail revealed that both the biphasic reaction to MdmX inhibition and the phase 2 period increase as inhibition strength is increased can be simulated. This holds true across all four models, which allows us to conclude that the reaction to parameter changes such as this seems to have a global character across several model formulations.

Discussion

The discussion in this chapter will focus on the experimental results in Sec. 6.1 and then on the results from numerical simulations in Sec. 6.2.

6.1 Experimental results

The experimental data is central to the investigations of the biphasic reaction to MdmX inhibition and as such, the amount of available data is relevant to discuss. When combining the data from both runs, the numbers of tracked cells are 347, 578, 469, 612, 653, and 722 for the control group and inhibition strengths 1-9, respectively (see Fig. 3.1). As only cells classified as oscillating and of type 2 or type 3 are considered in the data analysis, the actual numbers of analysed tracks are 235, 215, 359, 390, and 504 for inhibition strengths 1-9 (see right-hand side axis of Fig. 3.5). The reason that these numbers differ more *after* classification compared to *before* is that there are much more type 1 cells for the low inhibition strength, where the proliferation rate is higher. This can be seen from Fig. 3.2. One could argue that it would be feasible to collect more data for the low inhibition strength experiments, as the proportion of type 3 cells is lower for these inhibition strengths. On the other hand, analysing the accuracy of the mean periods found for all inhibition strengths in Fig. 3.8 yields that even for the lower inhibition strengths, the uncertainties are relatively small.

The classification process itself can also be a point for discussion. The motivation for classifying the dividing cells into both type 1 and 2 is that there needs to be a minimal amount of data points between MdmX inhibition and cell division to allow analysis of the dynamical behaviour, thus cells of type 1 can not be used for analysis of p53 dynamics.

Considering the difference between type 2 and type 3 cells, it is not known how many of the type 3 cells potentially divide after the 48 hours in which the cells are tracked. Analysis of the division times (not shown in this work) has shown that by far most type 2 cells divide for the first time during the first 25 hours after inhibition. Although this suggests that the results presented in this work would not differ much if the

cells were to be tracked for a longer period, a longer experiment could convincingly confirm that cells divide less and not just more slowly as the inhibition strength is increased.

Concerning the classification, the data analysis presented in this work has furthermore revealed that cells of type 2 oscillate faster than cells of type 3 at the same inhibition strength. This opens up for a very interesting question: Does the state of the cell affect the period of phase 2 oscillations, or does the period of phase 2 oscillations affect which state the cell is in? No clear answer to this question can be found directly from the data presented in this work, as another kind of experimental setup would be necessary to test this hypothesis.

The question also affects the interpretation of the increased period as inhibition of MdmX is increased. Does the inhibition of MdmX of different strengths have an impact on the state of the cell, which then affects the period? Or does the inhibition of MdmX affect the oscillatory period, which then causes the cell to enter a specific state? An answer to these questions can not be found from the experiments analysed in this work. However, analysing the distribution of periods presented in Fig. 3.8 yields that the period alone is insufficient to conclude anything about the cellular state. As the mean period for type 3 cells at inhibition strength 1 is approximately the same as the mean period of type 2 cells at inhibition strength 9, the period must be one of several factors affecting cellular decision making.

The timing of the big phase 1 pulse is yet to be fully understood. Previous investigations focusing on MdmX depletion have observed the phase 1 pulse to start immediately after mitosis (Heltberg *et al.*, 2019). For the experiments analysed here, the response instead happens immediately after MdmX inhibition. Although different MdmX inhibitors have been used for these experiments, it seems that mitosis has a still unknown effect on the p53/Mdm2 network and its reaction to MdmX inhibition. The possible effects of mitosis on the dynamics have been avoided in this work by cutting the cell type 2 data tracks before mitosis.

Batchelor *et al.* (2008) suggested that the oscillations in p53 levels after DNA damage are a product of oscillatory dynamics of upstream regulators of p53, such as ATM*. The results of this work show that oscillations in p53 levels can also occur as a reaction to changes only affecting the p53/Mdm2 network itself. Thereby, the negative feedback structure presented in the models here is necessary to obtain the experimentally observed reaction to MdmX inhibition, although it might not be necessary to explain the response after DNA damage, as the oscillations in this case can stem from oscillating upstream regulators.

The reason to have a control group in the experiment alongside the inhibition groups is to quantify *how well* the cells are doing during the experiment. As can be seen from Fig. 3.1 around 20 % of the control cells do not divide during the experiment, pointing to the fact that the conditions might not be optimal. The data presented in this work comes from two repetitions of the same experiment. For the first repetition, a relatively large amount of the control cells did not divide, for which reason it was chosen to repeat the experiment. When analysing the data for this work, only the data from the second run of the experiment was initially analysed. The data from the first run was then analysed and all the results were the same as for the second run (with exception from the high proportion of non-dividing control cells in the first run). As 1270 cells were tracked in the second run compared to 2111 cells in the first run, it was decided that the combined data could be used to improve the statistical analysis of the results, although an explanation on the large amount of non-dividing control cells in the first run is still to be found.

A final remark that should be made concerning the experimental data is that there could be some toxicity issues for the high inhibition cases. As the MdmX inhibitor is a small molecule that is added to the cells in some solution, there is a possibility that the cells experience cellular stress from this solution when the concentration is relatively high. This could then also alter the dynamics of the p53 response when the solution is added to the cells, which would have a stronger effect for the high inhibition experiments.

6.2 Numerical simulation results

Concerning the numerical investigations in this work, there are several points for discussion. The most important motivation for the *in silico* investigations in this work was to analyse how different model formulations react to the same MdmX-dependent changes in the p53/Mdm2 network. As several models have been introduced to analyse the same network, the question was if conclusions made from one of these models have a global character across models.

The models presented in this work originate from four different papers and have been used to model p53 dynamics in different situations. Although it was possible to relate the models to each other by deriving them from model A, the binding cooperativity between p53 and the Mdm2 promoter site is still up for debate.

It seems that there is a span between level of detail and simplicity of the mathematical model, where model A is the most detailed and model D the simplest model. Starting from the most detailed model, derivation of the other models was possible, but only

by introduction of new assumptions for each step of simplification. Whether these assumptions are valid in biological terms can in some cases be difficult to conclude. An example of this is the assumption that the total amount of p53 is much larger than the amount of p53-Mdm2 complex in the system. As the data from MdmX inhibition experiments only represents the total p53, not much is known about the amount of bound p53 present in the system.

Numerical investigations yield slightly different distributions between p53, Mdm2 and the p53-Mdm2 complex for the different models and different cooperativities. Especially the distribution for model D and cooperativity 2 yields that there is almost as much p53-Mdm2 complex as there is p53 in total. This seems strange, as this is one of the models that assumes that the total amount of p53 is much bigger than the p53-Mdm2 complex. Here, it is important to consider that the parameters used for simulation in this work have been chosen only to yield approximately the expected period of oscillation. As information is missing on the parameter values themselves, no conclusions should be made about the resulting levels as such.

The standard system configuration is of great importance for the results presented in this work. At the same time, not much is known about the parameter values. How can conclusions then be made from the *in silico* investigations using the standard parameter configuration? The answer lies in the comparative nature of the analyses done in this work. The main interest has been to relate the four models to each other and to see how the reaction to MdmX inhibition varies across different model formulations. Concerning the levels of proteins portrayed in Fig. 5.3, focus should therefore lie on the similarity of the distributions across different models, and not on the distributions themselves.

The same can be said about the temporal dynamics of p53 levels. As these are also strongly controlled by the parameter values, focus does not lie in the dynamics themselves, but rather the similarity in dynamics as the different models are used. From Fig. 5.1 and Fig. 5.2 it is apparent that models B and D show more spiky oscillations compared to model A and C modelled with the exact same parameters. This points to the fact that the introduction of an explicit time delay affects the dynamics quite heavily. This can also be seen from the bifurcation analyses in Fig. 5.6 and Fig. 5.7 (and also App. D and App. E). In these figures it can be seen, how the oscillatory nature of p53 levels is much more robust to parameter changes for model B and D compared to model A and C, as oscillations are found for almost all parameter combinations for model B and D.

Regarding the global character of reactions to changes in the p53/Mdm2 system, it seems that although the models are different in their mathematical formulation, the

reaction to changes is largely conserved across models. For the low cooperativity case, the Mdm2-independent p53 degradation rate κ is clearly the parameter with the strongest effect on phase 2 periods. As the cooperativity is raised to 2, the complex formation rate γ has also been shown to be able to cause period variations.

In general, the differences between the models seem to grow bigger as the high cooperativity is chosen for simulations. This can be explained by the fact that the production of Mdm2 from p53 is nonlinear in the case of the high cooperativity, thus the effective production rate of Mdm2 varies more in this case, resulting in more drastic changes in terms of dynamics.

Conclusion

In this work, the effect of MdmX on the regulatory network between p53 and Mdm2 has been investigated both by analysis of experimental data from the Lahav Lab and through numerical investigations of several mathematical models.

The analysis of experimental data showed that inhibition of MdmX leads to a biphasic oscillatory response in p53 levels. The phase 2 period of oscillation is different for cells that do divide compared to cells that do not divide during the course of the experiment. As the inhibition strength increases, the proportion of cells that divide during the experiment furthermore decreases. Lastly, when the inhibition of MdmX is increased, the phase 2 period also increases.

These observations lead to a phenotype design for the MdmX inhibition experiment that consisted of four parts: the biphasic response, the lowered proliferation as inhibition strength is increased, the difference in period between dividing and non-dividing cells, and the increase in period as the inhibition strength is increased.

The last of these points was the main focus for the numerical investigation using mathematical modelling. For this part, four models introduced in previous papers investigating the regulatory network of p53 were compared to each other. To allow a comparison such as this, the models first had to be related to each other. This was done by deriving all the models from the most detailed model, model A. With the formulations achieved through these derivations, a direct comparison of the models was enabled.

First, the four models were simulated using a set of standard parameters, making it possible to compare the obtained temporal dynamics. This was done both for the case with cooperativity 1 and cooperativity 2, yielding differences in the dynamics especially for model B and model D. Then, the bifurcation diagrams were investigated by simulating the model for a wide span of parameter combinations. These diagrams showed how the period of phase 2 oscillations can vary as the parameters of interest are varied.

The main focus of this comparison was how MdmX enters the regulatory network between p53 and Mdm2. Therefore, the parameters of interest for the bifurcation analysis above were chosen to be the parameters related to the complex formation process. For these parameters, the Mdm2-dependent p53 degradation rate was for all models the one that could best recreate the biphasic response to MdmX inhibition as well as the phase 2 period increase resulting from increased inhibition, indicating that MdmX affects this parameter in the p53/Mdm2 network.

A conclusion on the numerical investigations performed in this work is that the reaction to MdmX inhibition has a global character across the four models presented here. Although the models differ in mathematical formulation and in the assumptions necessary for derivation of the model, the reaction to changes in the parameters of interest are comparable across models.

Outlook

One of the main questions that has opened up through the analysis of the experimental data in this work is whether the cellular state is dependent on the period or the period is dependent on the state the cell is in. This has led to discussions as to how this question can be investigated further experimentally in the Lahav Lab. New experiments have already been conducted as a result of the findings in this work, aiming to relate cell fate to the period of phase 2 oscillations.

In these experiments, the period of p53 oscillations is altered by using the drug Nutlin. Nutlin has been introduced as an inhibitor of Mdm2 activity, as it binds to the p53-binding pocket of Mdm2, thereby prohibiting the complex formation between p53 and Mdm2 (Vassilev *et al.*, 2004). By introducing Nutlin periodically, p53 pulses can be induced at the desired period and thereby the effect of different periods on the cellular state can be investigated.

As this experiment is conducted on cells in which MdmX has not been inhibited, the reaction of the cells to p53 pulses does not necessarily result in the same cellular decisions. This still leaves a possibility for further analysis in terms of the role of MdmX in the regulatory network of p53.

Furthermore, in this new experiment, the downstream target of p53, p21, is also tracked in the cells. The p21 protein is known to be a vital part of the cellular decision-making process. By analysing if p21 levels rise differently as the period of p53 is varied, a deeper understanding of the role of p53 oscillation periods on the cellular decision making process can be obtained.

These new experiments correspond well to the second point of investigation proposed by the handout mentioned at the beginning of this work: *Downstream effects on protein production*. The motivation for this suggestion for future research is to investigate how the cooperativity of different genes affect how either constant or oscillatory levels can induce the production of these genes. Preliminary studies of this question done during this work have revealed the results in Figure 2 of the handout (77). As can be seen from this figure, oscillating levels of p53 can induce higher levels of low-cooperativity

and intermediate-cooperativity genes compared to constant levels of p53. Now, with the new experimental data that is available, this investigation can be expanded to also include the effect of the period on the production of downstream targets.

Another experiment that can help understand the effects and importance of oscillatory p53 levels has been conducted recently in the Lahav Lab by Alba Jiménez Asins. In this experiment, p53 oscillations are first initiated through DSB generating γ -irradiation. Then, Nutlin is introduced periodically to the system, acting as an external oscillator. The p53 oscillations can entrain to this external oscillator depending on the amplitude and period of the external oscillator. Preliminary experiments have shown, that p53 can entrain to this external Nutlin oscillator both at period ratios of 1:1 and 1:2. This opens up for interesting numerical investigations concerning entrainment of the p53/Mdm2 system, where theoretical Arnold tongues can be investigated experimentally as well.

This experiment corresponds to the third proposal of the handout: *Entraining oscillations to periodic parameter variations*. Preliminary studies of this research proposal have been conducted as part of this work as well and can be seen in Figure 3 in the handout. From sub-figure A it can be seen that varying the Mdm2-dependent p53 degradation rate can entrain the oscillations of p53 to the variations of the parameter. The example shows how the oscillation of p53 can synchronise to exact half of the period of the external oscillator. For different periods and amplitude of the external Nutlin-oscillator, this ratio changes, and different states such as 1:1 and 1:2 can be reached. Scanning across many amplitudes and periods of the external oscillation finally leaves the Arnold tongues plotted in sub-figure B.

Analysing these entrainment tongues experimentally could prove very valuable to our understanding of p53 and its function. Furthermore, understanding how the p53 oscillations in different cells might be synchronised to each other through introduction of an external oscillator could potentially be important for the design of cancer treatments. As shown by Chen *et al.* (2016), the survival rate of MdmX-depleted cells varies strongly if the DNA damage occurs during phase 1 of the biphasic reaction compared to phase 2. This indicates that the right timing is crucial for this kind of treatment. Further investigations of entrainment in the gene regulatory network of p53 could lead to a better understanding of this timing and the relation between internal and external oscillators in the p53 network.

Handout for meeting November 24, 2020

Liv Moretto Sørensen, Mathias Heltberg & Mogens Høgh Jensen

In close collaboration with Alba Jimenez

Outline of research

In this small write-up we outline the ideas and results that we have been working with and will give full attention in the years to come. Our fundamental research question is focused on how dynamics in the concentration of p53 can give knowledge about the underlying biological networks and how it may control and enhance downstream protein production and ultimately define and the cell state.

Reaction to parameter variations across models

Our fundamental question in this part is the following: Will different models, similar in network structure, lead to the same conclusions, if we measure a change in one of the observable parameters (for instance the period of p53).

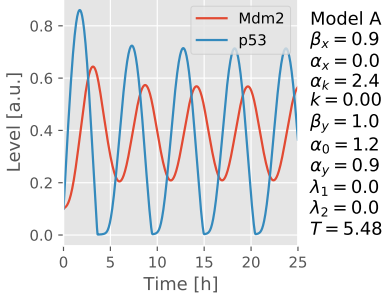
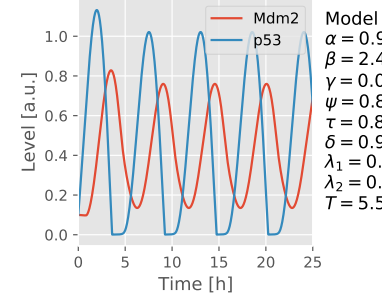
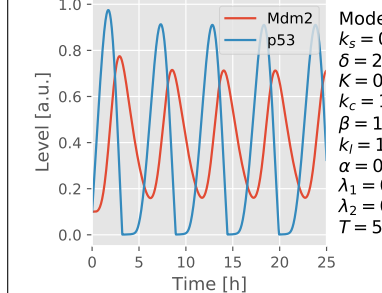
Model A	Model B	Model C
$\dot{x} = \beta_x - \alpha_x x - \alpha'_k y \frac{x}{x+k'}$ $\dot{y}_0 = \beta_y x - \alpha_0 y_0$ $\dot{y} = \alpha_0 y_0 - \alpha_y y$ <p>where</p> $\alpha'_k = \alpha_k \mu_1$ $k' = k \mu_2$ <p>and</p> <p>x: p53 level y_0: Mdm2 precursor level y: Mdm2 level</p>	$\dot{x} = \alpha - \beta' y \frac{x}{x+\gamma'}$ $\dot{y} = \psi x(t - T_{Del}) - \delta y$ <p>where</p> $\beta' = \beta \mu_1$ $\gamma' = \gamma \mu_2$ <p>and</p> <p>x: p53 level y: Mdm2 level</p>	$\dot{x} = k_s - \delta' y \frac{x}{x+K'}$ $\dot{y}_0 = k_c x^2 - \beta y_0$ $\dot{y} = k_l y_0 - \alpha y$ <p>where</p> $\delta' = \delta \mu_1$ $K' = K \mu_2$ <p>and</p> <p>x: p53 level y_0: Mdm2 precursor level y: Mdm2 level</p>
 <p>Model A $\beta_x = 0.9$ $\alpha_x = 0.0$ $\alpha_k = 2.4$ $k = 0.001$ $\beta_y = 1.0$ $\alpha_0 = 1.2$ $\alpha_y = 0.9$ $\lambda_1 = 0.0$ $\lambda_2 = 0.0$ $T = 5.48$</p>	 <p>Model B $\alpha = 0.9$ $\beta = 2.4$ $\gamma = 0.001$ $\psi = 0.85$ $\tau = 0.8$ $\delta = 0.9$ $\lambda_1 = 0.0$ $\lambda_2 = 0.0$ $T = 5.51$</p>	 <p>Model C $k_s = 0.9$ $\delta = 2.4$ $K = 0.001$ $k_c = 1.6$ $\beta = 1.1$ $k_l = 1.0$ $\alpha = 0.9$ $\lambda_1 = 0.0$ $\lambda_2 = 0.0$ $T = 5.50$</p>
$\beta_x = 0.9$	p53 production rate $\alpha = 0.9$	$k_s = 0.9$
$\alpha_y = 0.9$	Mdm2 degradation rate $\delta = 0.9$	$\alpha = 0.9$
$\alpha_k = 2.4$	saturation p53 degradation rate $\beta = 2.4$	$\delta = 2.4$
$k = 0.001$	p53 threshold for deg. by Mdm2 $\gamma = 0.001$	$K = 0.001$

Table 1: Model information for models A, B and C. Comparable parameters marked in colours.

In this analysis, three different models are simulated and the results are compared. The first model, called "Model A" in this handout, is the same as model IV without noise introduced by Geva-Zatorsky et al. [2006]. This noise-free variant of the model has been used by Stewart-Ornstein et al. [2017] as well. "Model B" refers to the model used by Heltberg et al. [2019a] in the exact same form. Lastly, "Model C" is taken from the paper by Mengel et al. [2010]. See Table 1 for more information on the three models.

As can be seen from the dynamics visualised for each model in Table 1, each model has been simulated with a standard set of parameters, that leads to a period of 5.5 h. The standard parameters are strongly inspired by the choice of parameters for model IV by Geva-Zatorsky et al. [2006], as also used by Stewart-Ornstein et al. [2017], but changed to show the wanted period of 5.5 h.

Since this analysis aims at comparing these three models, the comparable parameters are of interest. These are the p53 production rate (μ_1), the Mdm2 degradation rate (μ_2), the saturating p53 degradation rate (μ_3) and lastly the p53 threshold for degeneration by Mdm2 (μ_4), see Table 1. The last two of these are part of the term describing the complex formation between p53 and Mdm2, which is thought to be the term that is affected by Nutlin. The effect of varying these two parameters is investigated by multiplying the parameters with impact parameters μ_1 and μ_2 . This approach is inspired by the analysis done by Heltberg et al. [2019a].

Subfigures A1, B1 and C1 in Fig. 1 show how the three models react to varying impact parameter μ_1 , whereas subfigures A2, B2 and C2 illustrate the reaction to varying impact parameter μ_2 . In all six subplots, the connected grey data points show how the period of the p53 oscillations reacts to changing the impact parameter. The green dotted line shows how the ratio between the mean steady state value of Mdm2 and p53 varies over time. As can be seen, increasing impact parameter μ_1 results in a shorter period while decreasing it results in a longer oscillation period for p53. This holds true across all three models. One difference is that the ratio between the mean values of Mdm2 and p53 are decreasing for increasing impact factor μ_1 for model C but stays constant for the other two models.

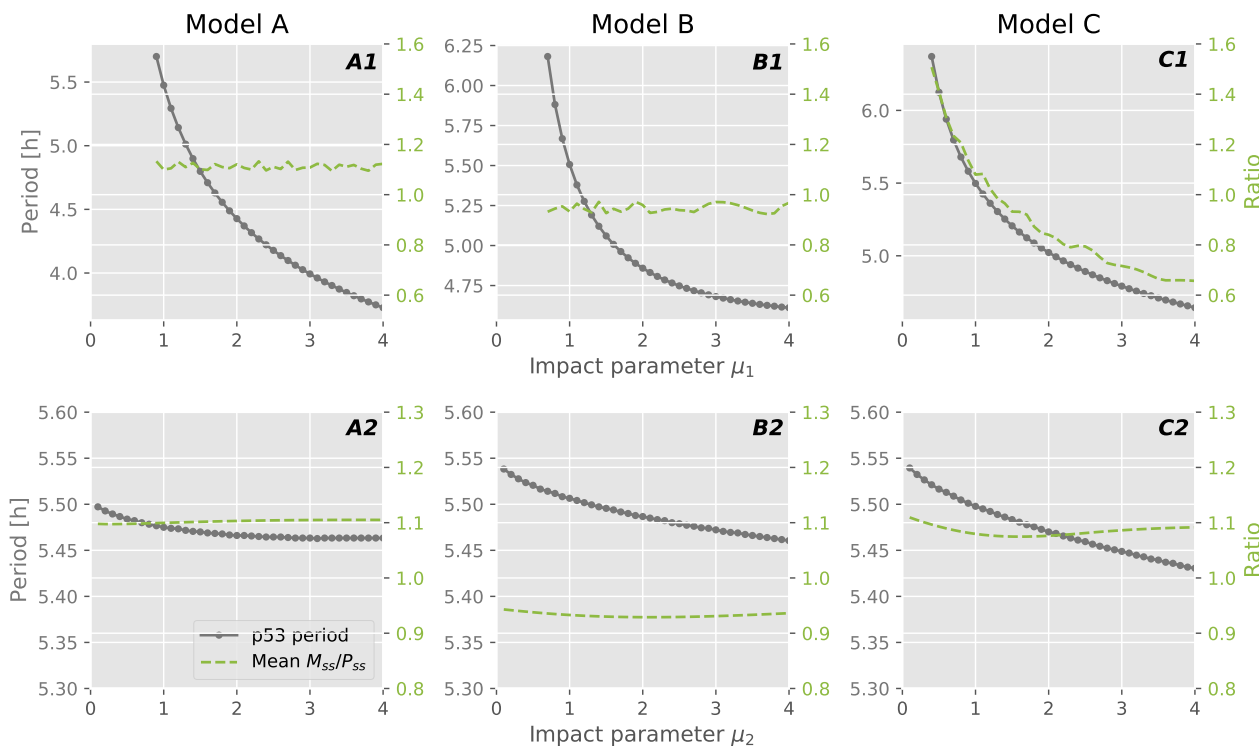


Figure 1: System reactions to changing the impact parameters μ_1 and μ_2 .

Downstream effects on protein production

Oscillations have been found in the concentrations of many different transcription factors, and we are investigating the different mechanisms that might lead to enhanced protein outcome generated by the properties of the oscillatory dynamics - the period and the amplitude of the oscillations.

To investigate how the downstream effects might be affected by the amplitudes in a transcription factor, the dynamics of genes that are regulated by p53 can be investigated by simulation. The method is inspired by Mengel et al. [2010] and Heltberg et al. [2019b]. A protein precursor z_0 is produced at a rate that is dependent on the concentration of p53 (x) through a Hill function. The protein z is then produced at rate cz_0 . The

protein and the protein precursor decay at rates d and b , respectively. The differential equations describing this process look as follows:

$$\begin{aligned} \dot{z}_0 &= a \frac{x^h}{x^h + k^h} - bz_0 \\ \dot{z} &= cz_0 - dz \end{aligned}$$

Depending on the nature of the p53 dynamics over time and on the steepness of the Hill function, different levels and dynamics are obtained for protein z . This is visualised in Fig. 2, where the rates $a = 0.5$, $b = 1$, $c = 0.5$ and $d = 0.1$ were used for simulation. The upper row shows the dynamics of protein z for oscillating p53 input (Fig. L2) and for steady p53 input (Fig. L3) for a low-affinity gene Hill-function with $k = 0.9$ and $h = 4$ (Fig. L1). The middle row shows the same for genes with intermediate affinity, with $k = 0.5$ and $h = 3$ (Fig. M1-M3). Lastly, the lower row shows the dynamics of a high-affinity gene with $k = 0.1$ and $h = 2$ (Fig. H1-H3). The oscillating p53 signal has been found by simulating Model A with standard parameters and the value of the steady state signal is the mean level of the oscillating signal, making the mean of both signals the same.

We are currently also investigating which fundamental networks might be regulated by the period of the p53 oscillations, in the sense that the exact timing might be of great importance. We have suggested for instance how this could have a potential role in the mechanisms of protein repair and how the mechanism we previously named "multiplexing" could cause enhancement of protein production.

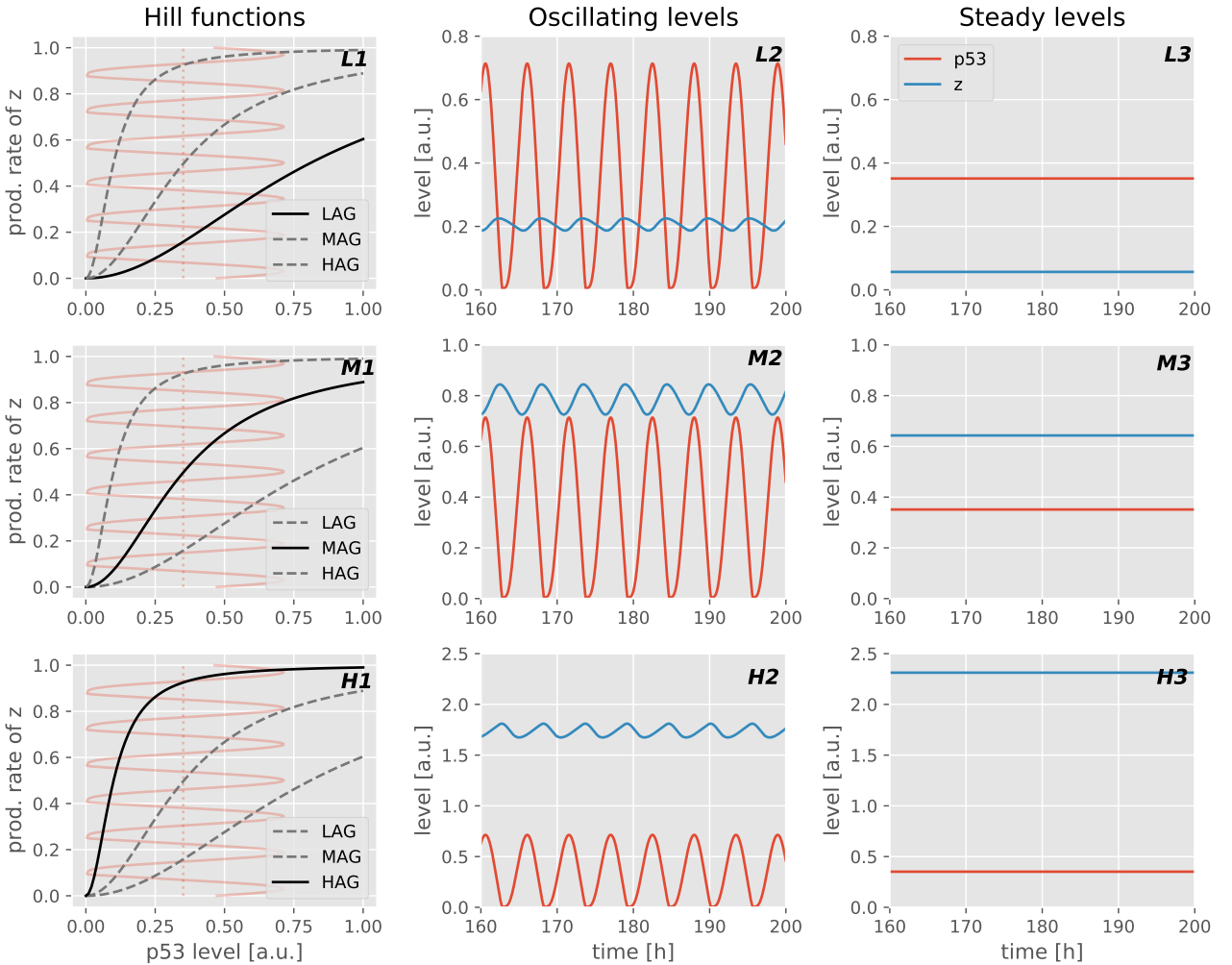


Figure 2: Protein levels and dynamics for proteins regulated by oscillating p53 signal (middle column) and steady p53 signal (right column). First row shows results for low-affinity gene, second row for intermediate-affinity genes and third row for high-affinity genes (Hill functions visualised in left column plots).

Entraining oscillations to periodic parameter variations

Since numerous proteins have the potential to show oscillatory dynamics in their concentrations, it is intriguing to study what happens when the oscillatory systems interact with each other.

As Fig. 1 illustrates, the period of p53 seems to depend strongly on the impact parameter μ_1 . Furthermore, as Fig. 2 shows, the produced downstream protein levels seem to be quite sensitive to the dynamics of the input signal. This makes the p53 oscillations under varying μ_1 values an interesting target.

By introducing $N(t)$, the concentration of Nutlin over time, as a signal with periodically spaced positive peaks, μ_1 can be re-written to:

$$\mu_1(t) = \frac{1}{1 + N(t)}$$

This indicates that for $N = 0$, $\mu_1 = 1$ and the standard parameter value is used for the saturating p53 degradation rate is used. For $N > 0$ on the other side, $\mu_1 < 1$ and the degradation rate is lowered, imitating how Nutlin inhibits the binding between p53 and Mdm2.

By simulating $N(t)$ with different amplitudes and periods, it can be investigated how and if the p53 oscillations somehow synchronise to the Nutlin modulations. This can happen in several ways; as an example, if $N(t)$ is oscillating with a period of 11.5 h and an amplitude of 0.25, the p53 oscillations will synchronise to exactly *half* the period of $N(t)$ - this is an 2:1 entrainment, see Fig. 3A.

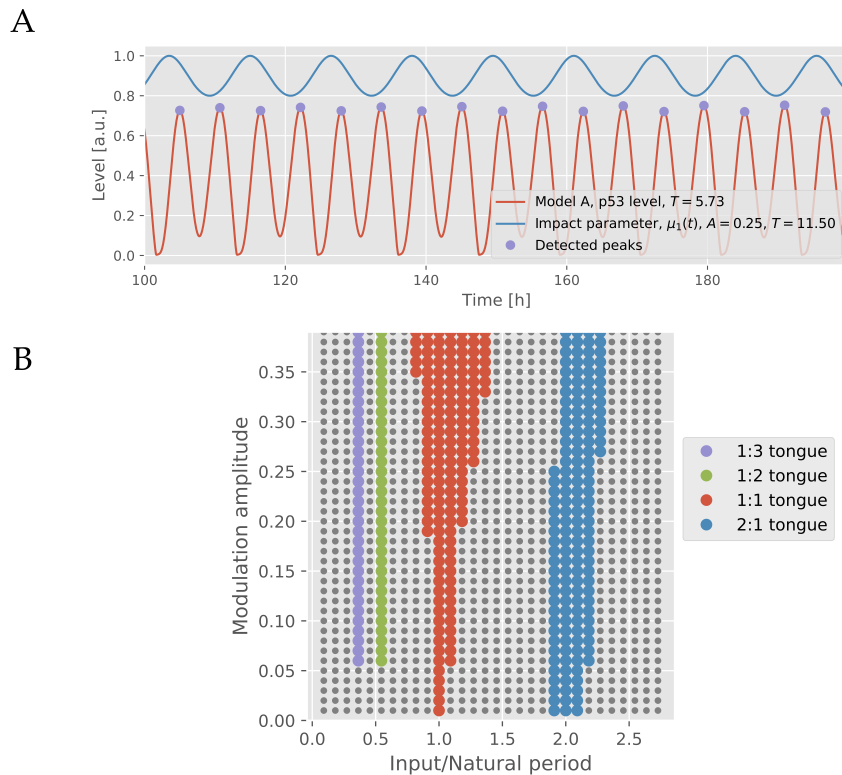


Figure 3: A) Arnold tongues for modulation of model A by signal $N(t)$ with varying period and amplitude. B) Arnold tongues for modulation of model A by signal $N(t)$ with varying period and amplitude.

Fig. 3B shows how this kind of entrainment happens for different combinations of the modulation amplitude and period. For the amplitudes and periods shown in the figure, 1:3, 1:2, 1:1 and 2:1 entrainment states are reached between the p53 oscillations and the Nutlin oscillations.

This suggest that the dynamics of p53 can be controlled by externally induced proteins. We are very interested to test if p53 can be "forced" to show even more complex dynamics, and how this might affect cancer cells, especially if certain types of dynamics might make them more vulnerable as has previously been suggested for chaotic dynamicis.

References

Naama Geva-Zatorsky, Nitzan Rosenfeld, Shalev Itzkovitz, Ron Milo, Alex Sigal, Erez Dekel, Talia Yarnitzky, Yuvalal Liron, Paz Polak, Galit Lahav, and Uri Alon. Oscillations and variability in the p53 system. *Molecular Systems Biology*, 2(1):2006.0033, 2006. ISSN 17444292. doi: 10.1038/msb4100068.

- Jacob Stewart-Ornstein, Ho Wa Jacky Cheng, and Galit Lahav. Conservation and divergence of p53 oscillation dynamics across species. *Cell Systems*, 5(4):410–417.e4, 410–417.e4, 2017. ISSN 24054720, 24054712. doi: 10.1016/j.cels.2017.09.012.
- Mathias L Heltberg, Sheng-Hong Chen, Alba Jiménez, Ashwini Jambhekar, Mogens H Jensen, and Galit Lahav. Inferring leading interactions in the p53/mdm2/mdmx circuit through live-cell imaging and modeling. *Cell Systems*, 9(6):548–558.e5, 548–558.e5, 2019a. ISSN 24054720, 24054712. doi: 10.1016/j.cels.2019.10.010.
- Benedicte Mengel, Alexander Hunziker, Lykke Pedersen, Ala Trusina, Mogens H Jensen, and Sandeep Krishna. Modeling oscillatory control in nf-b, p53 and wnt signaling. *Current Opinion in Genetics Development*, 20(6):656–664, 2010. ISSN 0959-437X.
- Mathias L. Heltberg, Sandeep Krishna, and Mogens H. Jensen. On chaotic dynamics in transcription factors and the associated effects in differential gene regulation. *Nature Communications*, 10(1):71, 2019b. ISSN 20411723. doi: 10.1038/s41467-018-07932-1.

Bibliography

- Bar-Or, Ruth Lev, Ruth Maya, Lee A. Segel, Uri Alon, Arnold J. Levine, and Moshe Oren (2000). „Generation of oscillations by the p53-Mdm2 feedback loop: A theoretical and experimental study“. eng. In: *Proceedings of the National Academy of Sciences of the United States of America* 97.21, pp. 11250–11255.
- Batchelor, Eric, Alexander Loewer, Caroline Mock, and Galit Lahav (2011). „Stimulus-dependent dynamics of p53 in single cells“. eng. In: *Molecular Systems Biology* 7.
- Batchelor, Eric, Caroline S. Mock, Irun Bhan, Alexander Loewer, and Galit Lahav (2008). „Recurrent Initiation: A Mechanism for Triggering p53 Pulses in Response to DNA Damage“. eng. In: *Molecular Cell* 30.3, pp. 277–289.
- Bennett, William P., S. Perwez Hussain, Kirsi H. Vahakangas, Mohammed A. Khan, Peter G. Shields, and Curtis C. Harris (1999). „Molecular epidemiology of human cancer risk: Gene-environment interactions and p53 mutation spectrum in human lung cancer“. eng. In: *Journal of Pathology* 187.1, pp. 8–18.
- Böttger, Volker, Angelika Böttger, Carlos Garcia-Echeverria, Yolande F.M. Ramos, Alex J. Van Der Eb, Aart G. Jochemsen, and David P. Lane (1999). „Comparative study of the p53-mdm2 and p53-MDMX interfaces“. eng. In: *Oncogene* 18.1, pp. 189–199.
- Chen, Sheng-hong, William Forrester, and Galit Lahav (2016). „Schedule-dependent interaction between anticancer treatments“. eng. In: *Science* 351.6278, pp. 1204–1208.
- Donehower, LA, M Harvey, BL Slagle, MJ McArthur, CA Montgomery, JS Butel, and A Bradley (1992). „Mice deficient for p53 are developmentally normal but susceptible to spontaneous tumours“. eng. In: *Nature* 356.6366, pp. 215–221.
- Fang, Shengyun, Jane P. Jensen, Robert L. Ludwig, Karen H. Vousden, and Allan M. Weissman (2000). „Mdm2 is a RING finger-dependent ubiquitin protein ligase for itself and p53“. eng. In: *Journal of Biological Chemistry* 275.12, pp. 8945–8951.
- Geva-Zatorsky, Naama, Nitzan Rosenfeld, Shalev Itzkovitz, *et al.* (2006). „Oscillations and variability in the p53 system“. eng. In: *Molecular Systems Biology* 2.1, msb4100068.

- Hamstra, Daniel A., Mahaveer S. Bhojani, Laura B. Griffin, Bharathi Laxman, Brian D. Ross, and Alnawaz Rehemtulla (2006). „Real-time evaluation of p53 oscillatory behavior in vivo using bioluminescent imaging“. eng. In: *Cancer Research* 66.15, pp. 7482–7489.
- Haupt, S., D. Buckley, J. M.B. Pang, *et al.* (2015). „Targeting Mdmx to treat breast cancers with wild-type p53“. eng. In: *Cell Death and Disease* 6.7, e1821.
- Heltberg, Mathias, Ryan A. Kellogg, Sandeep Krishna, Savaş Tay, and Mogens H. Jensen (2016). „Noise Induces Hopping between NF-kB Entrainment Modes“. eng. In: *Cell Systems* 3.6, 532–539.e3.
- Heltberg, Mathias L., Sheng hong Chen, Alba Jiménez, Ashwini Jambhekar, Mogens H. Jensen, and Galit Lahav (2019). „Inferring Leading Interactions in the p53/Mdm2/Mdmx Circuit through Live-Cell Imaging and Modeling“. eng. In: *Cell Systems* 9.6, 548–558.e5.
- Hollstein, M, D Sidransky, B Vogelstein, and CC Harris (1991). „p53 Mutations in Human Cancers“. eng. In: *Science* 253.5015, pp. 49–53.
- Hu, Baoli, Daniele M. Gilkes, Bilal Farooqi, Said M. Sebti, and Jiandong Chen (2006). „MDMX overexpression prevents p53 activation by the MDM2 inhibitor nutlin“. eng. In: *Journal of Biological Chemistry* 281.44, pp. 33030–33035.
- Hunziker, Alexander, Mogens H. Jensen, and Sandeep Krishna (2010). „Stress-specific response of the p53-Mdm2 feedback loop“. eng. In: *Bmc Systems Biology* 4.1, p. 94.
- Jackson, Mark W. and Steven J. Berberich (2000). „MdmX protects p53 from Mdm2-mediated degradation“. eng. In: *Molecular and Cellular Biology* 20.3, pp. 1001–1007.
- Jones, SN, AE Roe, LA Donehower, and A Bradley (1995). „Rescue of embryonic lethality in Mdm2-deficient mice by absence of p53“. eng. In: *Nature* 378.6553, pp. 206–208.
- Karolinska Institutet, Nobel Assembly (2017). *The 2017 Nobel prize in physiology or medicine*. URL: <https://www.nobelprize.org/prizes/medicine/2017/press-release/> (visited on Apr. 13, 2021).
- Kawai, Hidehiko, Dmitri Wiederschain, Hiroyuki Kitao, Jeremy Stuart, Kelvin K.C. Tsai, and Zhi Min Yuan (2003). „DNA Damage-induced MDMX Degradation Is Mediated by MDM2“. eng. In: *Journal of Biological Chemistry* 278.46, pp. 45946–45953.
- Kruse, Karsten and Frank Jülicher (2005). „Oscillations in cell biology“. eng. In: *Current Opinion in Cell Biology* 17.1, pp. 20–26.
- Kubbutat, Michael H.G., Stephen N. Jones, and Karen H. Vousden (1997). „Regulation of p53 stability by Mdm2“. eng. In: *Nature* 387.6630, pp. 299–303.
- Lahav, Galit, Nitzan Rosenfeld, Alex Sigal, Naama Geva-Zatorsky, Arnold J. Levine, Michael B. Elowitz, and Uri Alon (2004). „Dynamics of the p53-Mdm2 feedback loop in individual cells“. eng. In: *Nature Genetics* 36.2, pp. 147–150.
- Lane, DP (1992). „Cancer - p53, Guardian of the Genome“. eng. In: *Nature* 358.6381, pp. 15–16.

- Levine, Arnold J. (1997). „p53, the cellular gatekeeper for growth and division“. eng. In: *Cell* 88.3, pp. 323–331.
- Li, FP and JF Fraumeni (1969). „Soft-tissue sarcomas, breast cancer, and other neoplasms. A familial syndrome?“ eng. In: *Annals of Internal Medicine* 71.4, p. 747.
- Li, Mangmang, Yunlong He, Wendy Dubois, Xiaolin Wu, Jianxin Shi, and Jing Huang (2012). „Distinct Regulatory Mechanisms and Functions for p53-Activated and p53-Repressed DNA Damage Response Genes in Embryonic Stem Cells“. eng. In: *Molecular Cell* 46.1, pp. 30–42.
- Linares, Laëticia K., Arnd Hengstermann, Aaron Ciechanover, Stefan Müller, and Martin Scheffner (2003). „HdmX stimulates Hdm2-mediated ubiquitination and degradation of p53“. eng. In: *Proceedings of the National Academy of Sciences of the United States of America* 100.21, pp. 12009–12014.
- Loewer, Alexander, Eric Batchelor, Giorgio Gaglia, and Galit Lahav (2010). „Basal Dynamics of p53 Reveal Transcriptionally Attenuated Pulses in Cycling Cells“. eng. In: *Cell* 142.1, pp. 89–100.
- Malkin, D, FP Li, LC Strong, *et al.* (1990). „Germ Line p53 Mutations in a Familial Syndrome of Breast Cancer, Sarcomas, and Other Neoplasms“. eng. In: *Science* 250.4985, pp. 1233–1238.
- Marine, J. Chris, S. Francoz, M. Maetens, G. Wahl, F. Toledo, and G. Lozano (2006). „Keeping p53 in check: Essential and synergistic functions of Mdm2 and Mdm4“. eng. In: *Cell Death and Differentiation* 13.6, pp. 927–934.
- Mengel, Benedicte, Alexander Hunziker, Lykke Pedersen, Ala Trusina, Mogens H. Jensen, and Sandeep Krishna (2010). „Modeling oscillatory control in NF- κ B, p53 and Wnt signaling“. eng. In: *Current Opinion in Genetics and Development* 20.6, pp. 656–664.
- Migliorini, Domenico, Eros Lazzerini Denchi, Davide Danovi, Aart Jochemsen, Manuela Capillo, Alberto Gobbi, Kristian Helin, Pier Giuseppe Pelicci, and Jean Christophe Marine (2002). „Mdm4 (Mdmx) regulates p53-induced growth arrest and neuronal cell death during early embryonic mouse development“. eng. In: *Molecular and Cellular Biology* 22.15, pp. 5527–5538.
- Momand, J, GP Zambetti, DC Olson, D George, and AJ Levine (1992). „The mdm-2 Oncogene Product Forms a Complex with the p53 Protein and Inhibits p53-Mediated Transactivation“. eng. In: *Cell* 69.7, pp. 1237–1245.
- Monk, Nicholas A.M. (2003). „Oscillatory expression of Hes1, p53, and NF- κ B driven by transcriptional time delays“. eng. In: *Current Biology* 13.16, pp. 1409–1413.
- Parant, John, Arturo Chavez-Reyes, Natalie A. Little, Wen Yan, Valerie Reinke, Aart G. Jochemsen, and Guillermina Lozano (2001). „Rescue of embryonic lethality in Mdm4-null mice by loss of Trp53 suggests a nonoverlapping pathway with MDM2 to regulate p53“. eng. In: *Nature Genetics* 29.1, pp. 92–95.

- Purvis, Jeremy E., Kyle W. Karhohs, Caroline Mock, Eric Batchelor, Alexander Loewer, and Galit Lahav (2012). „p53 dynamics control cell fate“. eng. In: *Science* 336.6087, pp. 1440–1444.
- Shvarts, Avi, Wilma T. Steegenga, Nicole Riteco, *et al.* (1996). „MDMX: A novel p53-binding protein with some functional properties of MDM2“. eng. In: *Embo Journal* 15.19, pp. 5349–5357.
- Stewart-Ornstein, Jacob, Ho Wa (Jacky) Cheng, and Galit Lahav (2017). „Conservation and Divergence of p53 Oscillation Dynamics across Species“. eng. In: *Cell Systems* 5.4, 410–417.e4.
- Stewart-Ornstein, Jacob, Yoshiko Iwamoto, Miles A. Miller, *et al.* (2021). „p53 dynamics vary between tissues and are linked with radiation sensitivity“. eng. In: *Nature Communications* 12.1, p. 898.
- Stewart-Ornstein, Jacob and Galit Lahav (2017). „P53 dynamics in response to DNA damage vary across cell lines and are shaped by efficiency of DNA repair and activity of the kinase ATM“. eng. In: *Science Signaling* 10.476, eaah6671.
- Strogatz, Steven H. (2016). *Nonlinear Dynamics and Chaos : With Applications to Physics, Biology, Chemistry, and Engineering, Nonlinear Dynamics and Chaos*. eng. CRC Press.
- Surget, Sylvanie, Marie P. Khoury, and Jean Christophe Bourdon (2014). „Uncovering the role of p53 splice variants in human malignancy: A clinical perspective“. eng. In: *Oncotargets and Therapy* 7, pp. 57–67.
- Tiana, G., S. Krishna, S. Pigolotti, M. H. Jensen, and K. Sneppen (2007). „Oscillations and temporal signalling in cells“. eng. In: *Physical Biology* 4.2, R01.
- Tiana, Guido, Mogens H. Jensen, and Kim Sneppen (2002). „Time delay as a key to apoptosis induction in the p53 network“. eng. In: *European Physical Journal B* 29.1, pp. 135–140.
- Toledo, Franck, Kurt A. Krummel, Crystal J. Lee, Chung Wen Liu, Luo Wei Rodewald, Mengjia Tang, and Geoffrey M. Wahl (2006). „A mouse p53 mutant lacking the proline-rich domain rescues Mdm4 deficiency and provides insight into the Mdm2-Mdm4-p53 regulatory network“. eng. In: *Cancer Cell* 9.4, pp. 273–285.
- Toledo, Franck and Geoffrey M. Wahl (2007). „MDM2 and MDM4: p53 regulators as targets in anticancer therapy“. eng. In: *International Journal of Biochemistry and Cell Biology* 39.7-8, pp. 1476–1482.
- Vassilev, Lyubomir T., Binh T. Vu, Bradford Graves, *et al.* (2004). „In Vivo Activation of the p53 Pathway by Small-Molecule Antagonists of MDM2“. eng. In: *Science* 303.5659, pp. 844–848.
- Vousden, Karen H. and Xin Lu (2002). „Live or let die: The cell’s response to p53“. eng. In: *Nature Reviews Cancer* 2.8, pp. 594–604.
- Wade, Mark, Yunyuan V. Wang, and Geoffrey M. Wahl (2010). „The p53 orchestra: Mdm2 and Mdmx set the tone“. eng. In: *Trends in Cell Biology* 20.5, pp. 299–309.

- Wang, Hongbo, Xujun Ma, Shumei Ren, John K. Buolamwini, and Chunhong Yan (2011). „A small-molecule inhibitor of MDMX activates p53 and induces apoptosis“. eng. In: *Molecular Cancer Therapeutics* 10.1, pp. 69–79.
- Wasylishen, Amanda R. and Guillermina Lozano (2016). „Attenuating the p53 pathway in human cancers: Many means to the same end“. eng. In: *Cold Spring Harbor Perspectives in Medicine* 6.8, a026211.
- Wu, XW, JH Bayle, D Olson, and AJ Levine (1993). „The p53-Mdm-2 autoregulatory feedback loop“. eng. In: *Genes and Development* 7.7A, pp. 1126–1132.

Appendices

Appendix overview

Appendix A	Same as Fig. 3.3 but for all inhibition strengths
Appendix B	Same as Fig. 3.4 but for all inhibition strengths
Appendix C	Same as Fig. 3.7 but for all inhibition strengths
Appendix D	Same as Fig. 5.6 and Fig. 5.7 but for parameters ι and γ
Appendix E	Same as Fig. 5.6 and Fig. 5.7 but for parameters κ and ι
Appendix F	Same as Fig. 5.8 but for all models, both cooperativities, and parameters κ and γ
Appendix G	Same as Fig. 5.8 but for all models, both cooperativities, and parameters ι and γ
Appendix H	Same as Fig. 5.8 but for all models, both cooperativities, and parameters κ and ι

Appendix A

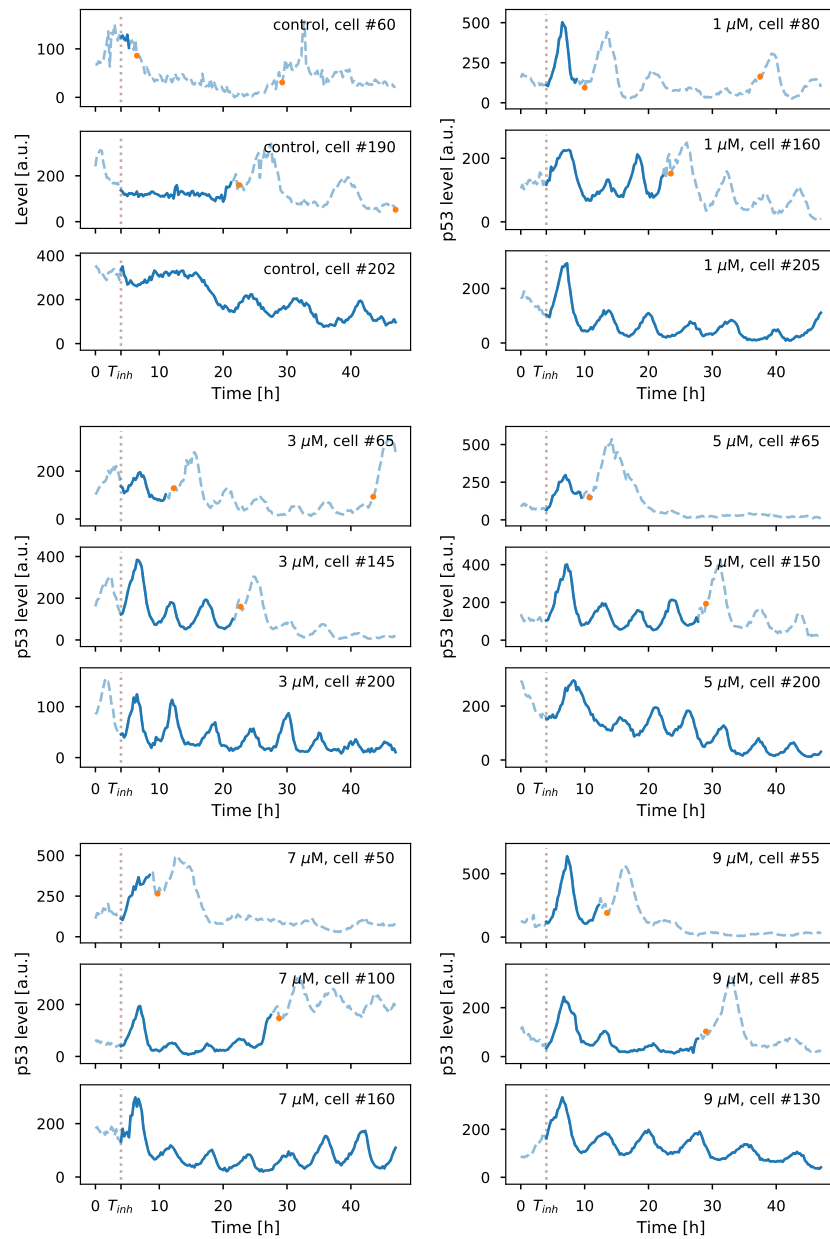


Figure 8.1: Examples of temporal dynamics in p53 levels for type 1 (upper panels), type 2 (middle panels) and type 3 (lower panels) cells. Two of these figures are shown in Fig. 3.3. The experimental data shown in this plot is unpublished data from the Lahav Lab at Harvard Medical School.

Appendix B

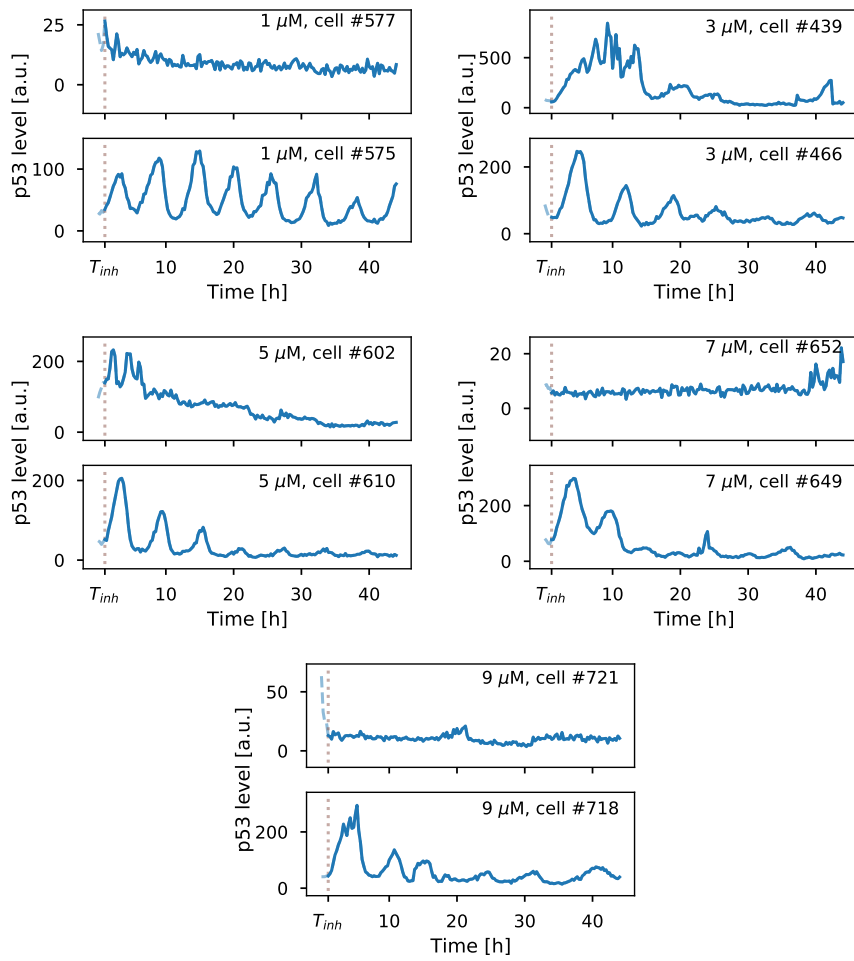


Figure 8.2: Examples of non-oscillating (upper panels) and oscillating cells (lower panels). Two of these figures are shown in Fig. 3.4. The experimental data shown in this plot is unpublished data from the Lahav Lab at Harvard Medical School.

Appendix C

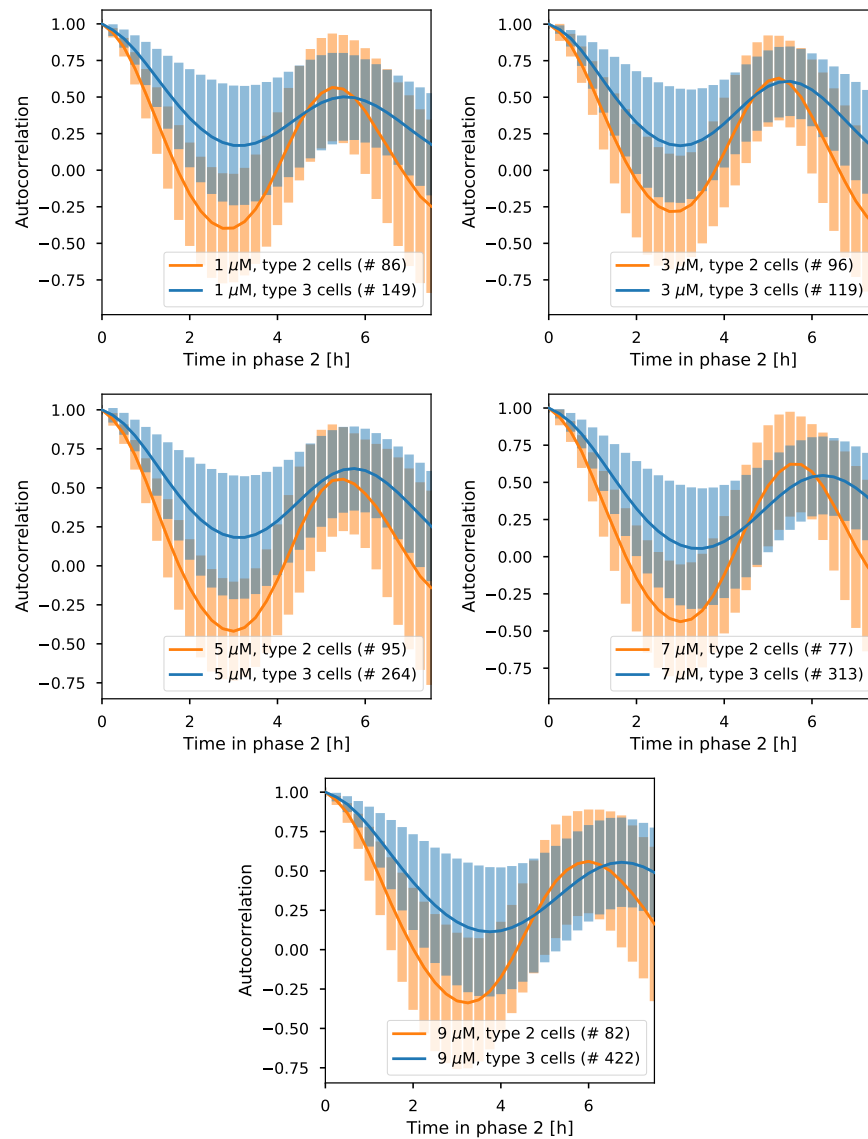


Figure 8.3: Mean autocorrelation plots. Each plot shows both the mean autocorrelation for type 2 and type 3 cells, including the standard deviation of the mean shaded in colour. The number of autocorrelations that have been averaged for each mean is indicated as well. Two of these figures are shown in Fig. 3.7.

Appendix D

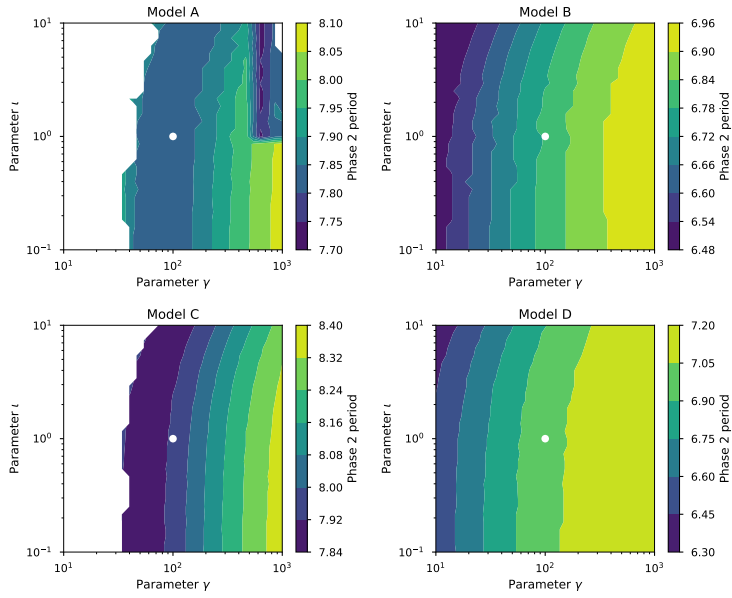


Figure 8.4: Period scans, same as Fig. 5.6 for γ and ι and $g(p) = p$.

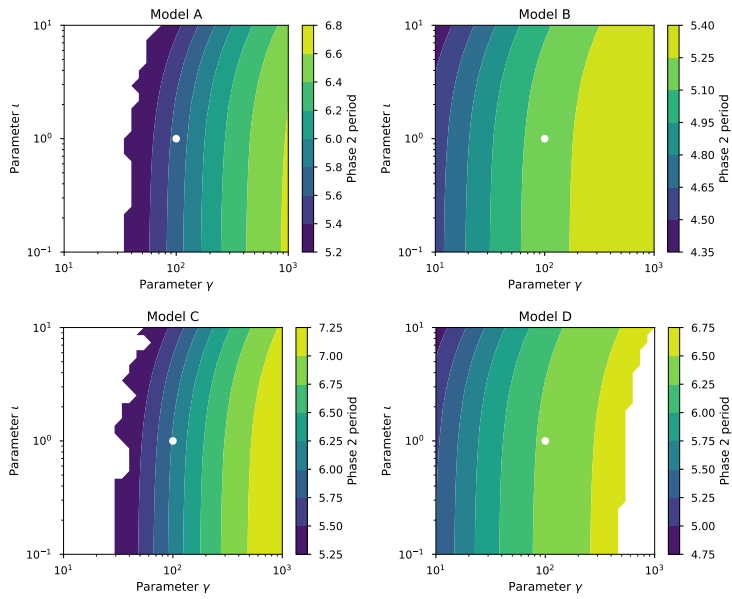


Figure 8.5: Period scans, same as Fig. 5.7 for γ and ι and $g(p) = p^2$.

Appendix E

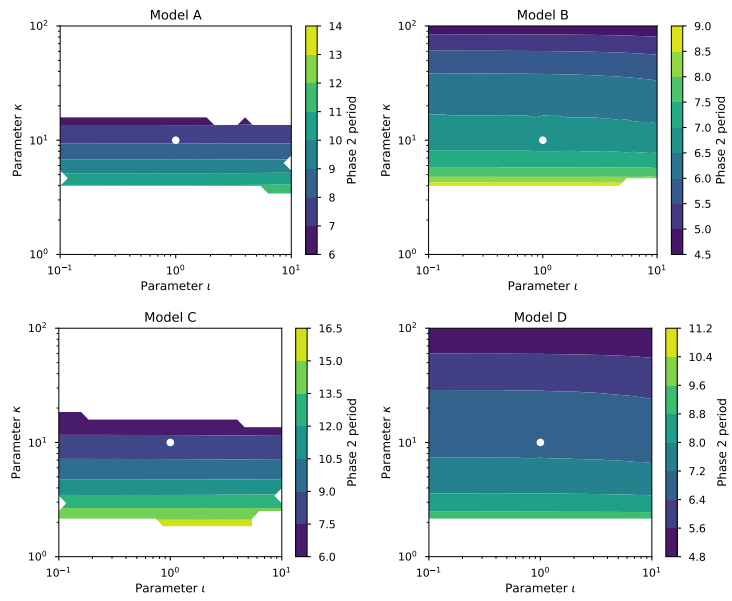


Figure 8.6: Period scans, same as Fig. 5.6 for ι and κ and $g(p) = p$.

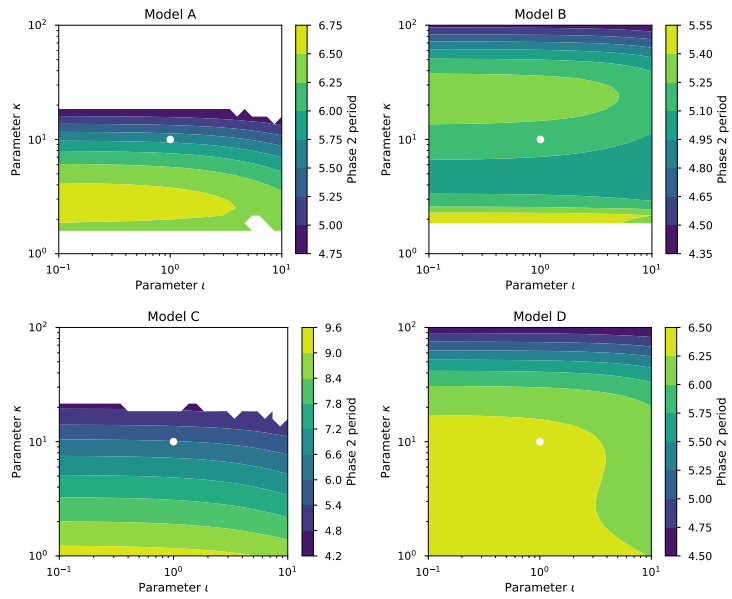


Figure 8.7: Period scans, same as Fig. 5.7 for ι and κ and $g(p) = p^2$.

Appendix F

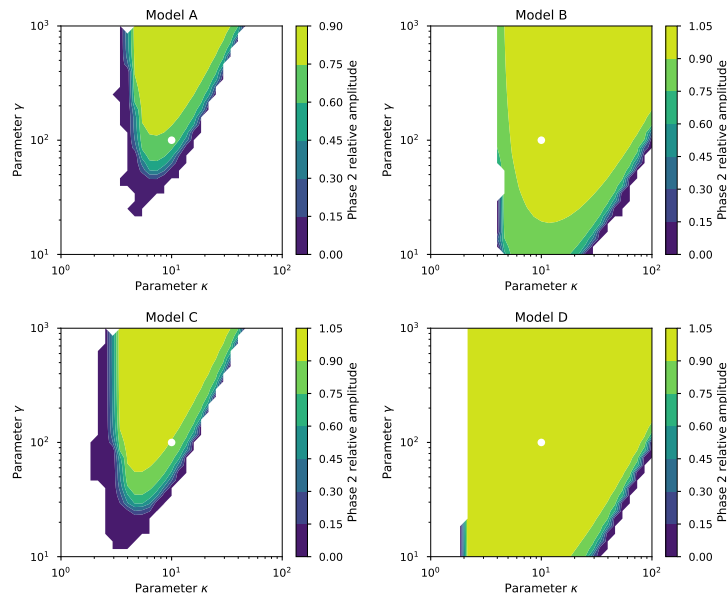


Figure 8.8: Relative amplitude scans, same as Fig. 5.8 for κ and γ and $g(p) = p$.

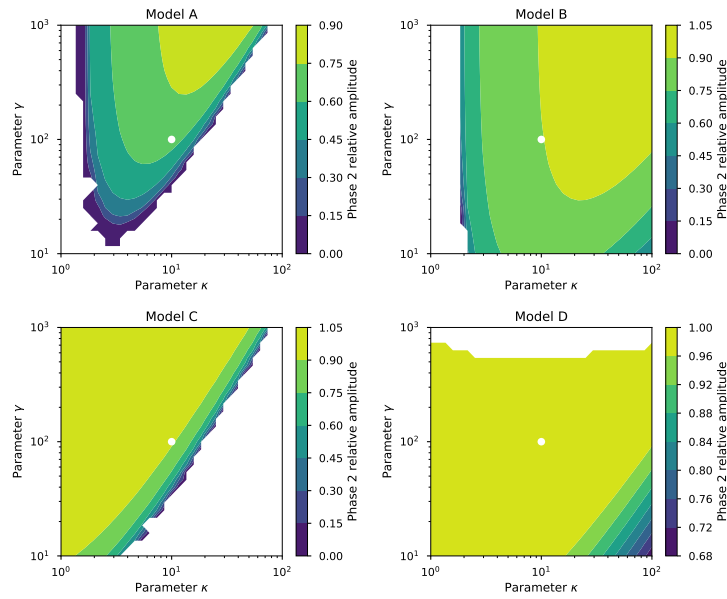


Figure 8.9: Relative amplitude scans, same as Fig. 5.8 for κ and γ and $g(p) = p^2$.

Appendix G

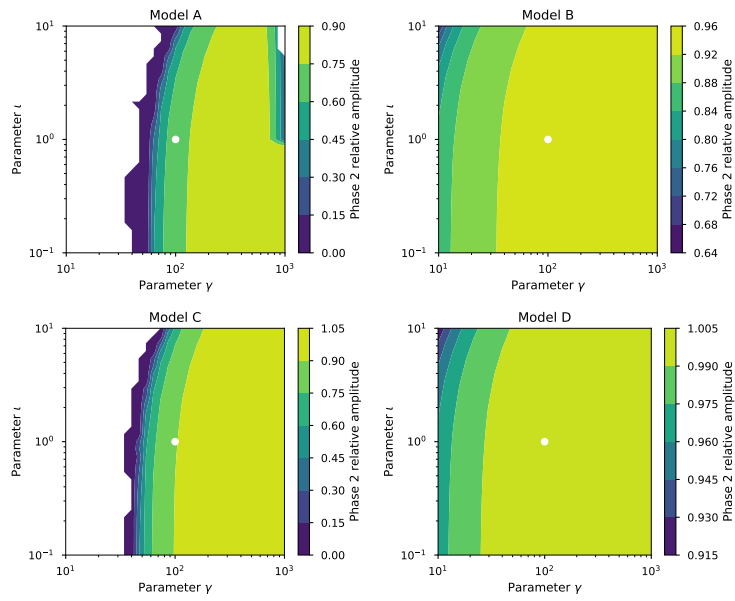


Figure 8.10: Relative amplitude scans, same as Fig. 5.8 for γ and ι and $g(p) = p$.

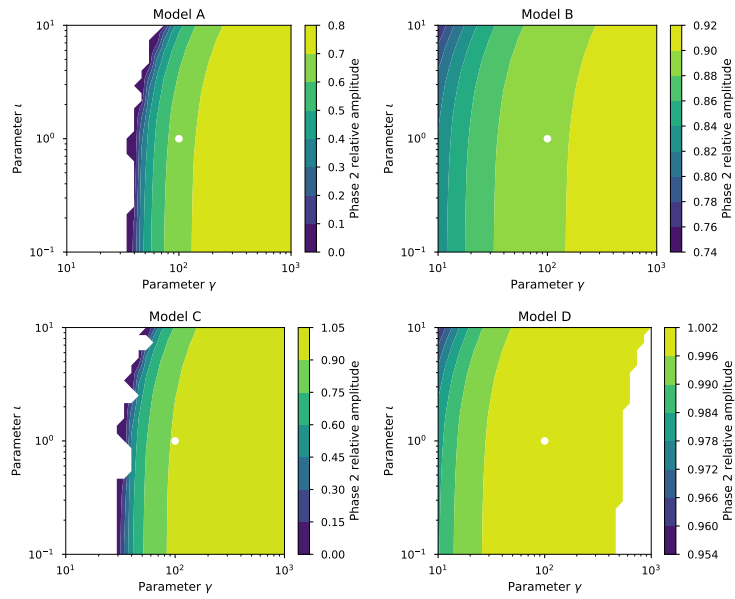


Figure 8.11: Relative amplitude scans, same as Fig. 5.8 for γ and ι and $g(p) = p^2$.

Appendix H

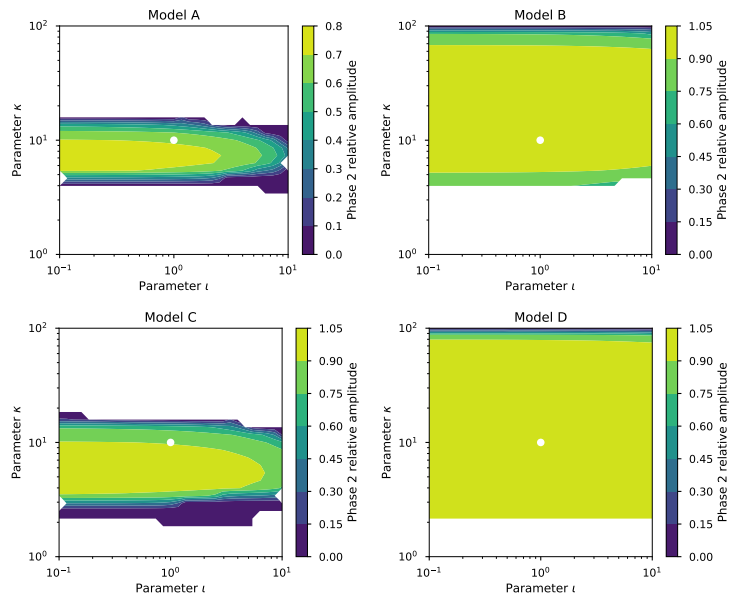


Figure 8.12: Relative amplitude scans, same as Fig. 5.8 for ι and κ and $g(p) = p$.

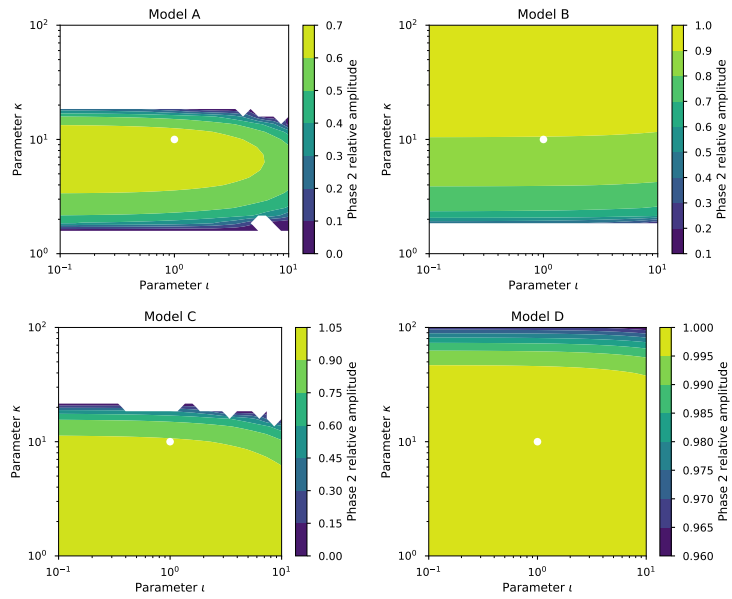


Figure 8.13: Relative amplitude scans, same as Fig. 5.8 for ι and κ and $g(p) = p^2$.